Innviðaráðuneytið

Hvassahraun

Analysis of lidar-derived observations of turbulence aloft

Assignment no.: **52107630** Document no.: **KVT/2023/R154/HÁ** Version: **J02** Date: **2024-03-15**

Norconsult

Client:	Innviðaráðuneytið
Client's Contact Person:	Friðfinnur Skaftason
Consultant:	Norconsult Norge AS, Tærudgata 16, NO-2004 Lillestrøm
Assignment Manager:	Hálfdán Ágústsson
Technical Advisor:	
Other Key Personnel:	Martin S. Grønsleth, Sibylle von Löwis (Veðurstofa Íslands), Einar Sveinbjörnsson (Veðurvaktin)

Version	Date	Description	Prepared by	Checked by	Approved by
J02	2024-03-15	Final	Hálfdán Ágústsson	Idar Barstad	Amund S. Haslerud
C01	2023-11-24	Draft for discussions	Hálfdán Ágústsson	Einar Sveinbjörnsson (Veðurvaktin)	

Contents

Glossary

Azimuth angle	Angle between the projection of the line of sight on the local horizontal plane and the geometric North. This angle is comprised between 0° and 360° (0° is the North and 90° is the East).
Elevation angle	Angle between the line of sight and the local horizontal plane. This angle is comprised between -90° and 90° (-90° is the Nadir, 90° is the Zenith).
LOS	“Line Of Sight” a constant azimuth angle and elevation angle scan.
RHI	“Range Height Indicator” a constant azimuth angle scan. This is a scan where the azimuth angle is kept constant while the elevation angle can vary.
PPI	“Plan Position Indicator” a constant elevation angle scan. This is a scan where the elevation angle is kept constant while the azimuth angle can vary.
RWS	Radial wind speed. The component of the wind along the laser beam of the lidar.
CNR	Carrier to Noise Ratio. This value depends on the aerosol concentration in the atmosphere. High atmospheric backscatter coefficient leads to high CNR. CNR level depends on weather conditions.
Spectrum width	A measure of the variation of the distribution of radial velocity data in a lidar sample.
Range	Distance between Lidar and measurement point (range gate centre)
Range gate length	Radial distance used along which lidar collects data for each lidar sample along the beam. This length is linked to the Laser pulse duration.
EDR	Eddy dissipation rate, a measure of turbulence strength
TI	Turbulence intensity, a measure of turbulence strength

Samantekt

Sem þáttur í rannsókn á veðuraðstæðum við mögulegt flugvallarstæði í Hvassahrauni þá var lidar-tæki til fjarmælinga á vindi notað til að mæla kviku (ókyrrð) í neðsta hluta lofthjúpsins. Í þessari skýrslu er gerð grein fyrir helstu niðurstöðum mælinganna.

Veðurstofa Íslands á lídarinn og rak hann í nærri tvö ár á vegum verkefnisins, á tveimur stöðum, við vindmælimastur í Hvassahrauni og nærri efnisnámu við Krísuvíkurleið, norðan undir Sveifluhálsi. Lídarinn var ekki í samfelldum rekstri heldur fluttur nokkrum sinnum milli staða auk þess að um tíma þurfti að sinna viðhaldi á lídarnum. Stærstan hluta verkefnisins náðust nothæf og góð gögn, en tæknileg vandamál ollu því að gæði gagnana voru lök um tíma, einkum í upphafi verkefnisins.

Gagnasafnið geymir mælingar á breytileika lóðrétta vindþáttarins, þ.e. kviku / ókyrrðar, frá yfirborði og upp í um 1000 m hæð. Gagnaheimtur er bestar nærri yfirborði og versna heldur með hæð, einkum ofan 500 m. Mælingar voru einnig gerðar eftir hallandi lídargeisla, en almenn túlkun þeirra gagna er flókin og gögnin því ekki ígrunduð frekar hér í samantektinni. Gögnin munu þó nýtast til kvörðunar á líkanreikningum kviku með fínkvarða CFD-líkönum, þegar og ef slíkar líkankeyrslur verða gerðar. Almennt séð eru gæði mæligagna nægilega mikil svo nota má þau til að greina kvikuástandið fjarri yfirborði, á sama hátti og var áður gert í sambærilegra rannsókn í Lófót í Noregi [1]. Gögnin eru nokkuð ítarleg fyrir þær vindáttir sem telja má að skipta mestu máli fyrir kviku við fyrirhugaðan flugvöll en fyrir sumar vindáttir er gagnamagn verulega takmarkað en það á þó einkum við áttir þar sem kvika er almennt fremur lítil. Við túlkun gagnanna þarf að hafa í huga að þeirra var aflað á tveimur ólíkum stöðum. Framsetning mælinga á kviku í þessari skýrslu byggir á staðalfráviki vindhraðans, sem er mælikvarða á orku kvikunnar. Svokallað EDR er einnig mælikvarði á kviku og náskyld stærð. Stærðirnar breytast líkt með styrk kvikunnar, þ.e.a.s. þegar kvika eykst þá stækka þær báðar, og öfugt þegar kvikan minnkar. Fylgnin er skýr og hlutfallið milli þeirra vel skilgreint í mælingum efst í mastri, en gera verður ráð fyrir því að hlutfallið breytist nokkuð með hæð yfir jörðu, a.m.k. í neðsta hluta jaðarlagsins.

Í upphafi verkefnisins var lídar staðsettur nærri 30 m mælimastri í Hvassahrauni og mælingar lídarsins sannreyndar á móti mælingum í mastrinu. Lídar og efsti mælir í mastri gefa sambærilegar mælingar, bæði varðandi meðalvind og -hraða, en einnig hvað varðar mælingar á styrk kvikunnar og kvikuorku. Megin takmarkanir mælinga með lídar m.v. háupplausnar mælingar með hefðbundnum sónískum vindmæli lúta að sjálfri mælitækninni. Lídarinn getur ekki mælt hátíðniþátt kvikunnar, það er að segja að lídarinn sér ekki minnstu hvirflana. Lídarinn mælir þann þátt kvikunnar sem er með lægri tíðni, sem er sá hluti sem knúinn er af árhifum frá landslagi og hrýfi. Þessar takmarkanir sjást í orkurófi mældrar kviku, en þar vantar gjarnan hátíðniþáttinn, og eins er hlutfallsstyrkur kvikunnar (TI, turbulence intensity) gjarnan vanmetinn um ~10 %.

Almennt þá gætir breytinga á hrýfi hærra í jaðarlaginu eftir því sem lengra er farið hlémegin breytinganna, þ.e.a.s. því lengra sem vindurinn hefur blásið frá þeim stað þar sem hrýfið breytist. Varlega má ætla að dýpt lagsins sem verður fyrir breytingum sé að lágmarki 1 / 10 af fjarlægðinni frá breytingunni en að almennt eykst dýpt lagsins töluvert hraðar. Full aðlögun jaðarlagsins að breytingum á hrýfi gerist þó hægar, þ.e.a.s. almennt vex dýpt lagsins hægar þar sem ekki lengur gætir áhrifa yfirborðs sem er fjær en fyrrnefnd breyting í hrýfi. Af ofangreindu og að teknu tilliti til landslags þá má ætla að almennt séu há gildi kviku nærri mastri fyrst og fremst fram komin vegna hrýfisáhrifa, þ.e.a.s. kviku sem verður til vegna bremsuáhrifa og vindskurðar við yfirborð jarðar.

Kvika sem verður til v. landslags berst með vindinum og eyðist smám saman. Ýmis þættir ráða því hve öflug kvikan verður og hver hratt hún eyðist, en vindhraði, hæð og lögun fjalla ásamt breytingum hita, vindhraða og vindáttar með hæð ráða þar mestu. Við hvassan vind yfir fjöll þá gætir oft við yfirborð enn áhrifa kvikunnar þó

komið sé fjær fjöllum en sem nemur tífaldri hæð þeirra. Öllu jöfnu má þó ætla að áhrifanna gæti ekki svo langt og kvikan eyðist fyrr. Við hagstæðar aðstæður þá getur þó áhrifa fjalla á loftstrauminn fjarri yfirborði enn gætt mun lengra hlémegin fjallanna. Að þessu má ætla að í mælingum kviku í sjálfu mastrinu í Hvassahrauni gæti fremur lítið eða sjaldan áhrifa frá kviku sem verður til vegna fjalla, en jafnframt að ofan mastursins sé á stundum kvikuástand tilkomið vegna áhrifa fjalla á vindinn.

Lídarmælingarnar sýna breytileika í styrk kvikunnar eftir vindátt, og að styrkur kvikunnar vex almennt með vaxandi vindhraða. Mæld kvika er jafnan minnst fyrir vestanáttir en takmarkað gagnmagn gerir það að verkum að ekki er hægt að túlka gögnin almennt. Norðanáttum er ágætlega lýst í gagnasafninu en mælingarnar sýna ekki almennt há gildi kviku næst jörðu fyrir þær áttir, en nokkuð afgerandi aukningu með hæð að ~300 m. Gögn úr veðurlíkönum gefa til kynna að í sterkum norðanáttum sé oft mikill breytileiki í vindasviðinu á svæðinu, mögulega nokkur kvika og vindsniði hár, þ.e.a.s. aukning vindhraða með hæð meiri en að jafnaði. Ætla má að þessi breytileiki sé vegna áhrifa frá landslagi. Ef frá eru skilin hægviðri þá virðist fremur lítill munur í lídarmælingum á báðum mælistöðum, en hafa ber í huga að mælitímabilin eru ólík og gagnamagn fremur lítið við mastrið.

Hæstu kvikugildin mælast í hvössum austan og suðaustanáttum, hlémegin 300 – 500 m hás fjallgarðs Reykjanesskagans. Kvikan mælist heldur minni í hreinum sunnanáttum. Hafa ber þó í huga að gagnaheimtur eru takmarkaðar þegar hvassast er í þessum áttum en þá er gjarnan úrkoma áköfust og skilyrði til mælinga erfið. Allra hæstu gildi kviku mældust ofan 600 – 700 m við mælistæð í námu, í langdreginni og hvassri austan- og suðaustanátt 2. – 4. maí 2023. Mæliskilyrði og gagnaheimtur voru þó óhagstæð og því ekki fyllilega ljóst um gæði mælinganna og breytingar í styrk kviku með hæð. Einnig mældust um tíma há gildi kviku á mælistað við námu í hvassri suðaustanátt þann 17. maí 2022 og voru þá hæst í 400 – 500 m yfir jörðu. Á sama tíma var hægt vaxandi austanátt og ekki hvasst við mastrið í Hvassahrauni. Nokkuð sambærilegar aðstæður voru daginn áður, 16. maí, en heldur minni kvika á mælistað við námu, hægt minnkandi austanátt og ekki hvasst í Hvassahrauni. Sama á við þann 20. mars 2023 en þá voru gagnaheimtur ofan 500 m engar svo ekki er hægt að fullyrða með vissu um að hámarkið hafi verið í 400 m yfir jörðu. Í meginefni skýrslunnar eru dæmi um fleiri tilvik með mikilli kviku, auk ítarlegri samantekt um mælingar þann 17. maí.

Kvikan í austan- og suðaustanáttum virðist almennt hærri neðan 500 m yfir jörðu en ofar, en það er þó ekki algilt. Í þeim hluta gagnasafnsins sem er með fullar gagnaheimtur þá mældust hæstu gildi kvikunnar í 400 – 500 m yfir jörðu á báðum mælistöðum, og voru aðeins lítillega lægri í 300 – 400 m. Fyrir hvassar austan og suðaustanáttir má líklega rekja uppruna hluta kvikunnar fjarri yfirborði til áhrifa frá landslagi og fjöllum fjarri mastrinu. Kvikan myndast vegna áhrifa frá Reykjanesfjallgarðinum á loftstrauminn yfir fjöllin, og kvikan berst svo áfram með vindinum hlémegin fjallanna. Vindstyrkur ásamt breytingum í vindi og hita með hæð ráða mestu um hve langt kvikan berst en með m.a. ítarlegri líkangögnum mætti leggja mat á hve langt það jafnan er í Hvassahrauni. Mælingar í mastrinu í þessum áttum virðast ekki endilega endurspegla vel há gildi kviku fjarri yfirborðnu.

Ítarleg kortlagning breytileika kviku í tíma og rúmi innan rannsóknasvæðisins er ekki gerð hér, en safnað hefur verið gögnum sem nýtast til þess. Líkt og í [1], þá má nota lídarmælingarnar til að kvarða háupplausna CFD-líkankeyrslur. Slíkar keyrslur má nýta til að lýsa ítarlegar vinda- og kvikuástandi á rannsóknarsvæðinu en hægt er með hefðbundnum veðurlíkönum, en CFD-líkönin herma þó ekki aðra veðurþætti en vind . Gögn úr slíkum líkankeyrslum eru ekki til en hægt er að framleiða þau með tiltölulega litlum tilkostnaði. Líkankeyrslurnar þarf þó að gera í nægilega hárri upplausn svo fínkvarða landslags á kviku sé hermt réttilega Fyrri rannsóknir (t.d. [1]) og gefa til kynna að lágmarki 100 m x 100 m reikninet sé æskilegt í sambærilegu landslagi, og að með grófara neti þá sé kvika kerfisbundið vanmetin, sér í lagi þegar kvika er mikil Ætla má að hærri upplausn bæti heldur niðurstöðurnar en að þá eykst mjög reiknitími og kostnaður. Gögnin þarf að framleiða fyrir allt tímabil lídarmælinganna, og mikilvægt er að líkanið sé á jöðrum sínum þvingað með raunverulegum vindagögnum. Eftir kvörðun m.v. lídargögn, þá má ætla að líkangögnin lýsi vel dreifingu kviku í rúmi innan reiknisvæðisins, en lídargögnin eru strjál bæði í tíma og rúmi. Það er dýrt að framleiða mjög langar

slíkar líkanraðir og því þarf að leiðrétta vinddreifinguna úr stuttum reiknirröðum svo hún endurspegli langtímameðaltöl. Það er gjarnan gert með samanburði við langtímameðaltöl úr löngum tímaröðum sem framleidd eru með veðurlíkönum sem eru keyrð í grófara reiknikneti. Slík grófkvarða líkangögn eru þegar til fyrir svæðið og meira en 40 ára langt tímabil.

1 Summary

As a part of a detailed investigation to assess the conditions at a possible airport site in Hvassahraun (background info in [2]), west of Reykjavík, a scanning lidar was deployed in order to quantify the occurrence and magnitude of turbulence aloft. Turbulence conditions are particularly favourable at the Keflavík international airport ~30 km further west while experience indicates that turbulence is on average more frequent and stronger at the Reykjavík national airport to the northeast, presumably due to urbanization and local terrain features. Previous studies and reports indicate that turbulence aloft may at times be problematic in the area near Hvassahraun, presumably due to mountains south and east of the site, but the evidence is not conclusive (see e.g. [3]). This report describes the lidar measurement campaign and its analysis. Other weather parameters relevant for aviation are studied in detail in a separate report [4] by the Icelandic Meteorological Office, which includes an analysis of turbulence in a 30 m high mast at the site in Hvassahraun.

The lidar (3D scanning Doppler lidar, pulsed single beam) was operated by the Icelandic Meteorological Office for almost two years at two different sites in the area of interest, but not continuously. Reliable and good data was collected for a large part of the campaign, while technical issues degraded somewhat the data quality during extended periods. Overall data availability and quality is considered good, and data are mostly adequate for the analysis of turbulence aloft, in particular for the wind directions which are considered of main interest. The dataset describes the variability of the vertical wind component, i.e. the vertical part of the turbulence, from the surface and up to roughly 1000 m above ground. Data availability is best near the ground and decreases with height, in particular above 500 m. Data interpretation must take into account that the data were collected at two different sites.

The main limitations of the lidar data with regard to traditional observations with sonic anemometer is related to technical differences pertaining to the observation platform and technique. Sonic anemometers are point observations which can typically be done with a frequency of 10 - 20 Hz, while a scanning lidar typically samples the atmosphere in a narrow but long interval along its beam, with a typical data acquisition time on the order of 1 second. In this sense lidar data are both a volume and temporal average. The lidar reproduces well the lower frequency turbulence, typically up to or well into the low-frequency end of the inertial subrange, while it cannot reproduce the higher temporal frequencies of the turbulence. A result of this is that bulk-estimates of turbulence such at the turbulence intensity are typically on the order of 10% lower than when observed with a sonic anemometer.

The lidar observations show a directional difference in the intensity of the turbulence and a general increase in turbulence with wind speed. Turbulence in the observations is generally weak from the west but the limited amount of available data for this sector means that the results are not easily generalized. Northerly wind is well represented in the data but is on average not associated with particularly strong turbulence at low levels but there is however a considerable increase with height up to ~300 m.

The strongest turbulence occurs in strong easterly and southeasterly flow, while the levels are slightly lower during southerly flow. Please note that data availability is limited during the strongest events, as they are typically associated with intensive precipitation. The strongest turbulence was observed during a strong southeasterly event at 600 – 700 m, but the variation with height is not well observed due to poor measurement conditions. Other strong events have a maximum at around 400 – 500 m, but also with high values down to 300 m. This is also the case for the subset of data with full data availability at all lidar levels within this directional sector. This suggests an orographic contribution to the turbulence aloft, related to the flow over the 300 – 500 m high mountains to the south and east.

Strong turbulence at the mast location is presumably mostly locally generated due to surface roughness while aloft there is presumably a non-local contribution for flow from the east and south. The mast data may not be an optimal indicator for strong turbulence aloft for these directions.

2 Introduction

Previous measurements campaigns and analysis work pertaining to siting of a new airport near Reykjavík, Iceland, have indicated that the Hvassahraun area west of Reykjavík (Figure 2-1) is the most optimal location with regard to climatic conditions. As a part of a detailed investigation to assess the conditions at a possible airport site in Hvassahraun, a scanning lidar was deployed in order to quantify turbulence occurrence and magnitude aloft, in a similar manner as previously done for Avinor, the Norwegian aviation authority, in Lofoten in Norway [1].

The measurement campaign also includes observations of other relevant atmospheric parameters, most relevant for the current analysis are the wind observations at high temporal resolution in a 30 m high mast in Hvassahraun [4], which are available for the whole period of lidar observations. A collection of measurement flights, mostly by ultralight aircraft, have been performed to map the spatial distribution of turbulence in the area of interest [5].

Long-time series of simulated atmospheric data produced at high spatial resolution with a numerical weather prediction model are also available and corroborate the observational data in the analysis. The KVTMeso (IceBox) hindcast covers January 1991 to September 2023 and allows for comparing the flow conditions during the measurement period with the wind climate. The hindcast is prepared with the WRF-model[1] and input data based on ERA5, at a temporal resolution of 1 hour, and a horizontal resolution of 2 km and high vertical resolution (details in appendix A). The dataset has been extensively validated in other project work.

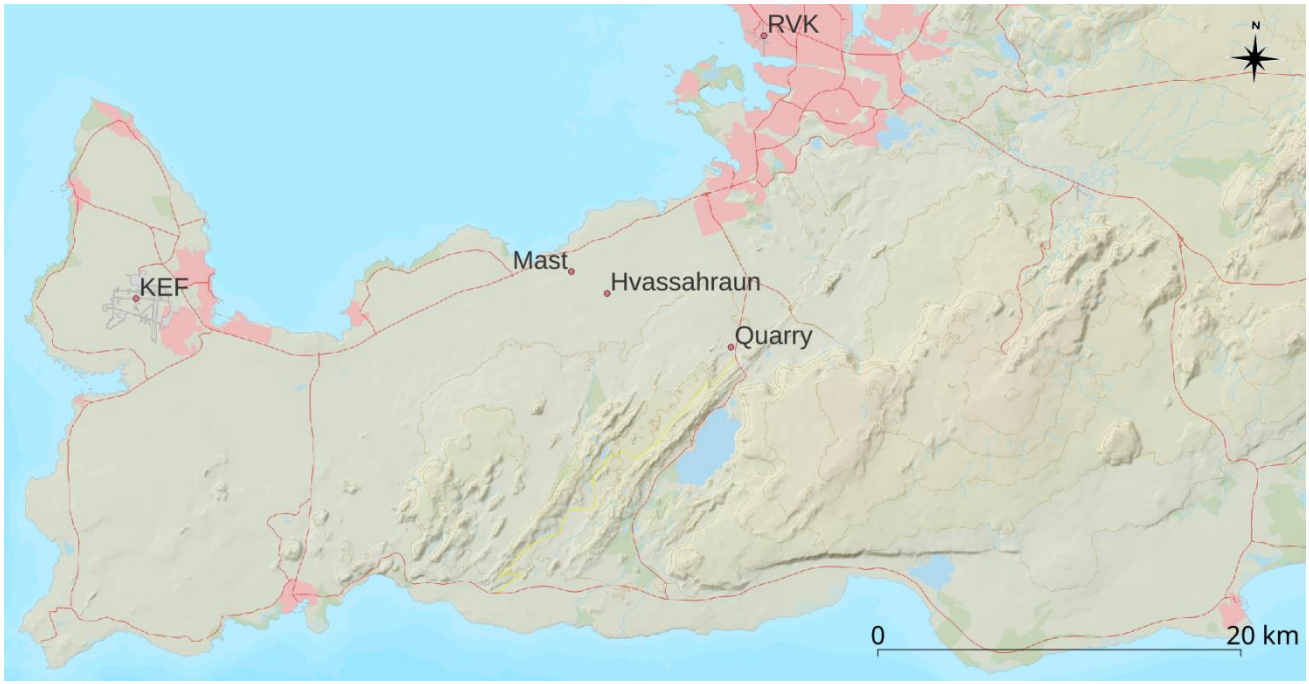

Figure 2-1 Overview map of the area of interest at Reykjanesskagi in Southwest-Iceland.

[1] https://www.mmm.ucar.edu/models/wrf

3 Instrumentation and lidar operation

3.1 What is a lidar and why is it used here?

A lidar is a remote sensing device that uses a laser and the doppler effect to measure the speed of airborne particles, aerosols, in the atmosphere. It measures the backscatter of light from the aerosols, processes the data, and returns the wind speed along the lidar-beam, which is termed the radial wind speed (RWS). It can do so simultaneously for multiple distances along the beam, out to the lidars maximum range. Depending on the type of lidar, the temporal granularity is on the order of seconds and up to 10 minutes.

One of the main advantages of using a scanning lidar, as compared to for example a tall mast, is that the lidar beam can be oriented in an arbitrary direction and measurements can be collected high aloft or at a large distance from the lidar, as well as at locations where it may not be possible to place masts. Scanning lidars can in particular be used to quantify atmospheric turbulence aloft, as has for example previously been done in Norway, where lidars were used to map the occurrence of topographically induced turbulence near multiple possible future airport locations in Lofoten [1].

The main limitations of the lidar data with regard to traditional observations of turbulence with sonic anemometer is that it gives only one component of the turbulence, and it cannot reproduce its higher temporal frequencies. The lidar reproduces well the lower frequency turbulence, typically up to or well into the low-frequency end of the inertial subrange. A result of this is that bulk-estimates of turbulence such at the turbulence intensity are typically on the order of 10% lower than when observed with a sonic.

3.2 Setup and technical details of the lidar

The current lidar is a Leosphere 200S scanning, pulsed, lidar, owned and operated by the Icelandic Meteorological Institute (IMO). The lidar has a wavelength of 1543 nm and is a class 1M lidar, meaning that the laser beam is not harmful to the naked eye, unless viewed through an optical instrument. The lidar head can be rotated at will and the laser beam hence pointed in any direction needed, from slightly below the horizontal and upwards.

The lidar probes the atmosphere along the whole lidar beam at a very high temporal resolution and returns measurements of the along-beam wind speed (radial wind speed, RWS) in so-called range gates which are distance intervals along the lidar beam. The radial wind speed value returned for each range gate is based on a large amount of lidar sampling along the whole distance of the range gate, weighted most at its centre. A range gate length of 50 m is employed here, which gives the highest spatial resolution possible with the lidar. The range gates are spaced at 50 m intervals, with the first range gate located 100 m away from the lidar, which is minimum allowed distance. With this setting the maximum range is 7200 m, given optimal atmospheric conditions, which is more than sufficient for the current setup.

In order to measure the wind, a lidar depends on the existence of aerosols in the air that it probes. If the air is very clear and there are too few aerosols, there will be no measurements. If there is heavy precipitation or there are too many aerosols, for instance fog, the signal will be attenuated quickly, and the measurement range will be reduced.

The lidar collects backscatter data at very high internal resolution while the highest possible temporal resolution for the resulting radial wind speed is ~1 second, which is what is used here.

Measurements have been done for a few different pointing angles, most notably for a vertical lidar beam and beam pointing a few degrees above the horizontal. In this context we note again that the lidar only measures the wind speed along the lidar beam, i.e. RWS, which means that with a scanning lidar in LOS mode only one one component of the turbulence can be reliably measured. Other modes, and other lidars, may suggest observations of the 3-dimensional wind but that assumes homogenous flow, which is not a valid assumption in complex terrain and introduces uncertainties not accepted for the turbulence estimates.

Measurements were performed at two different locations, near the 30 m mast in Hvassahraun (Mast) as well near the mountains ~7 km southeast of the mast (Quarry), as depicted in Figure 2-1.

3.3 Filtering of lidar data

Thorough filtering and detailed post-processing are required for extracting useful and reliable wind information from the raw lidar data. The post processing, including the time and space aggregation of the data, is to an extent dependent on the analysis to be done. As such, a conventional table of percentages of valid 10-minute mean values only describes a specific subset of the data used in the analysis. A part of the analyses, including that of turbulence, requires strict conditions on sampling frequency and data quality. The amount of reliable data is reduced with more stringent requirements.

Internally, the lidar calculates the Carrier to Noise Ratio (CNR) [dB] of each high frequency sampling, which is in essence the strength of the measured signal with regard to background noise. This value can then be used in filtering of the raw data. Previous analysis in similar conditions ([1] and [6]) as well as a review of the current data shows that good quality data typically has a CNR value greater than -27 dB, with lower values typically associated with insufficient aerosol content (i.e. too clean air). High CNR values are also often an indication of problematic measurements, e.g. due to too high aerosol content, fog or hydrometeors. We have here employed constant maximum and minimum thresholds of, respectively -15 and -27 dB to define reliable data, which removes most problematic data points.

The data can be filtered by other means than the CNR value alone. Further filtering is done using additional quality parameters from the lidar, namely the confidence index is 100 % and status is OK, both of which are internal quality parameters provided by the Leosphere software. The last filtering criteria requires that the spectrum width (a measure of the distribution of velocity data in a lidar sample) is less than 1, which is a somewhat arbitrary but removes spurious, unphysical, spikes that introduce noise into the dataset.

The analysis of the lidar data is typically done using 10-minute aggregated data, but shorter aggregation periods have also been checked. The use of 10-minute data is as customary in analysis of observational wind-data and allows for an easier comparison and correlation with other atmospheric data sources such as mast-data and simulated flow. For 10-minute data a minimum of 500 ~1-second samples are required (83 %), as a higher threshold would be too stringent with regard to the available data. The criteria are scaled accordingly for shorter aggregation periods.

3.4 Measurement locations and scenarios

The scanning lidar has been located in two different locations (Table 3-1) during the measurement period, near the mast in Hvassahraun as well as in an abandoned aggregate quarry (gravel mine/pit) at the foot of the mountain ridge to the south (Figure 2-1). At the start of the campaign in April 2021, the lidar was placed near the mast before it was moved to the location near the quarry in September 2021. The lidar was not in operation for a period in the spring of 2022, before it was again placed near the meteorological mast in the

autumn of 2023. The lidar was again moved to the quarry in January 2023 and finally decommissioned in early May 2023 (Table 3-2). The lidar was twice out for other use and maintenance, during summers of 2021 and 2022. All lidar operations and maintenance were done by IMO, with Norconsult providing support on measurement setup and organization.

Table 3-1: Coordinates of the lidar locations.

lidar	Latitude north [deg]	Longitude east [deg]	Elevation [m]
Mast	64.00995	-22.14143	35
Quarry	63.97646	-21.95782	140

The lidar has been set in a few different scanning modes that can used for collecting and analysing turbulence data aloft. During the first period at the met-mast (May and June 2021) the lidar was in line of sight mode (LOS) where the lidar was staring at fixed angles, approximately southwards at a low elevation angle passed the top sensor in the mast. This period was characterized by unstable operations because of issues with the remote power supply. The data is used for validating the lidar against the met-mast measurements, and also coincides with the first ultralight flights. Lidar directions were verified by hard-target scans against the mast.

The lidar was dismantled in June 2021 and moved to the site at the quarry further to the south, where it was on 30 September 2021 set to scan in LOS mode, southwards. Data is of degraded quality for approx. 4 weeks after 10. November, due to issues related to the scan settings, equivalent to a loss of ~30 % of good data. A short period of vertical LOS with different range gate settings was done in January and May 2022, in connection with ultralight flights. Hard-target scans were missing until 19. January 2023 after which lidar directions could be verified. The scanning direction was changed to a more appropriate south-westerly LOS on 31. January 2023. Due to in-adequate fastening of the lidar, vibrations induced by wind pressure contaminated the measurement data, especially during strong wind episodes. These issues were addressed on 2. February 2022 after which the conditions improved, as seen in the changes in the baseline value of the lidars rotation around its two horizontal axes of rotation (yaw and pitch, Figure 3-1). However, measurement data 30. September 2021 – 2. February 2022 is suspect to considerable uncertainty. Lidar was dismantled and sent to maintenance on 15 June 2022.

The lidar was installed again at the met-mast location, and set to vertical LOS scans, on 23. September 2022 and until 18. January 2023. The first month of data in the autumn of 2022 is missing most of data due to technical problems and high internal humidity causing dew and rime formation on the inside of the lidar lens during cold weather (internal relative humidity values exceeding ~30 % are typically a problem in cold temperature operations of this type of lidar, cf. Figure 3-2). Data after 6 December is of degraded quality due to issues related to the scan settings, equivalent to a loss of ~40 % of good data.

The lidar was again installed at the site at the quarry on 22. January 2023 and was in operation and set to vertical LOS until 10. May 2023.

A summary of the time and length of each scans used are provided in *Table 3-3* below. Scans which can potentially be used for mapping turbulence aloft are marked specifically. However, for technical reasons discussed above, these can for practical reasons be considered to be only the vertical scans.

The range-gates (distances away from lidar where observations are available) employed have for all practical considerations been held constant (*Table 3-4*). They range gates are the same for the periods of vertical and sloping lidar observations, except for a few days of vertical LOS where higher resolution and lower top maximum range was used.

Table 3-2: Periods of different lidar locations.

Position	Period start	Period end	Comment
Mast	30. April 2021	29. June 2021	Test and sloping scan past top sensor. Unstable operation due to power generator.
Quarry	30. Sep. 2021	15. June 2022	Sloping scan to south until 31. January, thereafter to southwest. Some days of vertical scans. Lidar not secured well to ground until 2. Feb. No hard target until 22. Jan.
Mast	23. Sep. 2022	18. Jan. 2023	Vertical scans. Unstable operations in start due to power problems and until 20 Oct. due to high internal humidity.
Quarry	22. Jan. 2023	10. May 2023	Vertical scans.

Table 3-3: Simple overview of scenarios (scanning modes) of the lidar. Scenarios marked in light grey can potentially be used in studies of turbulence. Note that duration does not indicate continuous operation for the stated number of days.

Period start	Duration (days)	Setup & tech. tests	Hard target scan	Validation at mast	Sloping south	Sloping southwest	Vertical scan	Comments
28. Apr. 2021	3	x						
29. Apr. 2021	1		x					Towards met-mast
30. Apr. 2021	61			x				Downtime due to power issues
24. Jun. 2021	1		x					Towards met-mast
28 Sep. 2021	*3*	*x*						
30. Sep. 2021	*124*				*x*			Incorrect scan direction, unstable operation
7. Jan. 2022	*3*						*x*	In connection with flight, high vertical resol.
19. Jan. 2022	*148*		*x*					Operational, against tower
31. Jan. 2022	*136*					*x*		
16. May 2022	*3*						*x*	In connection with flights
23. Sep. 2022	*118*						*x*	Unstable operation until 20. Oct.
22. Jan. 2023	*109*						*x*	

Table 3-4: Labelling of measurement distances away from lidar (until June 2022), as well as measurement heights above the lidar for a few days in January 2022 as well as since September 2022.

Distance [m], until June 2022	**345**	**395**	**445**	**495**	**545**	**595**	**645**	**695**	**745**	**795**	**845**
Label	N	M	L	K	J	I	H	G	F	E	D
Distance [m]	**895**	**945**	**995**								
Label	C	B	A								

Height [m], 7. – 10. January 2022	**100**	**120**	**140**	**160**	**180**	**200**	**220**	**240**	**260**	**280**	**300**
Label	Z	Y	X	S	R	Q	P	N	M	L	K
Height [m]	**320**	**340**	**360**	**380**	**400**	**420**	**440**	**460**	**480**	**500**	
Label	J	I	H	G	F	E	D	C	B	A	

Height [m], from September 2022	**100**	**150**	**200**	**250**	**300**	**350**	**400**	**450**	**500**	**550**	**600**
Label	X	S	R	Q	P	N	M	L	K	J	I
Height [m]	**650**	**700**	**750**	**800**	**850**	**900**	**950**	**1000**			
Label	H	G	F	E	D	C	B	A			

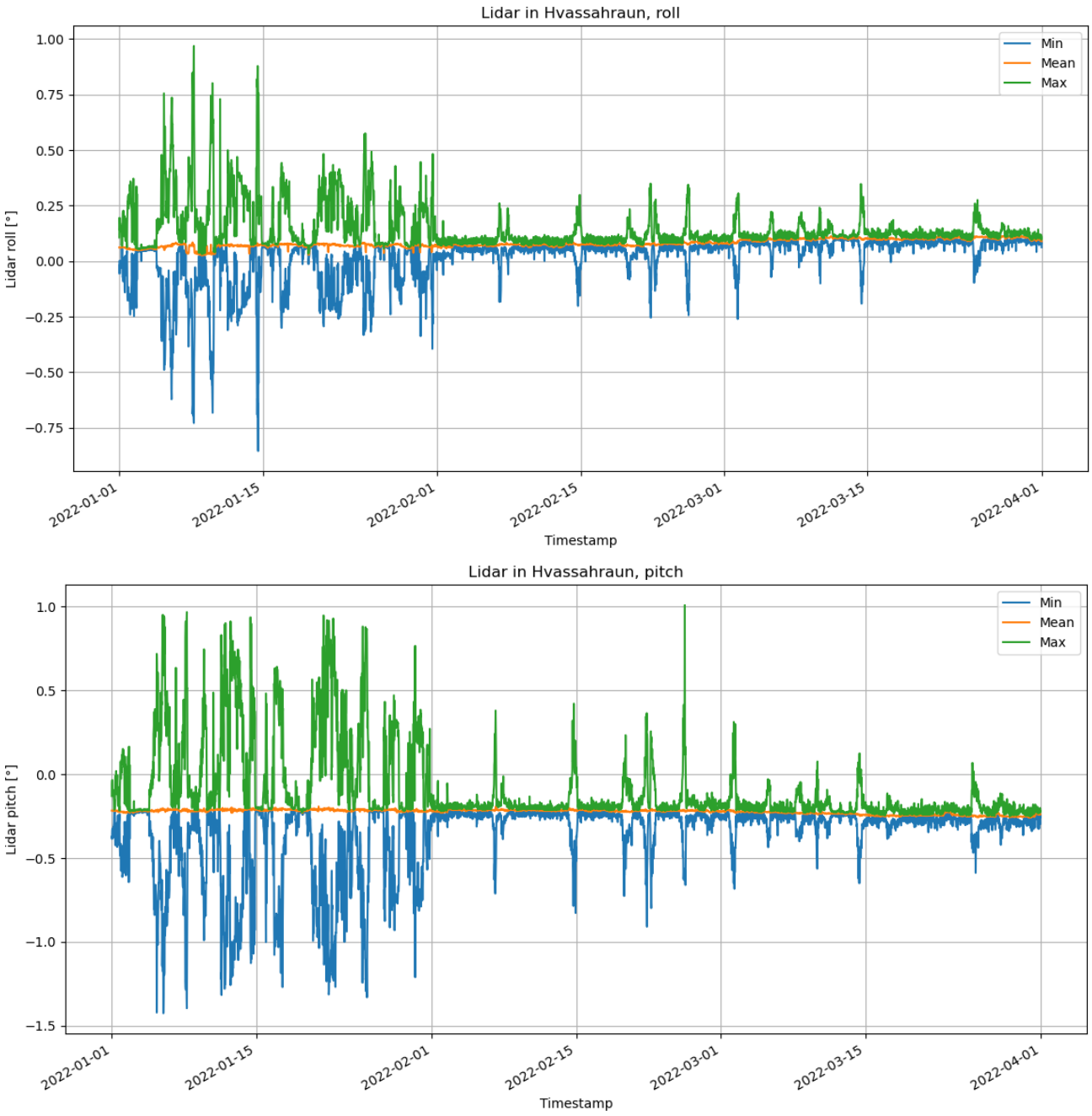

Figure 3-1 Time series of lidar baseline orientation, roll and pitch, for 1. January – 1. April 2022.

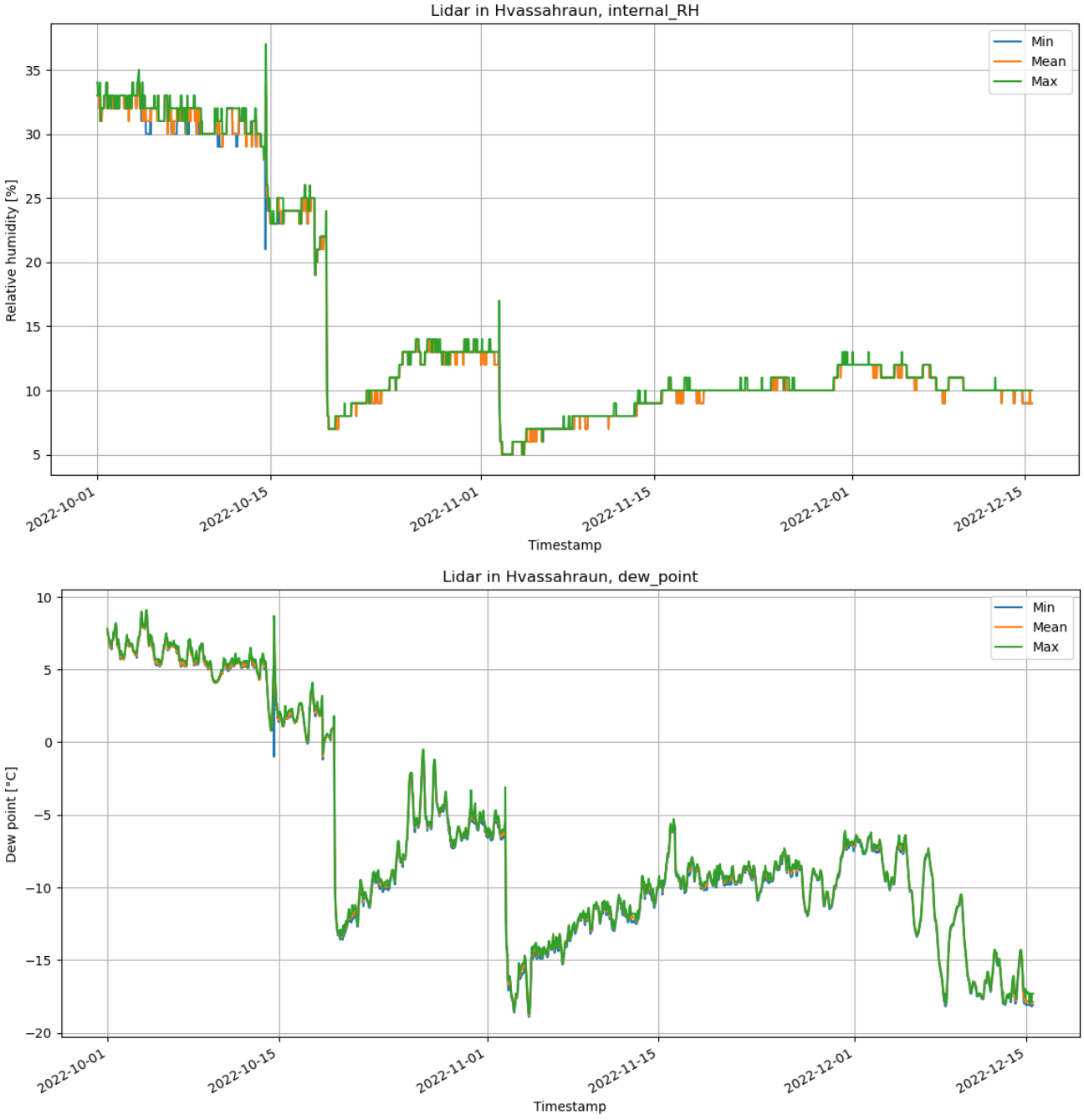

Figure 3-2 Time series of lidars internal dew point and relative humidity, for 1. October – 15. December 2022.

4 Atmospheric turbulence and lidar measurements

4.1 Turbulence in atmospheric timeseries

The velocity of an air parcel is typically described as the sum of a mean component, indicated by an overbar, and a turbulent part which is indicated by an apostrophe. For the full wind vector or any of the three wind components this becomes

$$u = \bar{u} + u'. \tag{1}$$

The mean is typically taken over a period that naturally separates the slow variation of the wind speed associated with large scale structures with variations associated with microscale turbulence. This separation is normally described as the spectral gap and is on the order of 10 minutes to 1 hour in most observational records. At the spectral gap there is typically an apparent lack of variation in the flow, compared to the variations at longer time and spatial scales (synoptic variations) compared to shorter scales associated with turbulence. More details can be found in for example [7].

Turbulent kinetic energy for a given averaging period, TKE, is a measure of the energy per unit mass caused by the turbulent part in an air flow. The TKE is defined as:

$$TKE = \frac{1}{2}\left(\overline{u'} + \overline{v'} + \overline{w'}\right) = \frac{1}{2}\left({\sigma_u}^2 + {\sigma_v}^2 + {\sigma_w}^2\right) \tag{2}$$

where σ_u, σ_v and σ_w are the measured standard deviations along three spatial directions:

- u: component along the wind direction
- v: component perpendicular to the wind direction
- w: vertical component of the wind

In typical boundary layer flow where the turbulence is roughness driven, the along-wind component of the turbulence is typically largest (see e.g. [7]), while it is slightly weaker in the transversal direction. The vertical part is smallest, as vertical motions are inherently limited due to the proximity to the surface of the earth. The vertical component is on average smallest, in particular near the surface of the earth due to the blocking effect from the surface. This is however not the case in convective situations, where the vertical component may be at least as large as the horizontal components.

Isotropic turbulence implies that turbulence has the same magnitude in all directions, such that:

$$\sigma_u = \sigma_v = \sigma_w, \tag{3}$$

and the TKE can be determined by knowing only the standard deviation of any one of the three wind components (σ_r):

$$TKE_{isotropic} = \frac{3}{2}{\sigma_r}^2 \tag{4}$$

This is particularly useful when measurements of only one turbulent component are available, as is for example the case with a scanning lidar, and the TKE can be approximated with the simple equation in (3). However, the turbulence is rarely observed to be isotropic in typical boundary layer flow with roughness driven turbulence. Turbulence in strong flow near large structures, above or in the lee of topographic features is often more isotropic. Aloft, topographically driven turbulence is more likely to be isotropic downstream of complex topography than of simple 2-dimensional ridges and hills (cf. e.g. [8] and [9]). Previous work in Norway, using 10 Hz wind data from tall masts, indicates that in complex terrain the turbulence can often be isotropic or nearly isotropic within 10 % [1].

Turbulence intensity, TI, is frequently used as a measure of turbulence:

$$TI = \sigma/\bar{u}\,, \tag{5}$$

where σ is the standard variation of the flow; often for the horizontal part of the flow but can also be defined for individual wind components. TI is normalized in this way as it removes the effect of increased turbulence near the ground when the mean wind speed increases.

The eddy dissipation rate (EDR) is an indirect measure of turbulence and describes the rate of kinetic energy transfer in the inertial sub-ranges, i.e. from where the turbulence is created at longer scales and to where it is dissipated at short length scales (overview in e.g. [10]). EDR is often estimated via turbulence spectra, as done in [4]. Although yet not widely used, aviation authorities are moving towards using the EDR as a turbulence indicator instead of using the turbulence itself. Reports [4] and [5] have employed EDR in their analysis but that has not been practically possible with the lidar data. Estimates of the EDR directly from the radial wind speed via the spectra are not practical as the observed spectra does not describe well the high frequency part in the inertial subrange. Methods using other setups than LOS introduce uncertainties and assumptions which are not valid in complex terrain or require accurate estimates of the mean wind aloft as in [11].

Due to its definition the eddy dissipation rate is directly correlated to the standard deviation of the wind speed. The eddy dissipation rate for a wind component locates the part of the turbulence spectra in the inertial sub-range, while the standard deviation of the component is equal to the area under the spectra (i.e. its integral). This is obvious when the EDR and standard deviation of the observed wind in the top of the mast are compared (Figure 4-1). However, the ratio is not necessarily the same at all levels away from the surface as the length scales of the turbulence will typically vary with height up to a certain level in the boundary layer.

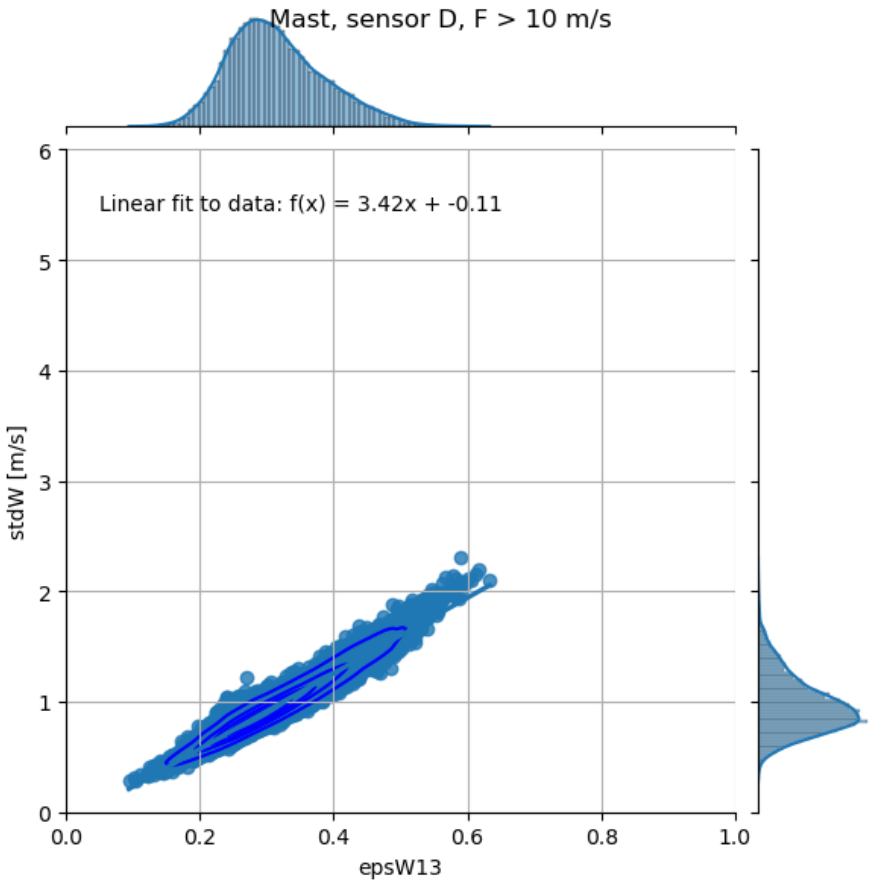

Figure 4-1: An example of the relation between the eddy dissipation rate (x-axis) and standard deviation of the wind, for the vertical component of the observed wind in the mast (data from April – June 2021).

4.2 Spatial averaging on turbulence observed in a scanning lidar

Since a doppler lidar measures the wind speed in an elongated volume along the laser beam, the observed radial wind speed is in fact a result of low pass filtering of the actual point velocity. Details are given in [11], but in short then the spatial filtering introduced by the sampling volume of the lidars will introduce an average deficit in the turbulence levels measured by the lidar. The reduction can be estimated directly when the mean wind is oriented along the lidar beam, but the reduction will vary with wind direction and speed, measurement noise and spatial resolution of the lidar.

For a Leosphere wind cube and lidar range gate length of 50 m (spatial resolution), the turbulence intensity, TI, can be reduced by approximately 14 % at 10 m/s, and slightly less at higher wind speeds. This is as depicted in Fig. 4 in [11], which is reproduced below for convenience. The reduction will vary with the direction of the flow with regard to the direction of the lidar beam, with a weaker reduction in TI when the flow is perpendicular to the beam.

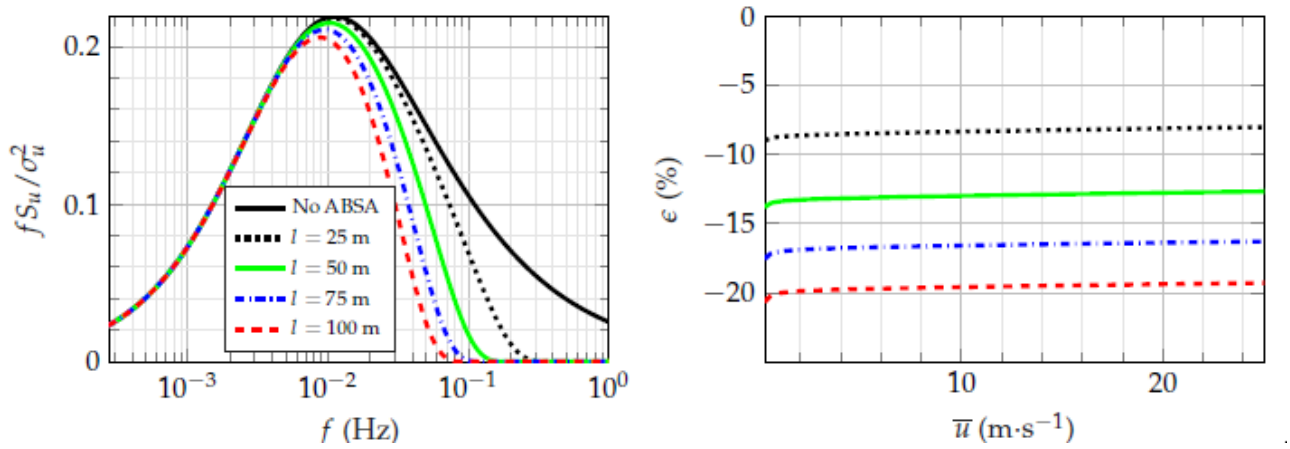

Figure 4-2: Reproduction of Fig. 4 from [11] © MPDI: (left) influence of the along-beam spatial averaging (ABSA) effect of the Wind Cube on the measured normalized spectrum defined in the Handbook N400 (Kaimal), using an arbitrary mean wind velocity u = 10 m/s at z = 25 m agl; (right) estimate of the corresponding deficit ε of the estimated standard deviation of the along-wind velocity due to the ABSA.

5 Data collection

In this chapter an overview of the collected data from the scanning lidar and its quality is presented. The campaign setup is based on the scenarios described in the previous chapter.

5.1 Lidar data availability

Power has been supplied via a temporary grid connection at the quarry site, and a remote power supply at the mast site. Data transfer, system control and monitoring has been done via a mobile connection (3G/4G/5G). The grid connection at the quarry worked well with no major outages during the campaign while the remote power supply has had intermittent trouble, particularly in June 2021.

The weekly data availability is presented as the percentage of 10-minute intervals with quality-controlled data at approximately 350 m away from the lidar (Table 5-1 and Table 5-2). Quality controlled, or good, data is defined as in the previous section, with given criteria on the minimum amount of 1-second data, CNR, etc. The availability will typically be lower for locations further away from, or higher above, the lidar. The availability for the days of vertical scans in January and May 2022 is combined with the sloping scans in the period.

Table 5-1: Weekly availability of 10-minute lidar-data at ~350 m away from the lidar. Continued in Table 5-2.

Year	Week	Availability [%]	Year	Week	Availability [%]
2021	**17**	81	**2021**	**35**	0
	18	14		**36**	0
	19	32		**37**	0
	20	0		**38**	0
	21	8		**39**	0
	22	3		**40**	49
	23	9		**41**	48
	24	56		**42**	22
	25	2		**43**	58
	26	0		**44**	52
	27	0		**45**	28
	28	0		**46**	16
	29	0		**47**	17
	30	0		**48**	13
	31	0		**49**	21
	32	0		**50**	36
	33	0		**51**	33
	34	0		**52**	31

Table 5-2: As for Table 5-1.

Year	Week	Availability [%]	Year	Week	Availability [%]
2022	**1**	28	**2022**	**37**	0
	2	18		**38**	7
	3	18		**39**	8
	4	44		**40**	4
	5	52		**41**	0
	6	47		**42**	31
	7	35		**43**	22
	8	26		**44**	58
	9	42		**45**	51
	10	47		**46**	56
	11	45		**47**	67
	12	38		**48**	41
	13	36		**49**	27
	14	18		**50**	24
	15	36		**51**	21
	16	55		**52**	37
	17	86			
	18	14	**2023**	**1**	16
	19	58		**2**	10
	20	80		**3**	0
	21	86		**4**	13
	22	25		**5**	13
	23	7		**6**	16
	24	0		**7**	43
	25	0		**8**	25
	26	0		**9**	17
	27	0		**10**	95
	28	0		**11**	87
	29	0		**12**	84
	30	0		**13**	47
	31	0		**14**	20
	32	0		**15**	69
	33	0		**16**	29
	34	0		**17**	70
	35	0		**18**	55
	36	0		**19**	55
				52	24

The technical availability (lidar operational and sending data) is inherently higher than presented in the tables but not discussed here. Apart from its dependence on the technical availability, the availabilities presented in Table 5-1 and Table 5-2 are typically most affected by scan settings which at times were not optimal, as well as limiting atmospheric conditions such as precipitation and very clean air.

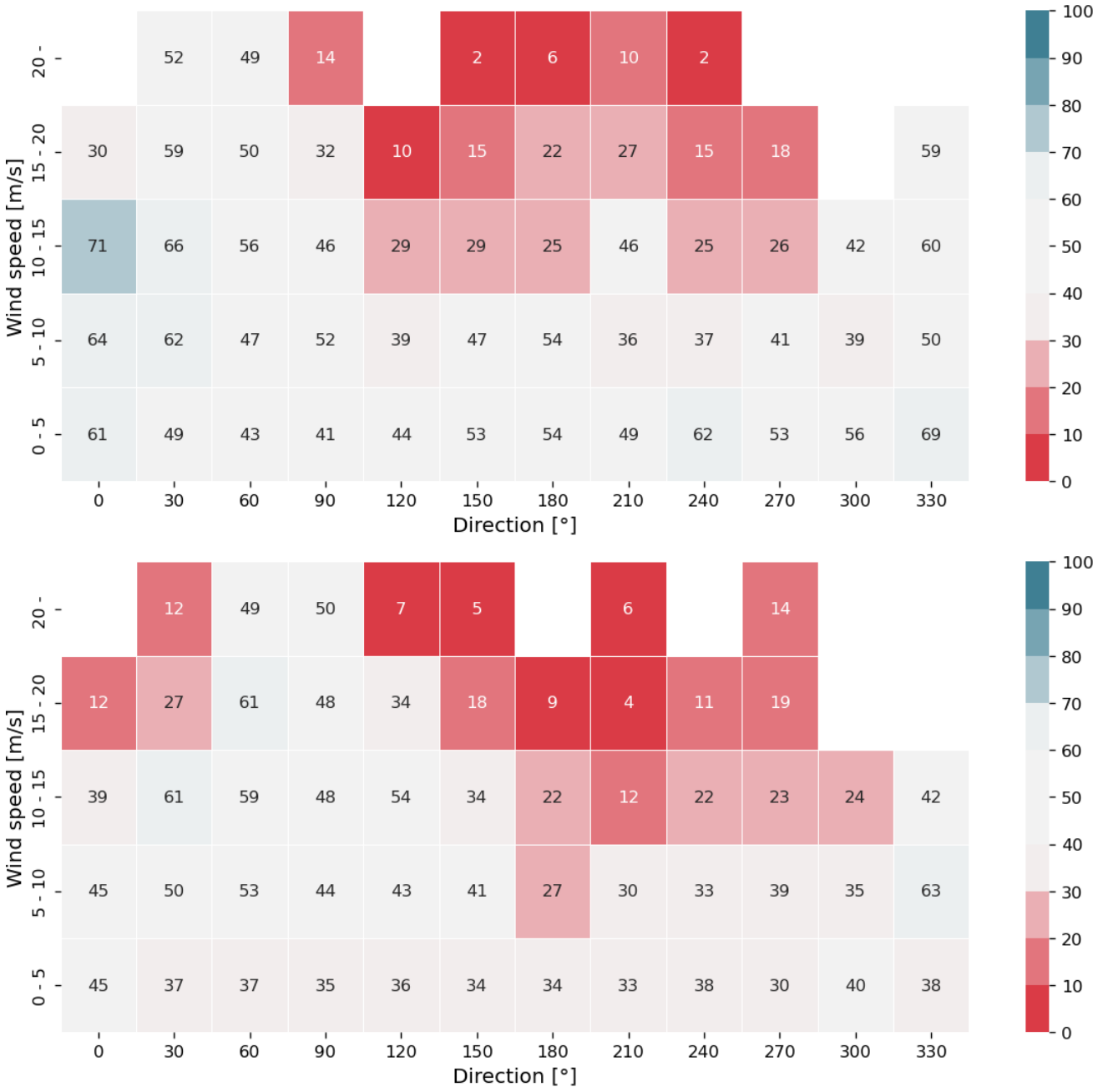

Figure 5-1: The availability [%] of the lidar observations, as a function of the simulated wind speed and direction at a ~350 above the mast location. Above: observations for Sept. 2021 – June 2022, with a sloping beam. Below observations for Sept. 2022 – May 2023 with a vertical beam.

An indication of the relative availability [%] of the lidar measurements, as a function of simulated wind speed and direction at ~350 m above the mast location, is given by the heatmaps in Figure 5-1. The available lidar data are binned with based on simulated wind data (WRF500M, described in Appendix F) which is a good indicator of the actual wind conditions.

Overall, 30 – 50 % of flow situations with winds weaker than 10 m/s have been sampled by the lidar. For higher wind speeds only easterly wind directions have been sampled as well during the period with a vertical lidar beam. The lower relative availability during southerly than for easterly directions may be related to higher frequency of precipitation during the southerly events observed but the precipitation climatology is however similar for these directions [12]. Winds from the west were relatively infrequent during the measurement period and are poorly represented in the lidar data.

5.2 Comparison of lidar data with mast data

During 30 April – 29 June 2021 the lidar was located close to the mast in Hvassahraun and the laser beam was pointed so it would measure the wind very close to the top sensor in the mast. Issues with the power supply led to downtime at the lidar, but the data collected is however well suited for comparing lidar derived wind data with the sonic anemometer wind data. Details on the mast observations are found in [4].

Figure 5-2 and Figure 5-3 show an excellent agreement by the projection of the measurements from the top sensor in the mast at 30 m agl onto the lidar beam vector and the lidar when measuring right beside the sensor. Differences in the observations from the lidar and mast are explained by the differences in measurement technology; one is a 10 Hz point observation while the other is a 1-second average over a 50 m elongated volume. Furthermore, a small error in the baseline wind direction estimate will introduce a bias while flow disturbances due to the mast may also contribute to increase the difference in wind speeds. The agreement is also good for the standard deviation of the radial wind speed (Figure 5-4), but lidar underestimates slightly the wind speed variability compared to the 10 Hz measured data from the sonic.

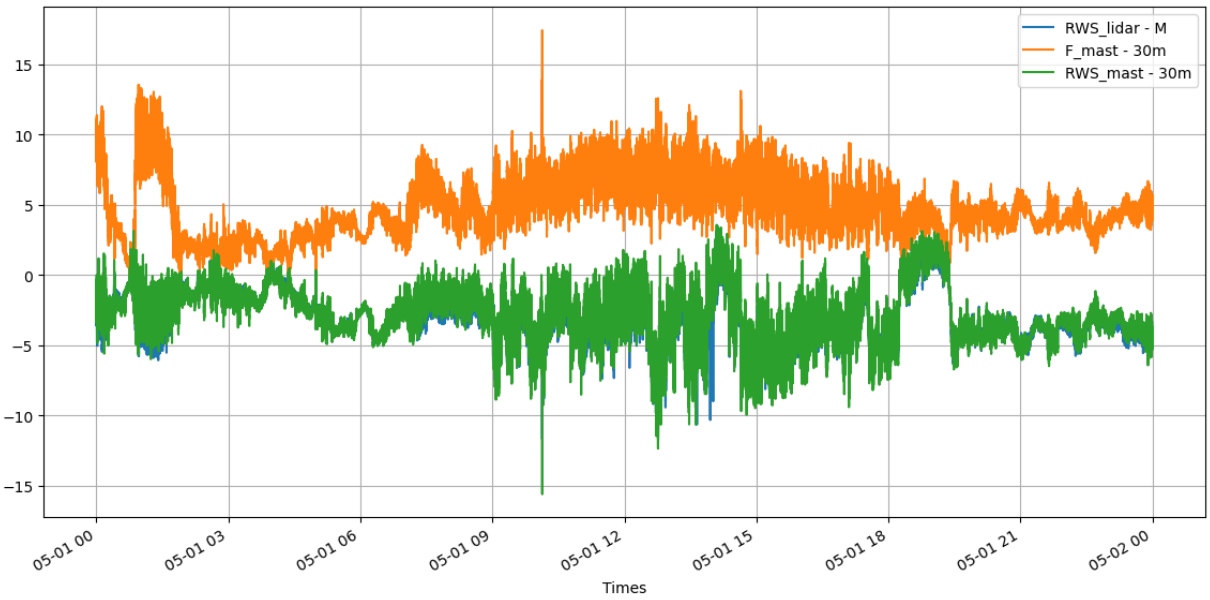

Figure 5-2 Example timeseries of observed wind (y-axis) in the top sensor of the mast (F, orange) and its projection onto the laser beam vector (radial wind speed along the vector, RWS, green), for 1 May 2021. The radial wind speed from the lidar in a volume right beside the mast-sensor (RWS, blue) is nearly identical to the RWS from the mast, and thus obscured by the green curve.

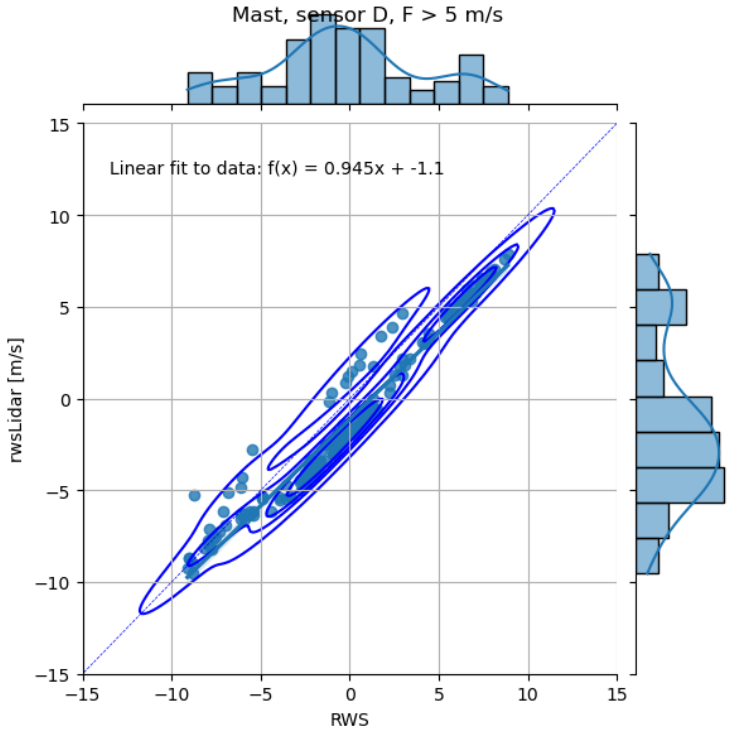

Figure 5-3 Scatterplot of projection of observed wind from mast top sensor onto the laser beam vector (abscissa) vs the radial wind speed from the lidar (ordinate) in a volume right beside the mast-sensor (30 April – 27 June 2021).

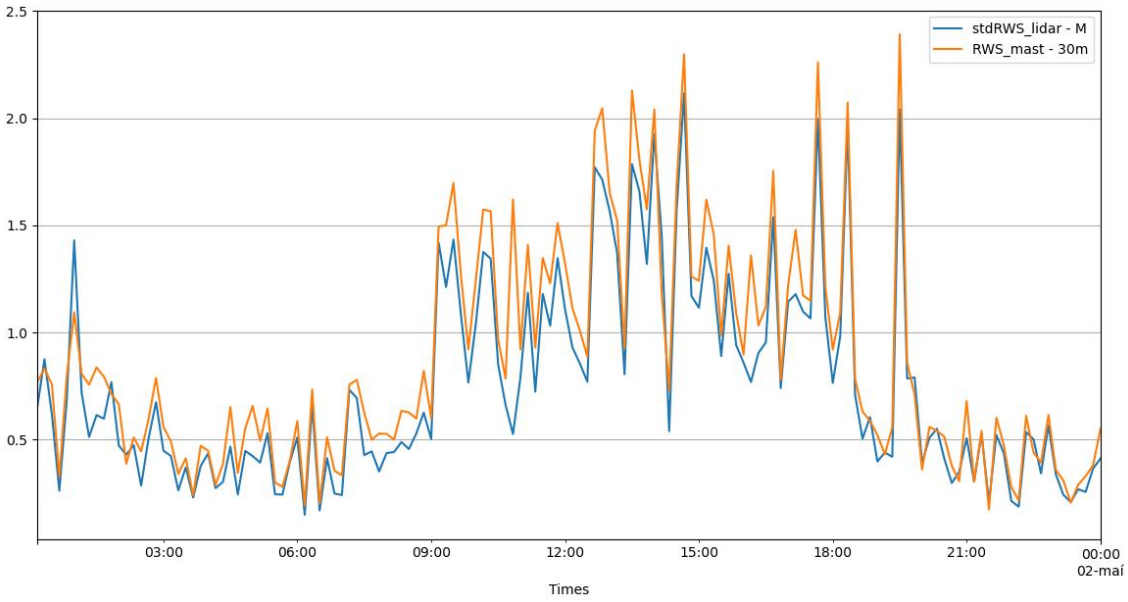

Figure 5-4 Example timeseries of the standard deviation of the projection of the observed wind in the top sensor of the mast onto the laser beam vector (orange) and of the radial wind speed from the lidar (blue), for 1 May 2021.

5.3 Lidar measurements during aircraft flights

The standard deviation of the radial wind speed from the lidar measurements is plotted (Figure 5-4 - Figure 5-14) for all days where lidar data is available and measurement flights were done, as listed in Table 5-3. Detailed information on observed wind and estimated EDR in the met-mast are found in [4]. For information on the turbulence conditions measured during the flights we refer to [5].

Table 5-3: Dates locations where lidar-data is available concurrent with measurement flights. Also shown are the location of the lidar and the type of scan employed. The column Ok indicates the data quality. Weather comments are based on simulated wind at ~200 m agl and ~350 m agl for, respectively, sloping and vertical scans.

Date	Location lidar	Type scan	Ok	Comment
20210430	Mast	Sloping	x	First flight, first day of operational lidar. Weak northerly flow.
20210525	Mast	Sloping		Lidar not operational
20210823				Lidar not deployed
20211222	Quarry	Sloping	x	Weak easterly, stronger in evening
20211229	Quarry	Sloping	x	From northeast, relatively strong but varying
20220104	Quarry	Sloping		Poor data quality. Weak easterly, increasing in afternoon
20220108	Quarry	Vertical	x	Very strong but decreasing in afternoon. Reduced vert. res.
20220502	Quarry	Sloping	x	Weak easterly and strong increase in late morning
20220515	Quarry	Sloping		Poor data quality. Strong wind except late morning
20220516	Quarry	Both	x	Strong but decreasing southeasterly
20220517	Quarry	Vertical	x	Moderate and then strongly increasing southeasterly
20220527	Quarry	Sloping	x	Weak northerly, increasing in evening
20220607	Quarry	Sloping		Relatively poor data quality. Strong but decreasing southeast
20220823				Lidar not deployed
20221106	Mast	Vertical	x	Moderate and varying wind from east
20221201	Mast	Vertical		Poor data quality. Strong southerly wind
20230308	Quarry	Vertical	x	Moderate wind from south
20230312	Quarry	Vertical	x	Weak and moderate northeasterly
20230328	Quarry	Vertical	x	Moderate and increasing easterly
20230516				Lidar not deployed

Complications with the physical and technical setup of the lidar until 2 February 2022 introduced increased data loss and complications with regard to the interpretation of the data. Furthermore, the vertical scans are in practice easier to interpret as measurements along the sloping scans will in some instances include a contribution from large scale wind direction changes. Definition of height levels is given in *Table 3-4*.

The following summaries in short the available lidar observations of the turbulence conditions for the dates in Table 5-3 and presented in Figure 5-4 - Figure 5-14 (also stated are location of lidar and beam direction).

- 30 April 2021 (mast/sloping): The first flight at the time of lidar operation at the mast was in the late afternoon, when the lidar measured relatively weak and homogenous atmospheric turbulence. There was relatively little variation in the turbulence along the sloping lidar beam.
- 22 December 2021 (quarry/sloping): The lidar is immediately downstream of the mountains and indicates relatively strong turbulence levels on 22. December and a peak in the early morning. The

reason is not clear but high-resolution simulated wind data indicates large spatial variability in the regional wind field and lee side accelerated flow, often associated with strong turbulence.

- 29 December 2021 (quarry/sloping): Turbulence levels appear relatively high, but lower than on the 22., during relatively strong large-scale northeasterly flow which is mostly oriented along the mountain ridge.
- 8 January 2022 (quarry/vertical): The lidar was scanning vertical on 8. January but with an increased vertical resolution and reduced max range (500 m). Turbulence is stronger in the morning and increasing with height, during very strong easterly flow aloft, but gradually weakens throughout day as winds get weaker.
- 2 May 2022 (quarry/sloping): Turbulence levels started low and increased in early morning, in relation to increasing southeasterly winds. High-resolution simulated wind data indicates large spatial variability in the wind field above the mountain slopes near the lidar (quarry/sloping) which is located immediately downstream of the mountains.
- 15 May 2022 (quarry/sloping): Turbulence levels started high, but quality is poor. Strong southeasterly and presumably large spatial variability over mountain slopes.
- 16 May 2022 (quarry/sloping and quarry/vertical): Turbulence levels started high when the beam was in a sloping orientation but decrease with weakening wind. Increasing in strength again in early evening, with a vertically oriented beam and a considerable vertical gradient. Strong southeasterly and large spatial variability in simulated wind over mountain slopes, with lidar immediately downstream of the mountain.
- 17 May 2022 (quarry/vertical): High and varying turbulence levels with lidar located downstream of mountain ridge. Strong easterly wind and large spatial variability in simulated wind over mountain slopes. This case is discussed in slightly more detail in the following subsection.
- 27 May 2022 (quarry/vertical): Weak but increasing turbulence levels. Relatively weak northerly winds near surface, but likely strong forward shear. Possible thermal effects.
- 6 November 2022 (mast/vertical). Moderate or weak turbulence levels, during moderate easterly flow. Large spatial variability with stronger winds at mountains.
- 1 December 2022 (mast/vertical). Poor data quality, presumably due to precipitation during strong southerly flow.
- 8 March 2023 (quarry/vertical). Weak turbulence in morning but stronger during afternoon with considerable vertical gradient, and weakening again in evening. Moderate northeasterly winds oriented along the mountain ridge but indications of large variability in the wind field.
- 12 March 2023 (quarry/vertical). As for 8 March above.
- 28 March 2023 (quarry/vertical). At times large turbulence levels and varying. Strong easterly flow, with lidar immediately downstream of mountain ridge.

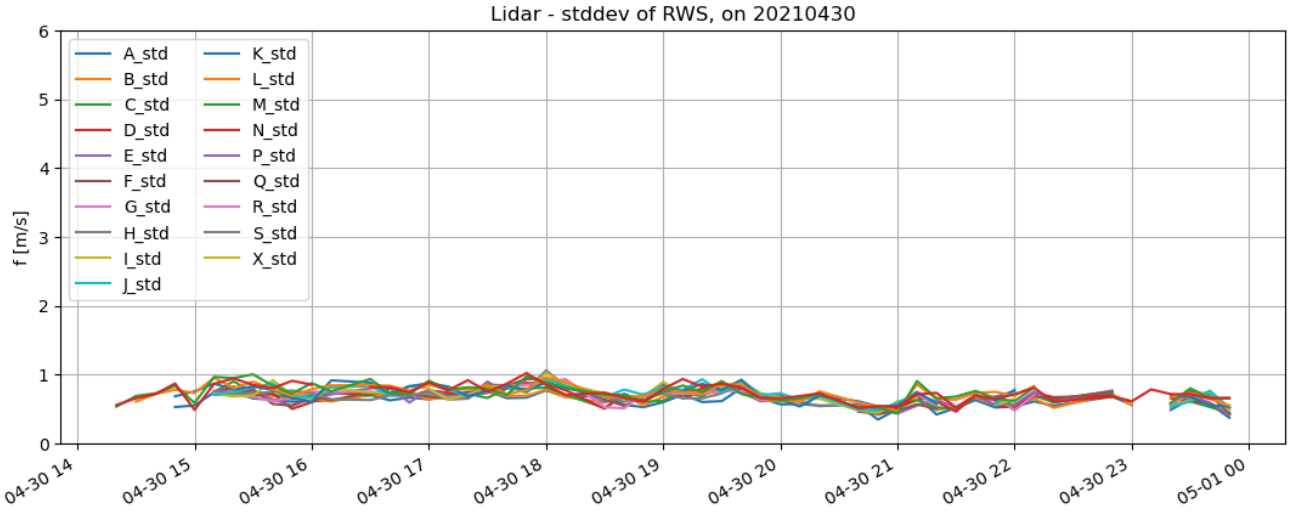

Figure 5-5 Timeseries of the standard deviation of the radial wind speed from the lidar. Lidar located at mast and in sloping LOS-mode. Height levels are indicated by letters A-Z, with reference to Table 3-4.

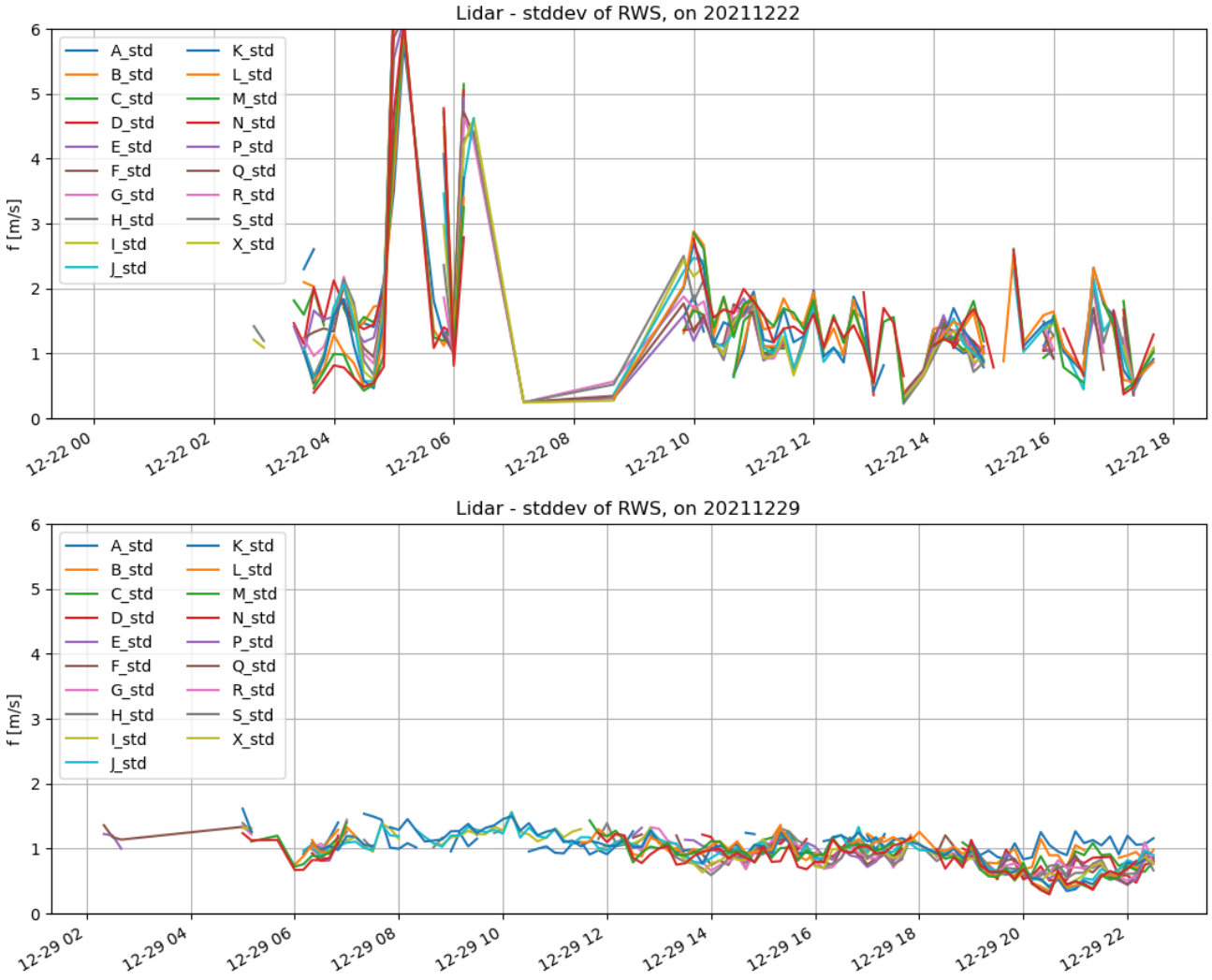

Figure 5-6 Timeseries of the standard deviation of the radial wind speed from the lidar. Lidar located at quarry and in sloping LOS mode. Height levels are indicated by letters A-Z, with reference to Table 3-4.

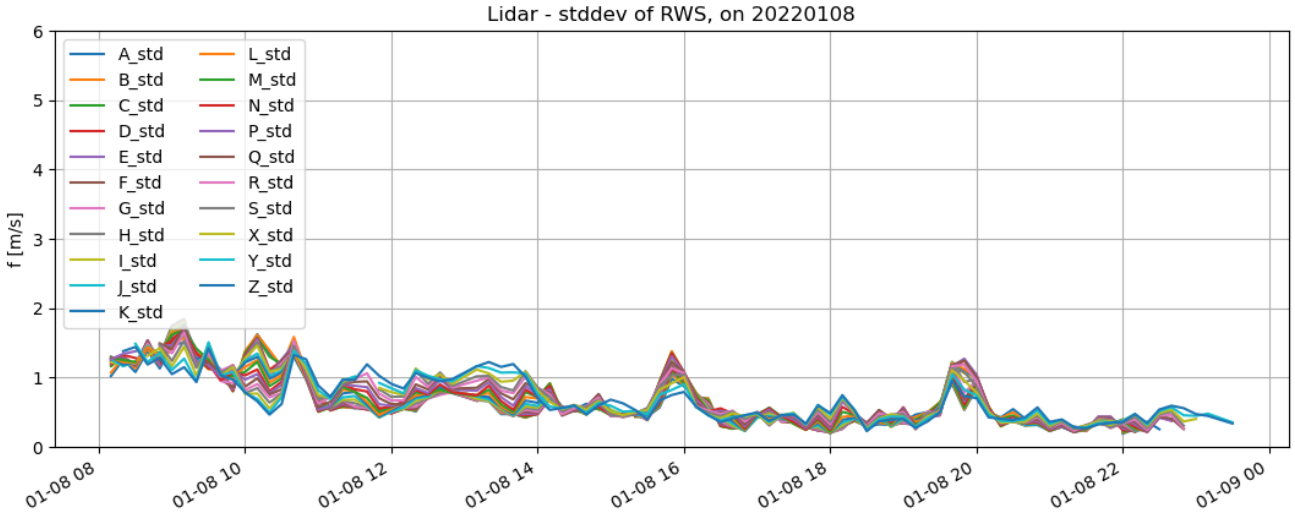

Figure 5-7 Timeseries of the standard deviation of the radial wind speed from the lidar. Lidar located at quarry and in vertical LOS mode, but with an increased vertical resolution and reduced maximum range (500 m). Height levels are indicated by letters A-Z, with reference to Table 3-4.

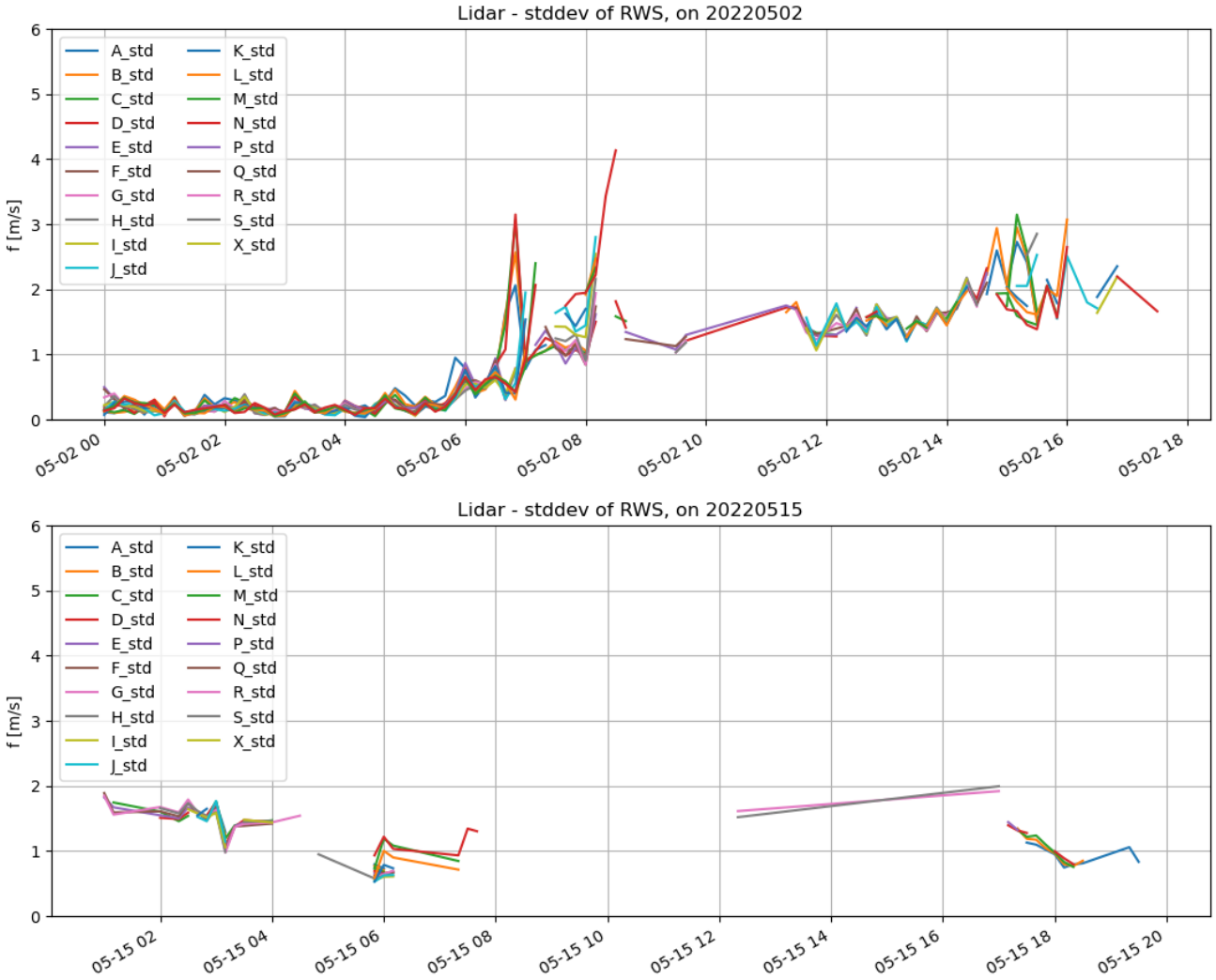

Figure 5-8 Timeseries of the standard deviation of the radial wind speed from the lidar. Lidar located at quarry and in sloping LOS mode. Height levels are indicated by letters A-Z, with reference to Table 3-4.

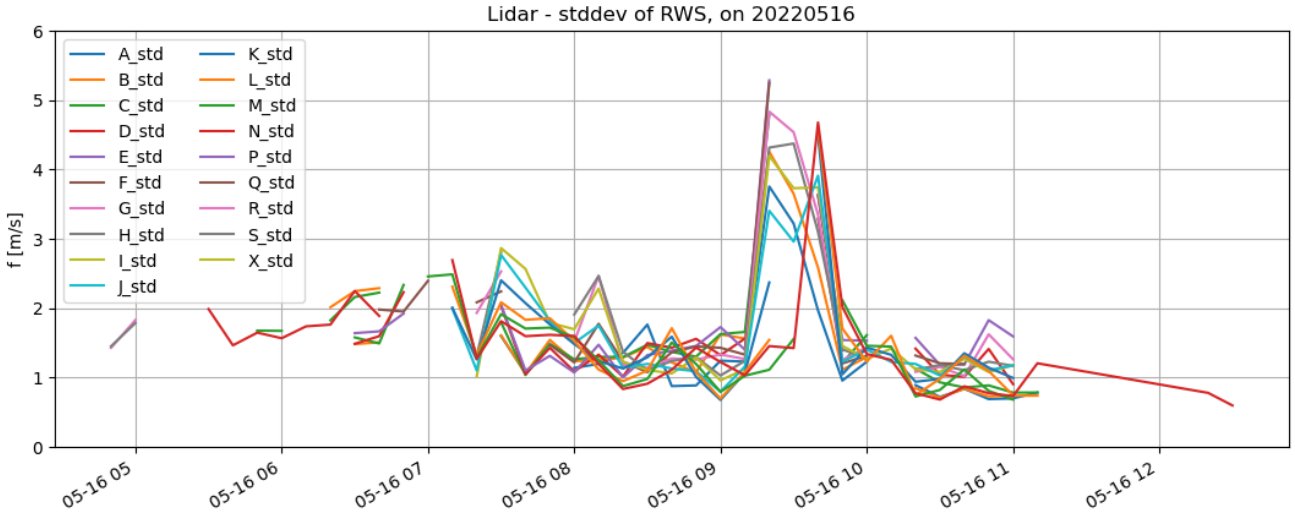

Figure 5-9 Timeseries of the standard deviation of the radial wind speed from the lidar. Lidar located at quarry and in sloping LOS mode. Height levels are indicated by letters A-Z, with reference to Table 3-4.

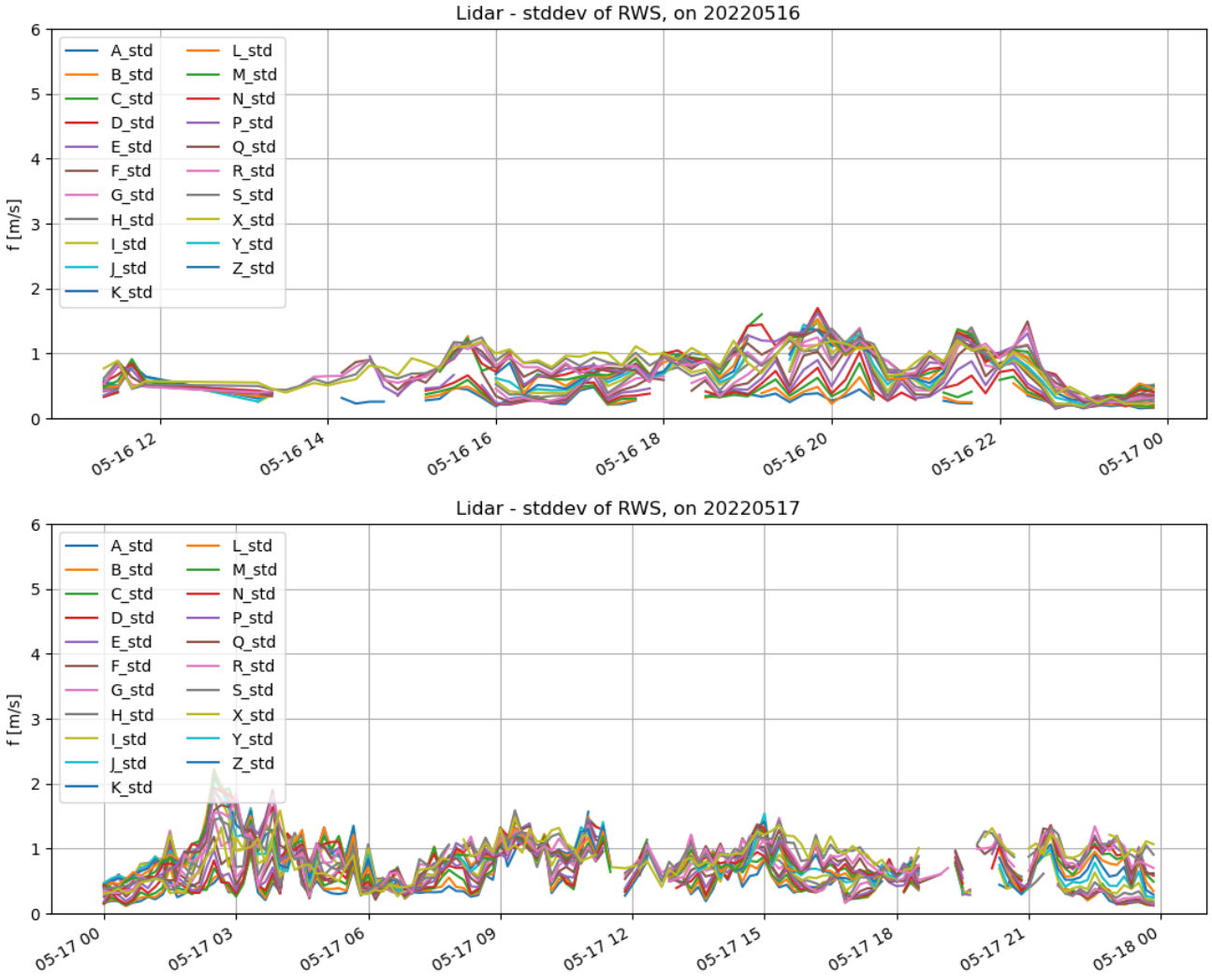

Figure 5-10 Timeseries of the standard deviation of the radial wind speed from the lidar. Lidar located at quarry and in vertical LOS mode. Height levels are indicated by letters A-Z, with reference to Table 3-4.

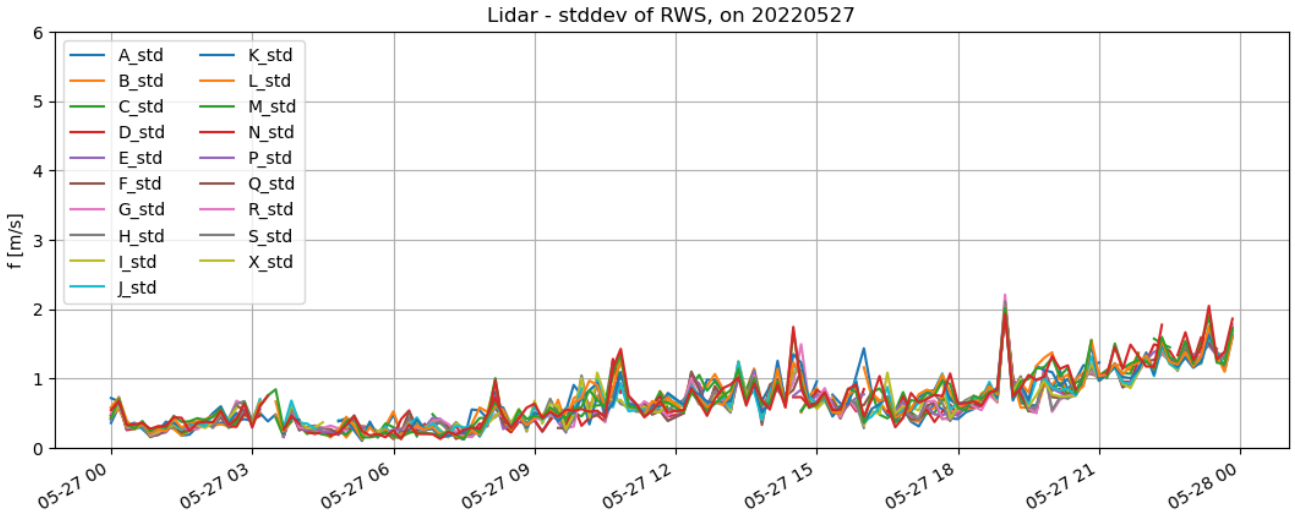

Figure 5-11 Timeseries of the standard deviation of the radial wind speed from the lidar. Lidar located at quarry and in sloping LOS mode. Height levels are indicated by letters A-Z, with reference to Table 3-4.

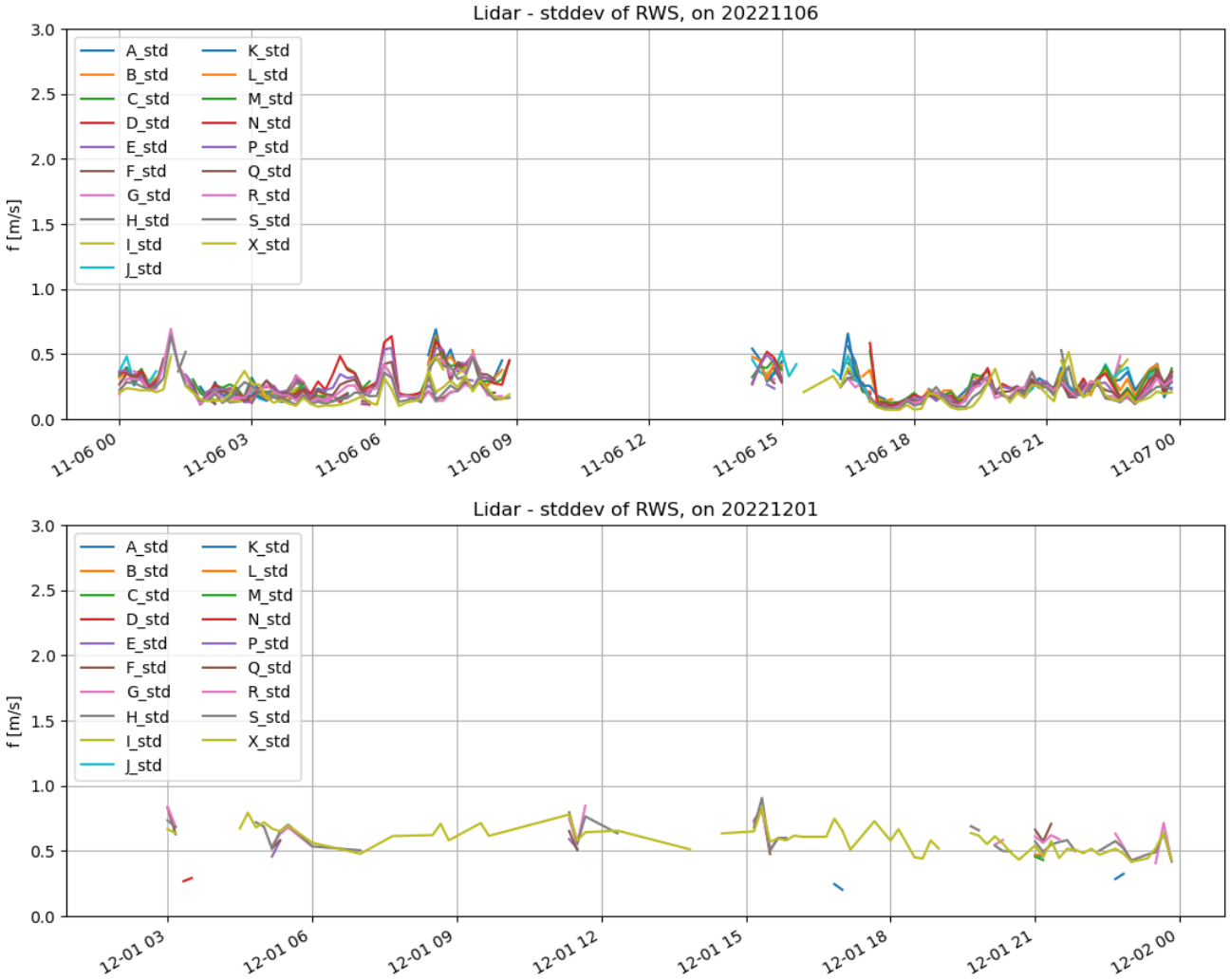

Figure 5-12 Timeseries of the standard deviation of the radial wind speed from the lidar. Lidar located at mast and in vertical LOS mode. Height levels are indicated by letters A-Z, with reference to Table 3-4.

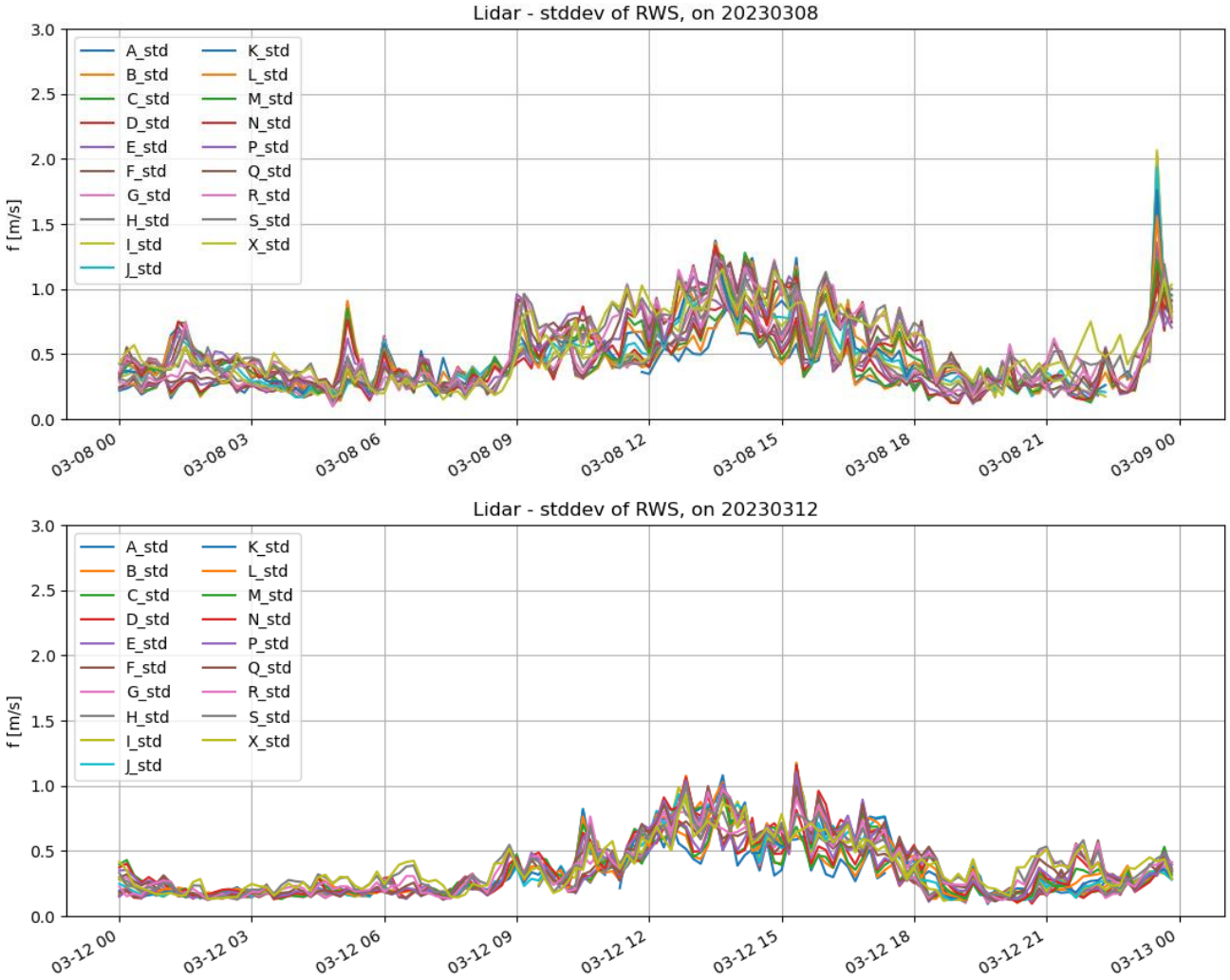

Figure 5-13 Timeseries of the standard deviation of the radial wind speed from the lidar. Lidar located at quarry and in vertical LOS mode. Height levels are indicated by letters A-Z, with reference to Table 3-4.

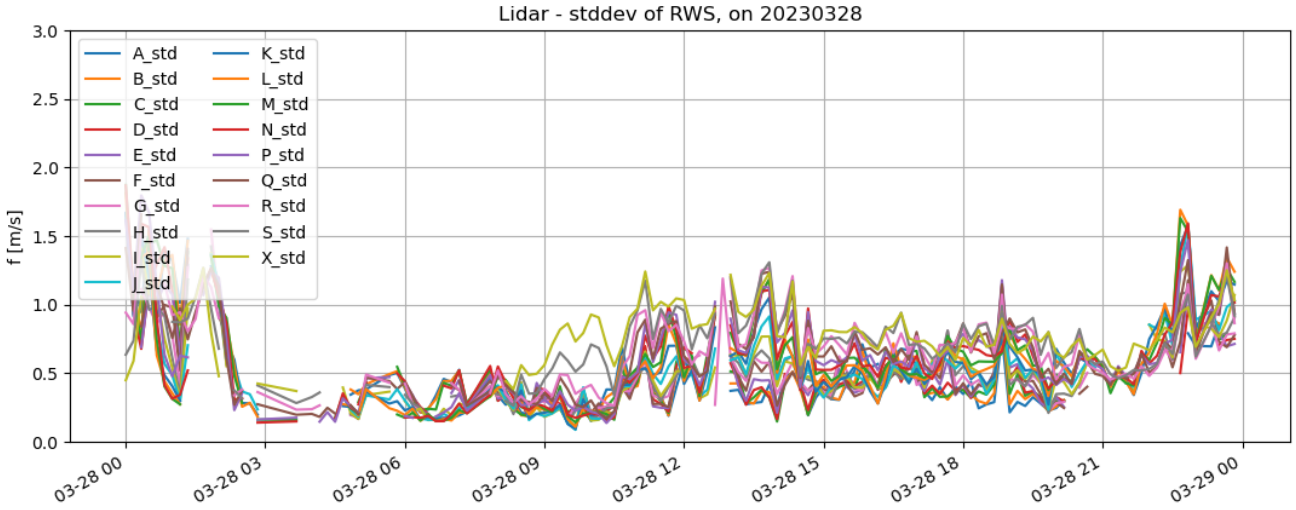

Figure 5-14 *Timeseries of the standard deviation of the radial wind speed from the lidar. Lidar located at quarry and in vertical LOS mode. Height levels are indicated by letters A-Z, with reference to Table 3-4*.

5.4 Lidar and mast measurements on 17 May 2022

Measurements on the 17 May 2022 are discussed in more detail here, in an attempt to relate the lidar and mast measurements during this day. Test flights [5] were also performed on this day but are not discussed here.

The lidar was set in vertical mode and was located at the quarry location. As before, flow conditions aloft are described by simulated data at 350 m above ground level. The wind at the quarry location (Figure 5-15) was relatively strong from the east in the early night (~14 m/s) but decreasing with very weak wind in the late morning. In the afternoon there is a strong increase in wind speed with ~20 m/s aloft from the late afternoon. The simulated wind at 350 m above the mast is similar and only slightly weaker (not shown). These conditions are not well reflected by the 30 m observed wind in Hvassahraun, which has weak winds in the morning and slowly increasing to roughly 12 m/s in the evening. Assumes that the models are not too wrong then this indicates a large spatial variability and strong vertical shear in the region, as supported by surface wind speed forecasts from a different atmospheric model (Icelandic Met. Office, Figure 5-16).

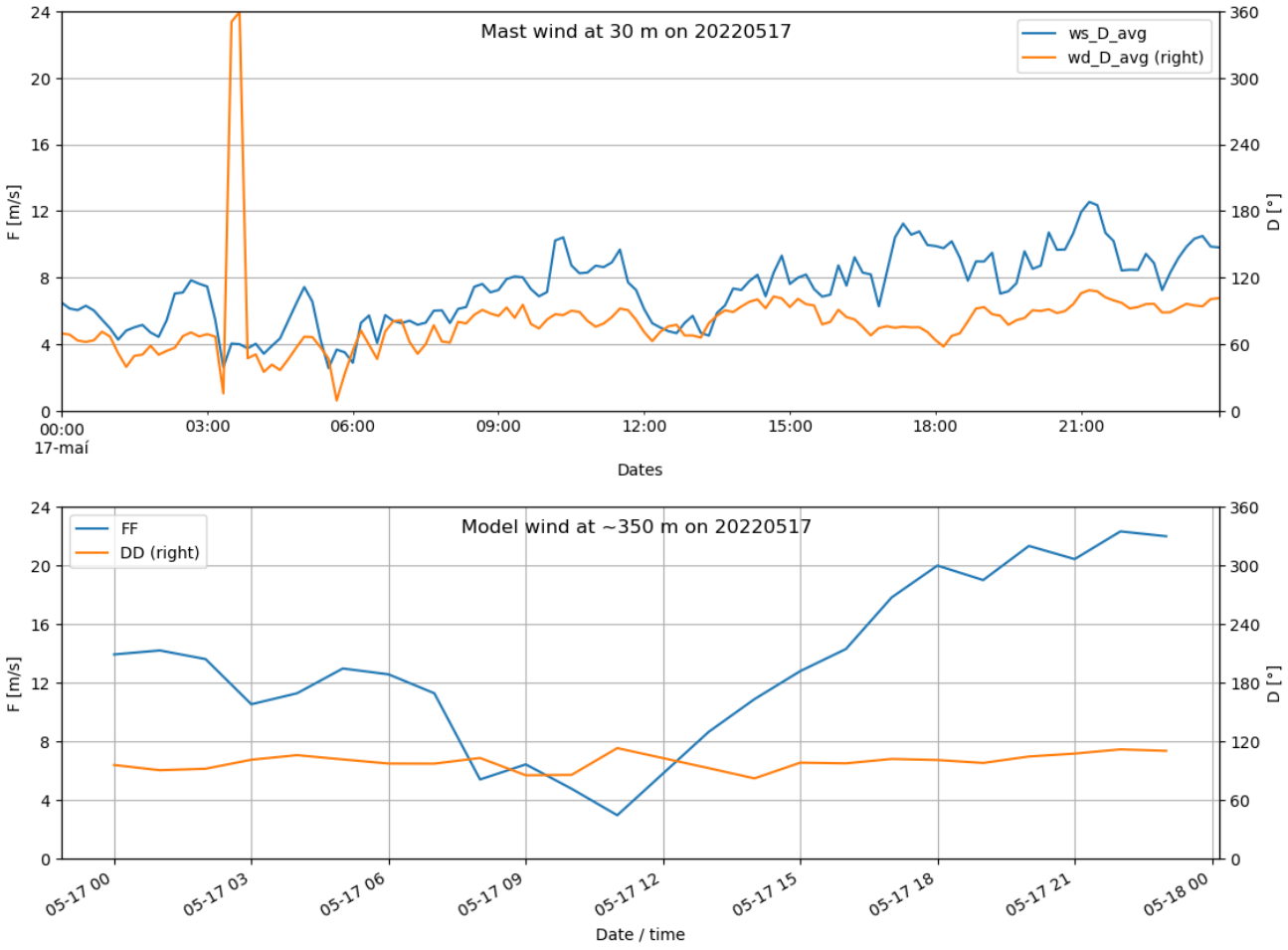

Figure 5-15 Observed wind at 30 m in mast at Hvassahraun (above) and simulated wind at 350 m at quarry location (below).

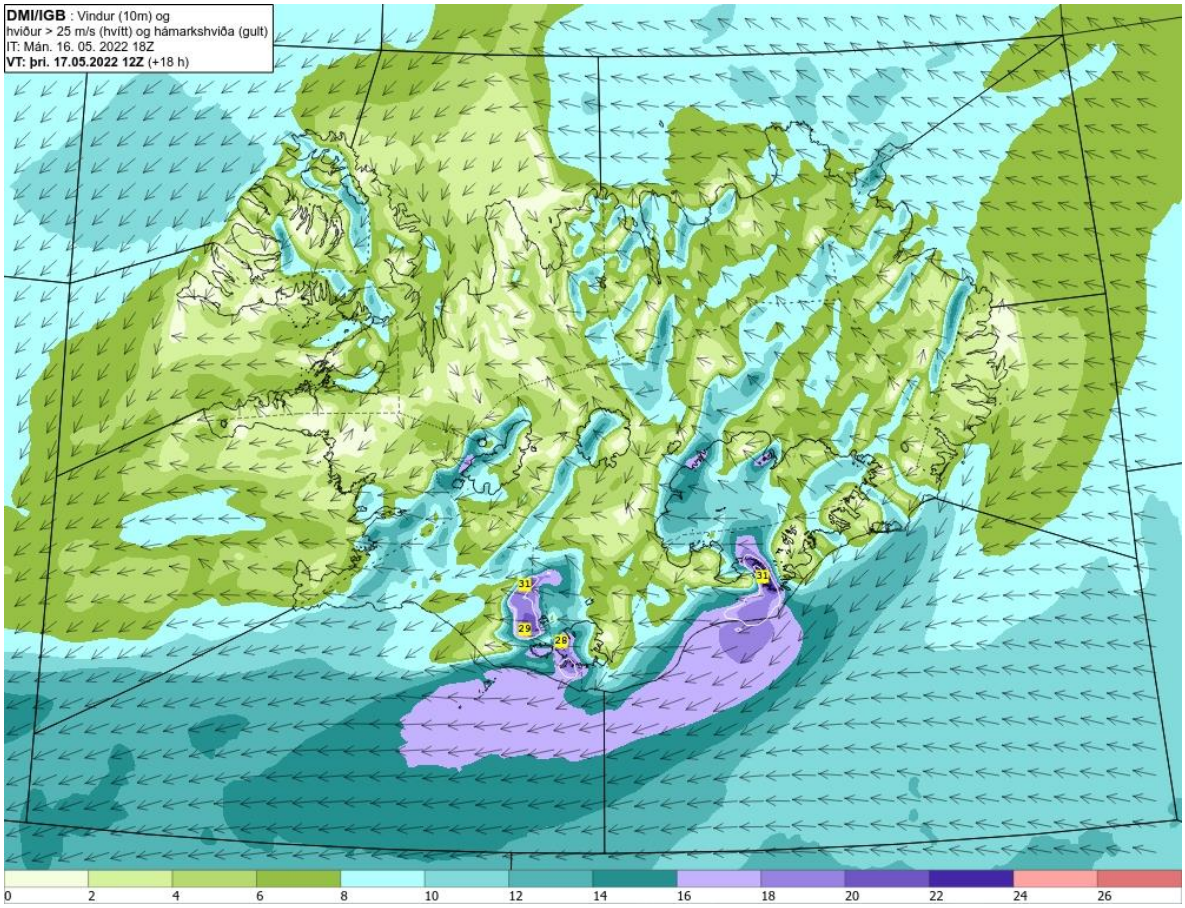

Figure 5-16 Simulated surface wind from the Icelandic Meteorological Office, valid at 18 UTC on 17 May 2022. Retrieved from “https://spakort.vedur.is/kort/spakort/”.

The standard deviations of the observed wind (turbulence kinetic energy) are shown for both and mast and lidar in *Figure 5-17*. Also shown is the eddy dissipation rate in the mast for the along-wind component, as calculated by the the Icelandic Met. Office. The largest values of the variation in the vertical wind speed from the lidar are seen in the early night and are strongest at roughly 400 m. This maximum is reflected in the horizontal components in the mast but only weakly in the vertical component. A comparison with the observed wind indicates that this peak is related to a short period of directional shear at the mast (wind becomes northerly), which is not resolved by the simulated wind.

Relatively high levels are observed by the lidar for the rest of the day and are typically stronger below ~500 m than above. Except for the aforementioned peak, turbulence in the mast is in generally at a minimum during the night and at noon, while not particularly high, it is still considerable in the morning and afternoon. This is reflected in both the eddy dissipation rate as well as the standard deviation of all three wind components. We note that the at 30 m, the vertical and horizontal components of the observed turbulence (standard deviation) scale well with the eddy dissipation rate (factors of 1/3 and 1/8, respectively).

Overall, there is a clear correlation between the mast and lidar observations of the mast, both when considering the eddy dissipation rate and the turbulence kinetic energy. However, in this case the mast observations of wind appear not to reflect as well the observed conditions aloft as they do in many of the other

events. Lidar was not located at the mast in this event and there was presumably a large horizontal and vertical variability in the wind field on this day.

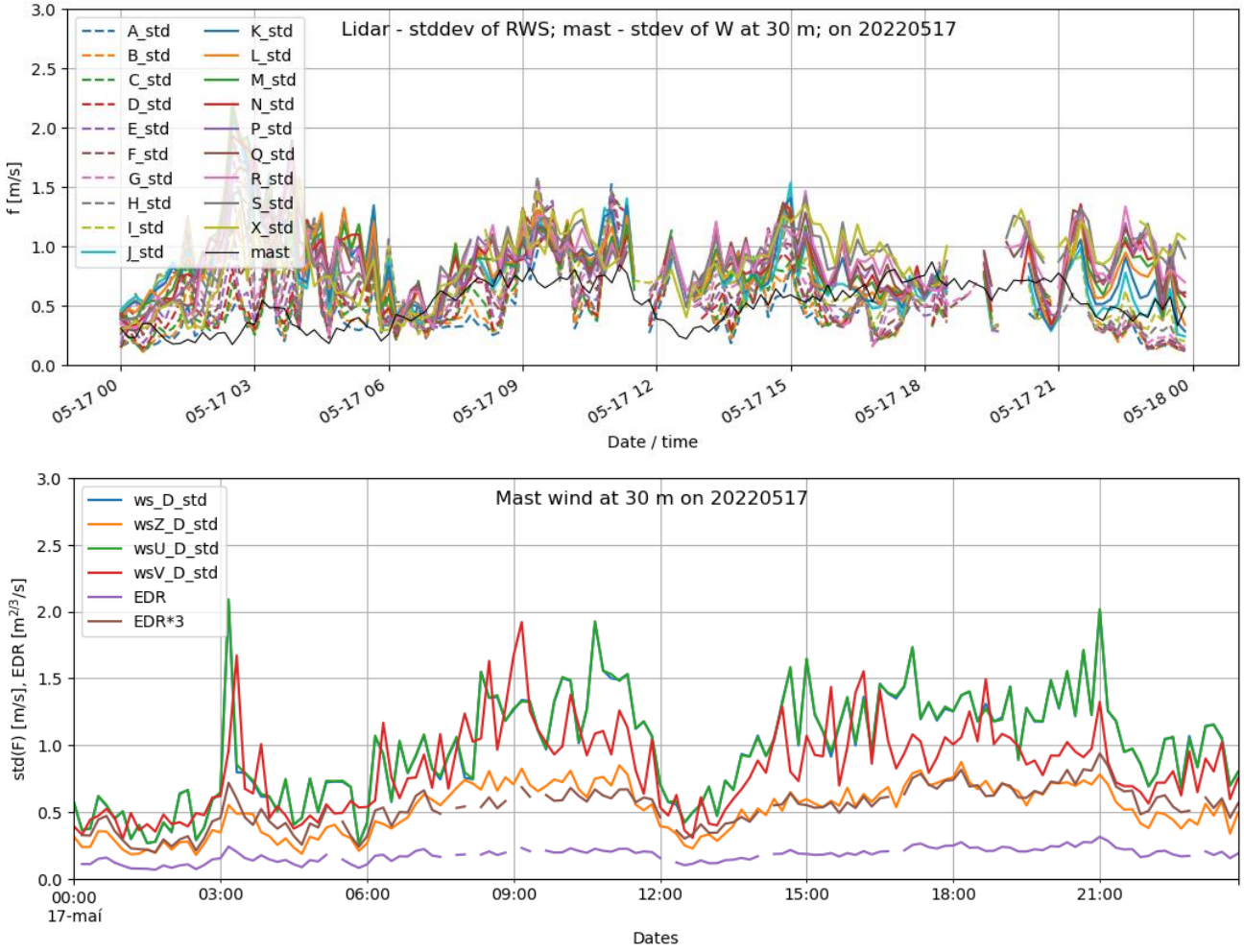

Figure 5-17 Above: Timeseries of the standard deviation of the radial wind speed from the lidar. Lidar located at quarry and in sloping LOS-mode. Height levels are indicated by letters A-Z, with reference to Table 3-4. Below: The eddy dissipation rate for along-wind component and standard deviation of observed wind at 30 m in mast (shown for full horizontal wind, as well as for the along-wind, across-wind and vertical components. Also shown is the eddy dissipation rate scaled by 3, for facilitating comparison with the standard deviation of the vertical wind component. Note that blue line is mostly covered by the green line, indicating that horizontal wind turbulence is on average the same as the along-wind turbulence.

5.5 Lidar measurements during strong wind events

Orographically induced turbulence of relevance for aviation is typically associated with relatively strong wind. Other factors are also important in this aspect and may be conclusive to whether strong turbulence is generated or not. However, these are not considered here; but include for example wind shear, atmospheric

stability, terrain height and shape, as well as surface roughness. Below are examples of lidar observations collected during storm situations.

Simulated wind data at roughly 350 m above the mast and quarry locations have been used to identify days with wind speed of at least 20 m/s during the period of lidar observations. The simulated data aloft is on average a good indicator of the larger scale flow, as previously validated by comparison with observed data (not shown). Mast data is also consulted but not used in choosing the events as there are indications in the observed data that strong flow aloft may in some cases be separated from the observed surface flow. Only the period of observations with a vertical lidar beam have been considered here, as the measurements with a sloping beam are more challenging to interpret in this context. Note that the number of lidar heights with available data varies in the data shown, which must be accounted for in the interpretation.

The following summaries the lidar-based observations of turbulence, i.e. standard deviations of the vertical radial wind speed presented in *Figure 5-18 -Figure 5-23*, for a subset of the days of strong wind (also stated is the lidar location). Figures for timeseries of simulated and observed wind are given in Appendix B.

- 17 May 2022 (quarry): Increasing southeasterly and easterly wind at mast but not particularly strong. Close to 20 m/s from east at quarry from late afternoon. Turbulent throughout day at quarry and average strongest at lower lidar levels. A measurement flight was performed on this day. Mast turbulence is poorly correlated with lidar in the morning but better correlation in afternoon.
- 14 November 2022 (mast): Varying direction at mast but southeasterly during strong wind in late morning. Turbulence levels correlated with observed wind and turbulence, similar or increasing with height in the lowest few hundred metres. Data availability poor during strongest wind.
- 16 November 2022 (mast): Mostly as for 14 November but strong from east after noon. Peaks in observed turbulence which are poorly correlated with observed wind and turbulence in mast.
- 19 November 2022 (mast): Mostly as for 14 November but strong from southeast in late morning and afternoon. Relatively poor data availability. Clear correlation of turbulence aloft with observed wind and turbulence in mast.
- 22 November 2022 (mast): Strongest wind in the late night, from southeast but weakening and veering to east. Clear correlation of turbulence levels with mast wind and turbulence, similar or increasing with height in the lowest few hundred metres. Data availability poor during strongest wind.
- 23 November 2022 (mast): Very strong from southeast and east aloft in late morning and afternoon. A slight increase in observed TI but not for wind speed. High turbulence levels in lidar, in particular away from the surface. Relatively poor correlation with mast wind and turbulence.
- 25 January 2023 (quarry): Strong but decreasing from west until late morning and increasing and strong from south in afternoon. Relatively poor data availability but stronger turbulence in mast than at lower levels from lidar during westerly flow but considerably lower in mast than from lidar during southerly flow in afternoon.
- 9 February 2023 (quarry): Quite similar to 25 January but more southeasterly in afternoon. Lidar turbulence in afternoon at times far higher than in mast.
- 7 March 2023 (quarry): Strong from northeast during most of day. Poor correlation between lidar turbulence and mast, presumably due two difference in locations.
- 20 March 2023 (quarry): Strong but varying from east aloft, weaker and from east-northeast in mast. Lidar turbulence mostly larger than from mast and poor correlation (different locations).
- 21 March 2023 (quarry): Wind conditions stronger but otherwise similar to 20 March. Stronger turbulence in mast than in lidar, and poor correlation (different locations).
- 22 March 2023 (quarry): Wind conditions stronger, decreasing in late afternoon, but otherwise similar to 20 March. Somewhat better correlation in turbulence levels from lidar and mast, than for 20 and 21 March.

- 28 March 2023 (quarry): Similar to 20 – 22 March but not as strong. Correlation in turbulence levels from lidar and mast.
- 30 March 2023 (quarry): Strong easterly aloft but decreasing in morning. Relatively weak wind in mast. Far stronger turbulence in lowest 500 m in lidar than from mast or further aloft. Relatively poor correlation between mast and lidar.
- 4 May 2023 (quarry): Weak from east in morning but increasing from southeast in afternoon. Poor correlation between mast and lidar in afternoon with far stronger turbulence in lidar.

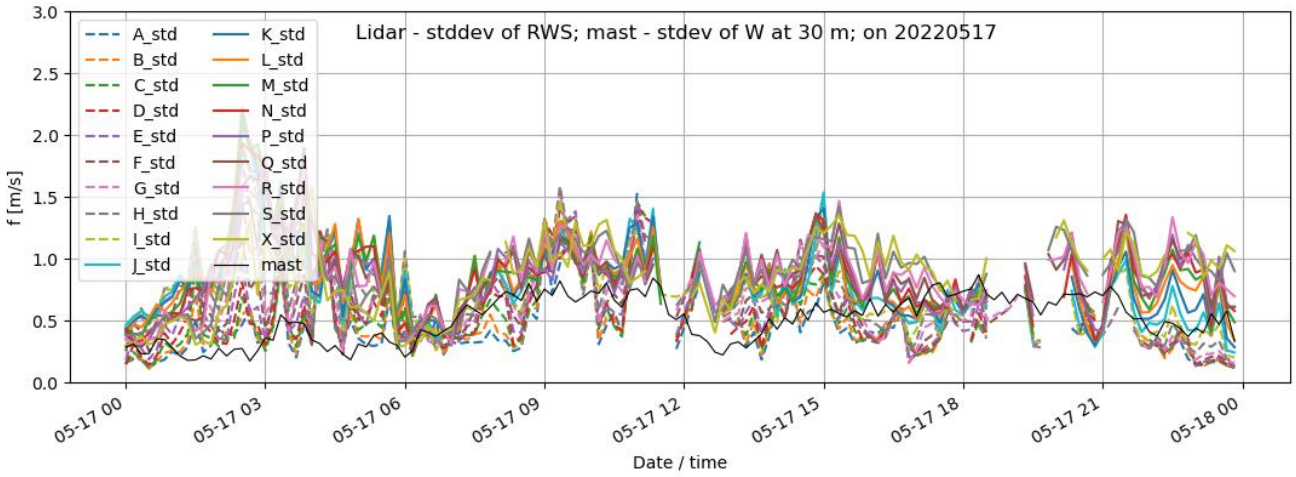

Figure 5-18 Timeseries of the standard deviation of the radial wind speed from the lidar and vertical wind at top of mast. Lidar located at quarry and in vertical LOS mode. Height levels are indicated by letters A-Z, with reference to Table 3-4.

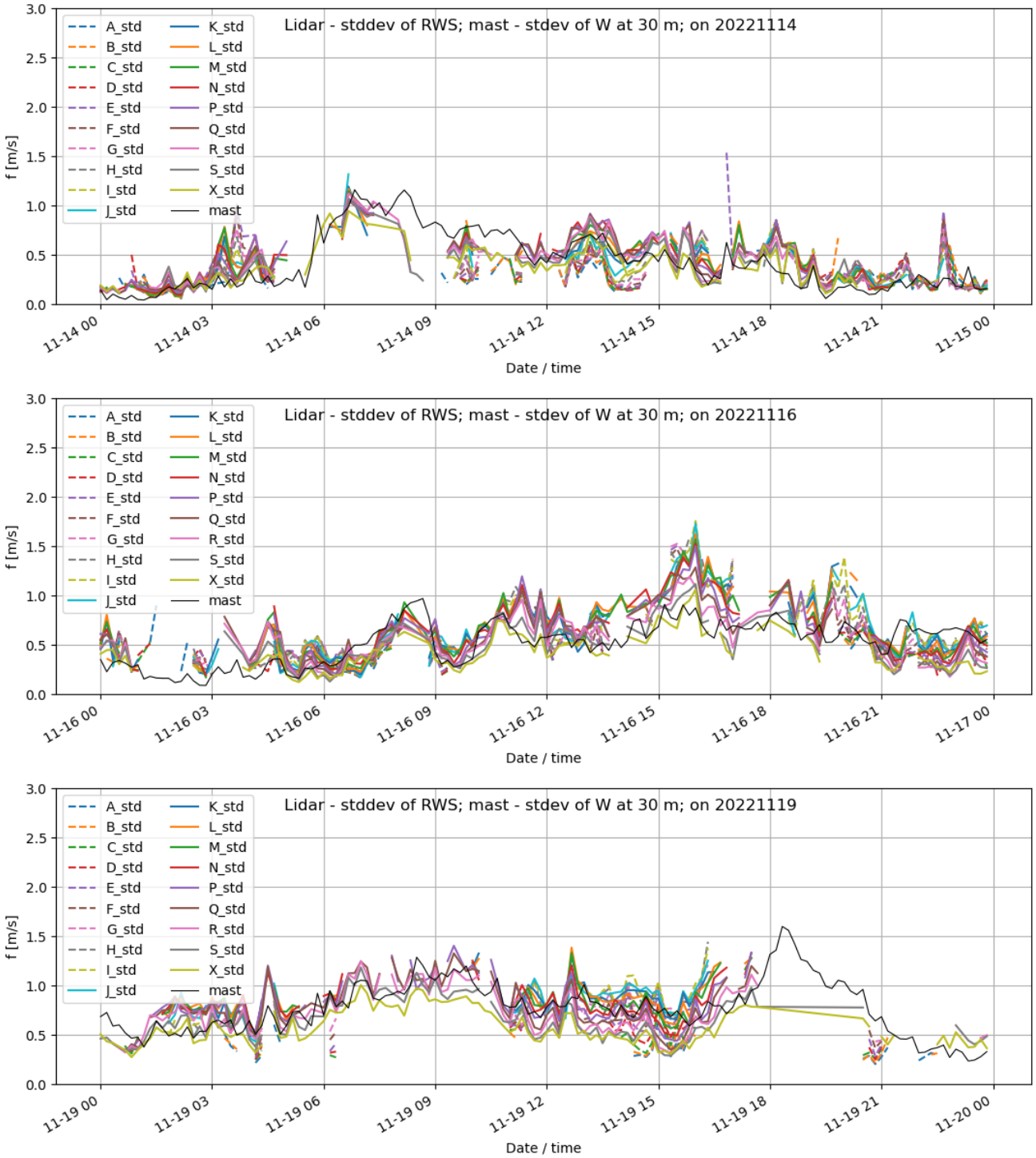

Figure 5-19 Timeseries of the standard deviation of the radial wind speed from the lidar and vertical wind at top of mast. Lidar located at mast and in vertical LOS mode. Height levels are indicated by letters A-Z, with reference to Table 3-4.

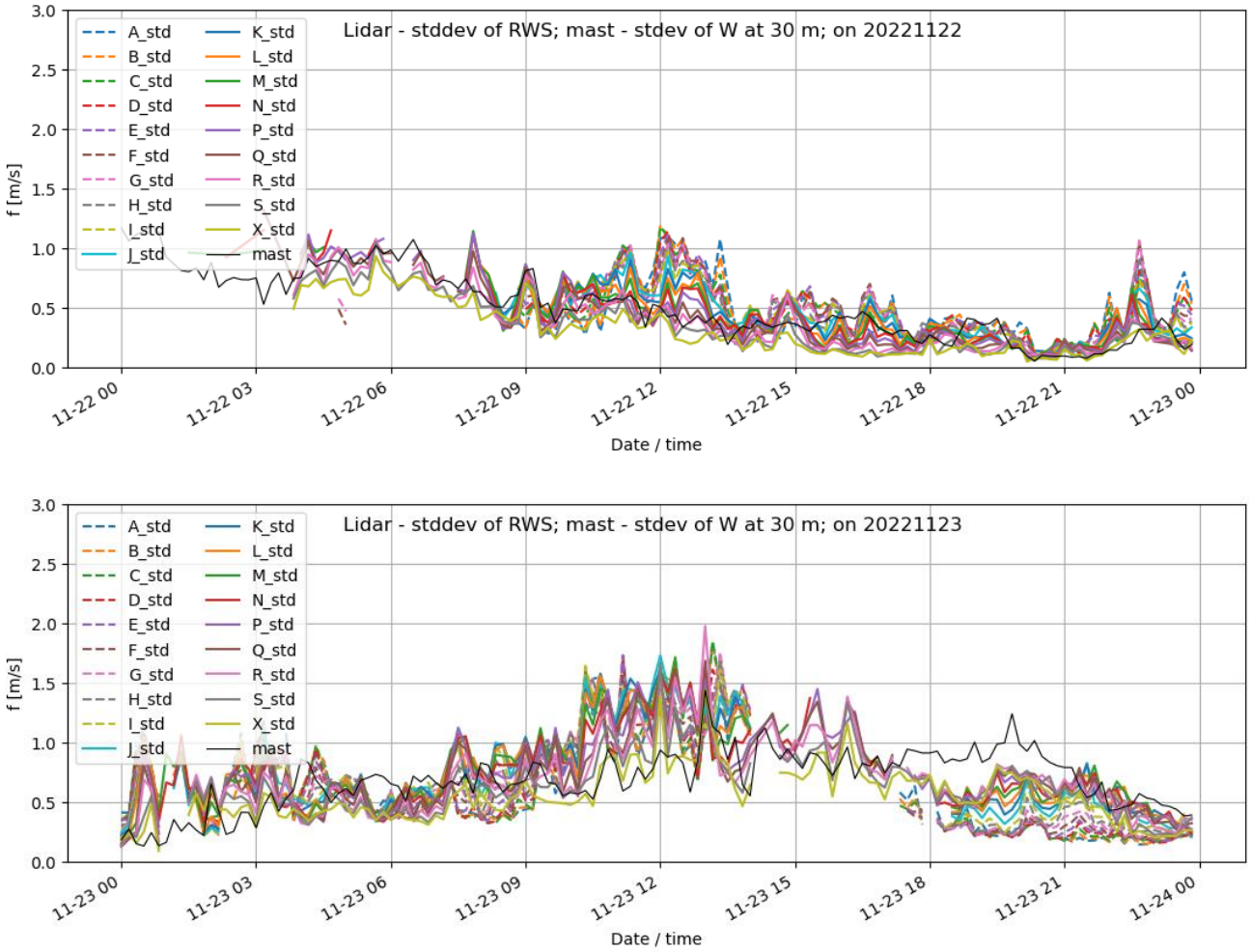

Figure 5-20 Timeseries of the standard deviation of the radial wind speed from the lidar and vertical wind at top of mast. Lidar located at mast and in vertical LOS mode. Height levels are indicated by letters A-Z, with reference to Table 3-4.

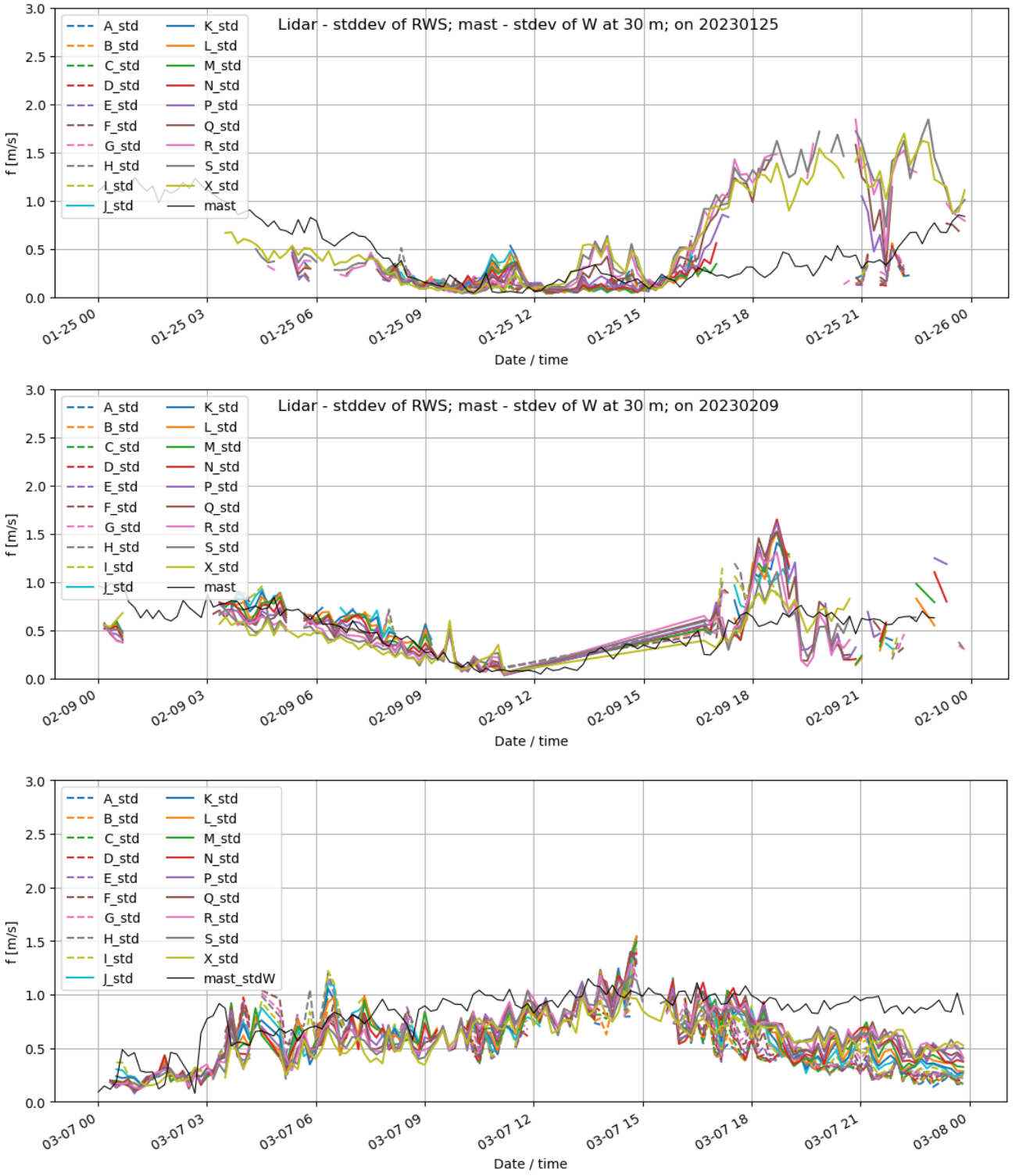

Figure 5-21 Timeseries of the standard deviation of the radial wind speed from the lidar and vertical wind at top of mast. Lidar located at quarry and in vertical LOS mode. Height levels are indicated by letters A-Z, with reference to Table 3-4.

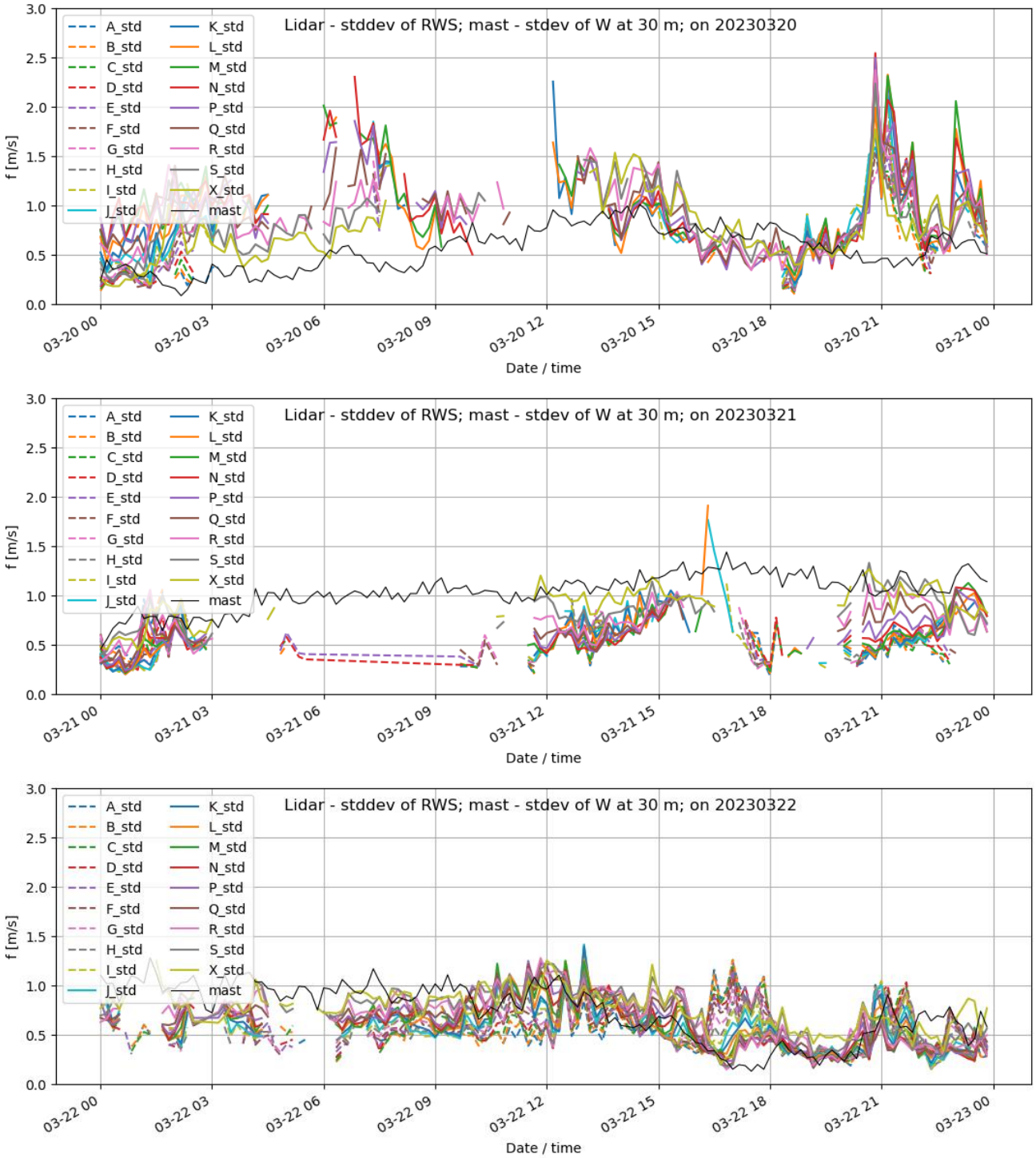

Figure 5-22 Timeseries of the standard deviation of the radial wind speed from the lidar and vertical wind at top of mast. Lidar located at quarry and in vertical LOS mode. Height levels are indicated by letters A-Z, with reference to Table 3-4.

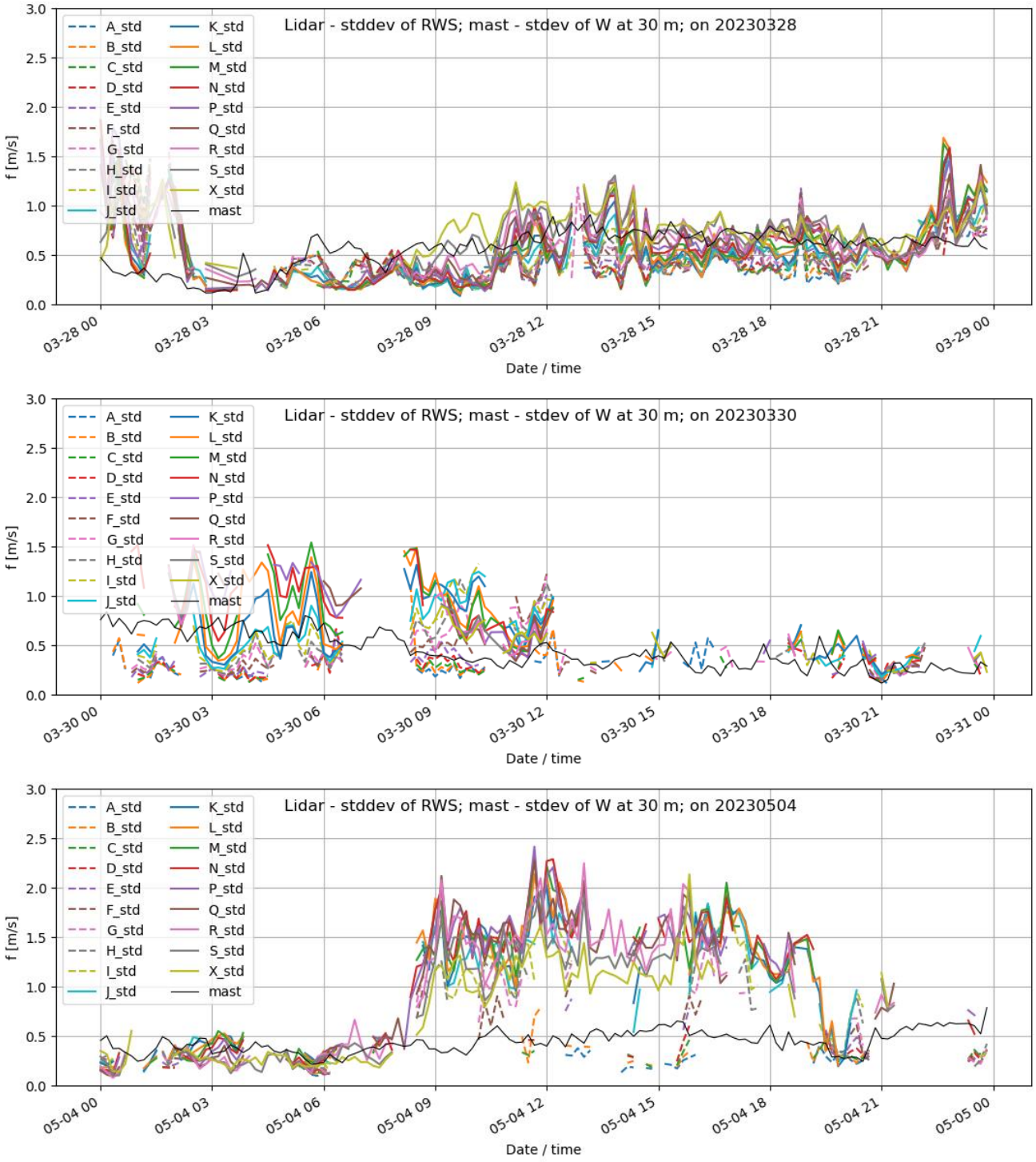

Figure 5-23 Timeseries of the standard deviation of the radial wind speed from the lidar and vertical wind at top of mast. Lidar located at quarry and in vertical LOS mode. Height levels are indicated by letters A-Z, with reference to Table 3-4.

5.6 Lidar measurements for different flow types

In order to assess the impact of upstream orography and wind direction on turbulence aloft, the lidar measurements are binned with regard to wind speed and direction. The binning is done for chosen wind speed intervals as well as specific sectors, but an overview is also given for all wind speeds and 8 standard wind speed sectors with a width of 45° (Appendix C). The results are presented as quantile, i.e. data are sorted in order of increasing size, showing the range from the median up to the 0.999 quantile (99.9 % percentile). Data shown are the lidar derived observations of turbulence, i.e. the standard deviation of the radial wind speed, as well as the standard deviation of the vertical wind component in the top sensor at 30 m in the mast.

Simulated wind speed and direction data at roughly 350 m above the mast locations have been used in the binning. We opt to use the simulated wind as it better represents the flow aloft than the mast observations, but similar results are found based on mast data. Only the period of observations with a vertical lidar beam have been considered here, as the measurements with a sloping beam are more challenging to interpret in this context. To increase the amount of data, data from both lidar sites must be used. Note that we require that concurrent data are available at all lidar heights and for mast top sensor for data shown in the figures below. Otherwise, the results would be skewed as the lidar data availability is greater at low levels than further aloft.

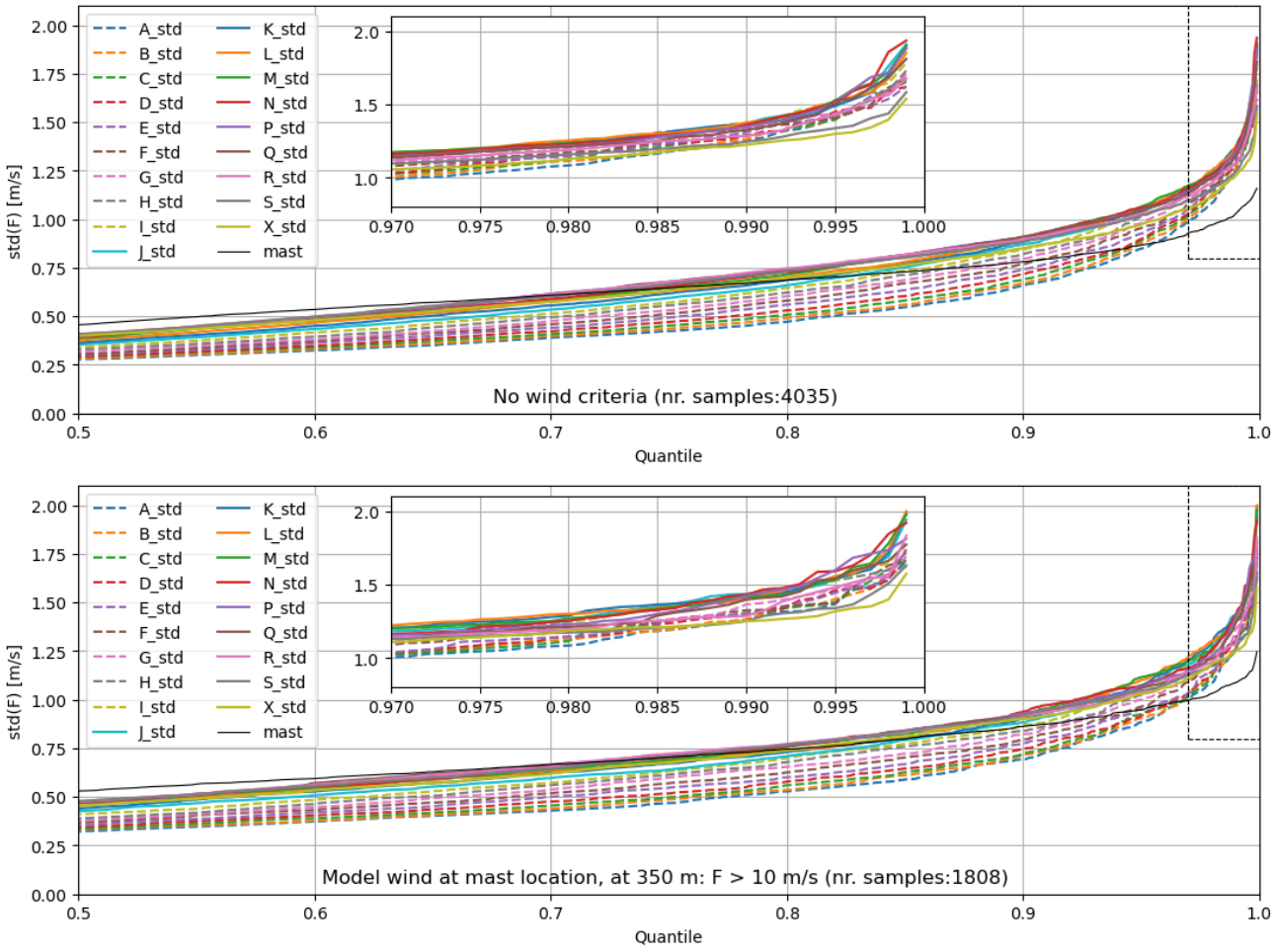

Figure 5-24 Quantile plots of the standard deviation of the radial wind speed from the lidar and vertical wind in top of mast. Above: No wind speed criteria, below: wind speed aloft greater than 10 m/s.

Figure 5-24 shows concurrent data from all lidar levels, i.e. from the surface and up to 1000 m agl, as well as from the mast. The form of the quantile plot is typical for atmospheric turbulence (see e.g. [1]), i.e. the bulk of the wind data have low turbulence levels and there is an approximately linear increase in intensity towards higher quantiles. For roughly the highest 10 % of the data, the increase is faster and non-linear.

As expected, mast values are higher than the lidar values for weak turbulence, while for the high quantiles the lidar values are higher. Presumably because the proximity to the surface limits the extent of vertical movements of the air more strongly than further aloft. Lidar values are on average higher below ~500 m agl and decrease with height above. However, the difference in turbulence values between the lidar levels is smaller at the highest quantiles than for weaker turbulence. A comparison of the two panels in Figure 5-24 confirms that the turbulence on average increases with stronger wind speed.

Due to the considerable reduction in lidar data availability with height, only the lowermost levels are considered when binning the data in more detail with regard to wind direction. This reduces the noise in the data as some of the wind speed sectors are poorly populated, in particular at wind speeds over 10 m/s.

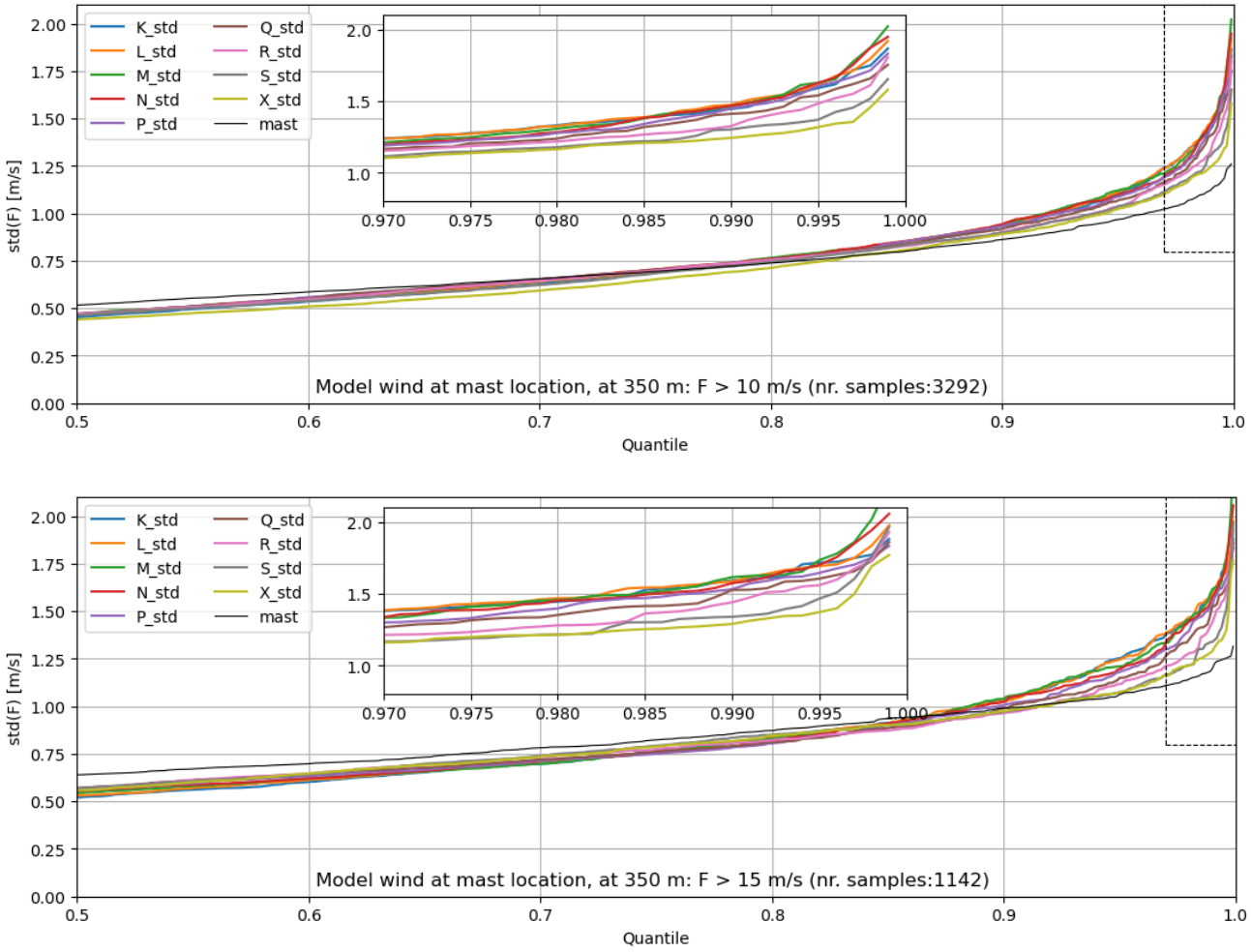

Figure 5-25 Quantile plots of the standard deviation of the radial wind speed from the lidar turbulence and vertical wind in top of mast. Wind speed aloft greater than 10 m/s (above) and 15 m/s (below).

Figure 5-25 can be compared to Figure 5-24, confirming the increase in turbulence strength with the wind speed. The turbulence increases with wind speed at all lidar levels in Figure 5-25 for the highest quantile, and the same is true for levels above 500 m agl. However, the amount of available data is halved and results not as smooth as for data below 500 m.

Wind speeds stronger than 10 m/s and for two sectors are presented in Figure 5-26. For wind from southwest and west, i.e. 225°-315°) there are a very limited number of observations but similar results are found for a slightly larger subset of the data using no wind speed criteria (see Appendix C). Lidar derived turbulence values are weak, also for the high quantiles. The high value at the lowest lidar level may be influenced by noise. The overall low data availability in this sector indicates that general conclusions should not be made based on the current data. The high mast values are a result of the anemometer being in the mast shadow in this sector and must be discarded.

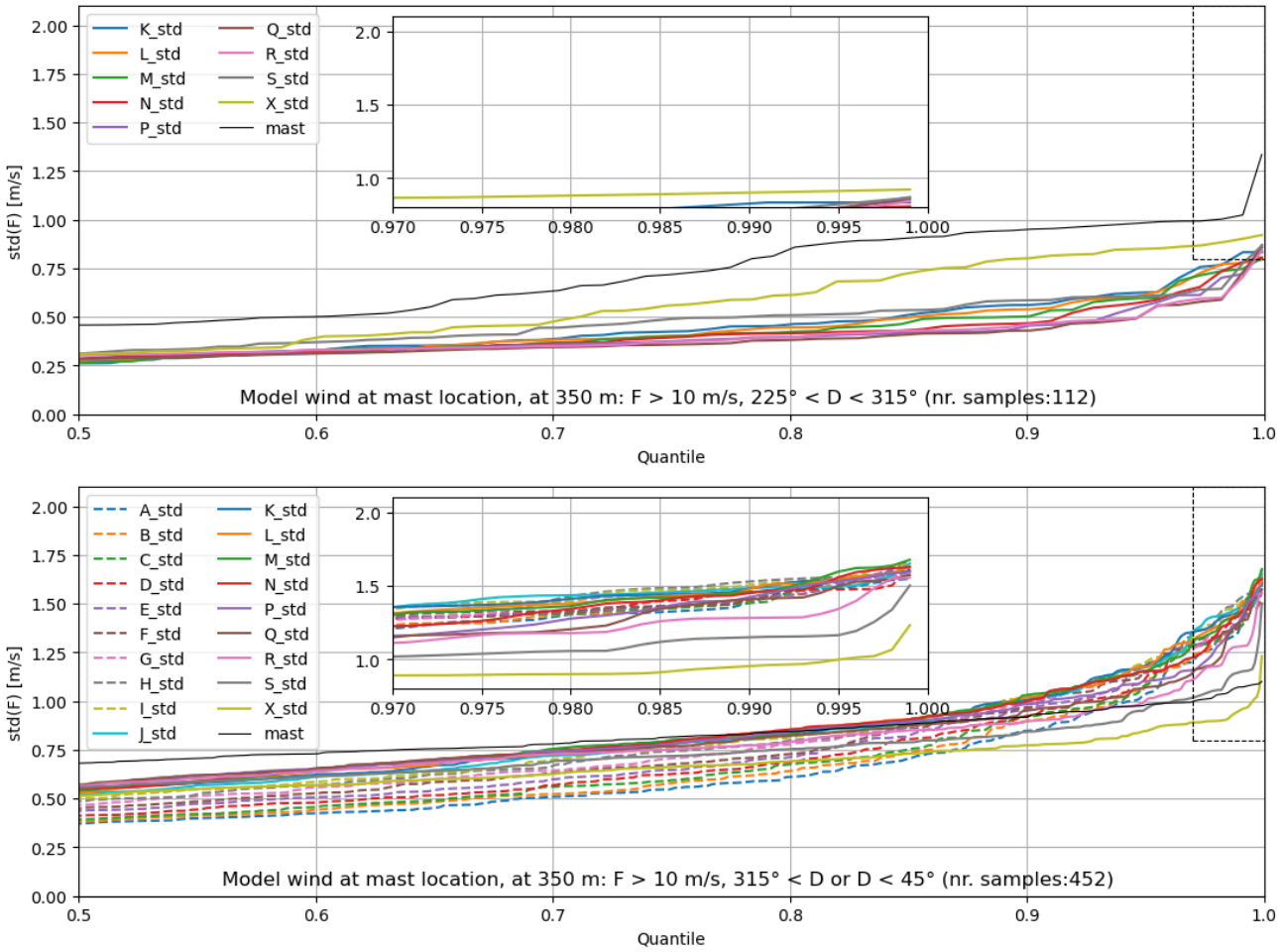

Figure 5-26 Quantile plots of the standard deviation of the radial wind speed from the lidar turbulence and vertical wind in top of mast. Wind speed aloft greater than 10 m/s, and wind from west-southwest (above, 225°-315°) and north (below, 315° - 45°).

For wind from the north (315° - 45°) turbulence values are much higher than from the south, and mostly higher in the lower 500 metres than above. For the large quantiles, the turbulence is strongest aloft, above roughly

200 -300 m. Simulated wind results indicate a complex spatial wind field for northeasterly flow, with strong vertical wind shear and orographic effects.

Figure 5-27 shows southeasterly (90°-180°) flow for two different wind speed criteria. Lidar derived observations indicate that the strongest turbulence occurs during flow from the south and east. For these directions and for high wind speed, it may be assumed that turbulence is only partly local or roughness generated. That is, a large part of the turbulence is non-local and there is a large orographic contribution to the turbulence. Mast turbulence values are far lower than in the lidar data, in particular for the high quantiles, indicating that mast observations may not be an optimal indicator of the stronger turbulence aloft. This as one would expect and can be interpreted such that the mast is a good indicator of locally generated turbulence (i.e. roughness-generated in the near-field) while on average the non-locally generated turbulence due to orographic effects is on average not present at low levels so far from the mountains. We note that the lidar results are a combination of data from the two lidar locations and the high quantiles are likely to be dominated by data from the quarry location. This should be considered in the interpretation of the data.

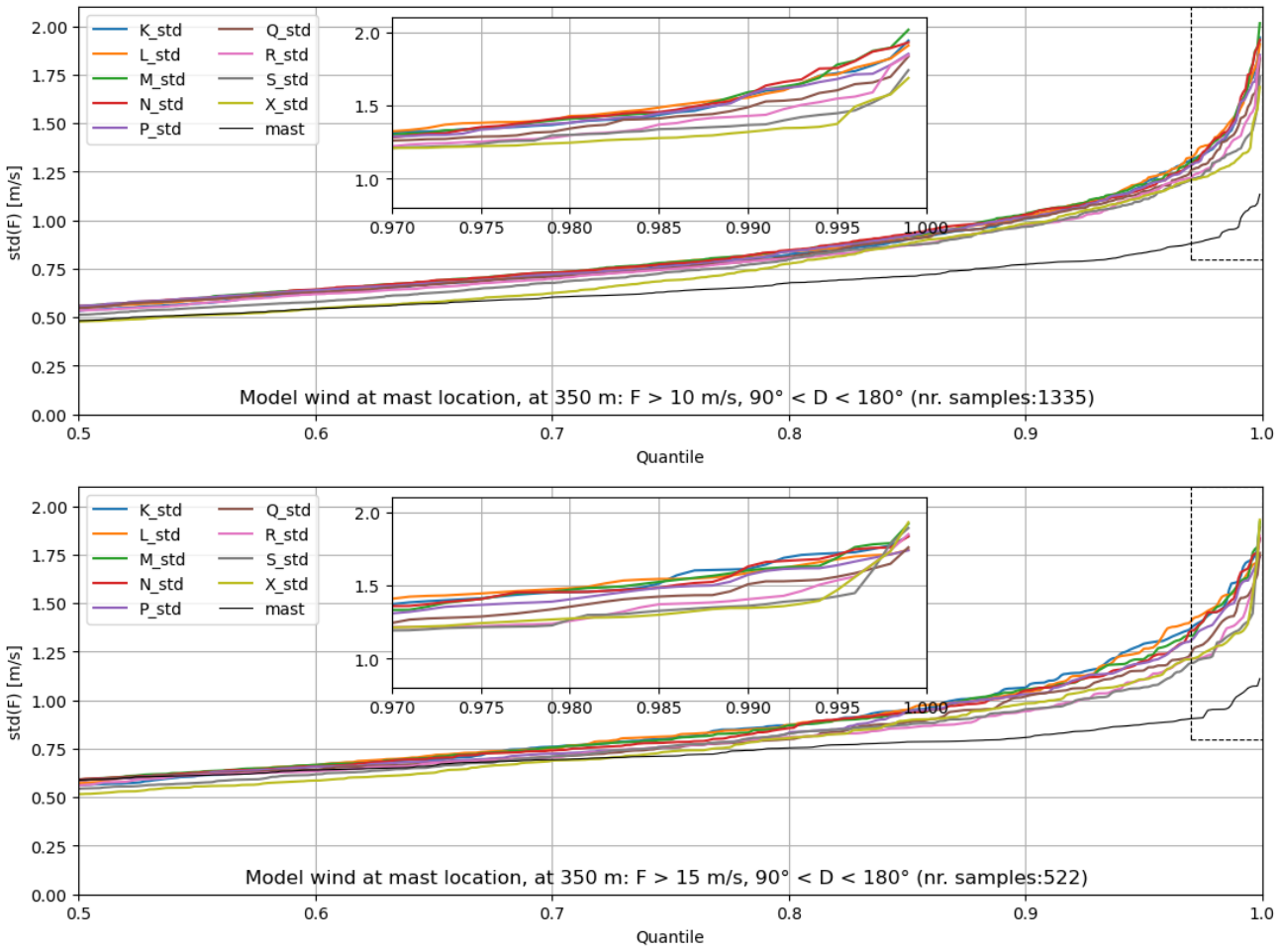

Figure 5-27 Quantile plots of the standard deviation of the radial wind speed from the lidar turbulence and vertical wind in top of mast. Wind direction is from the southeast (90°-180°), and wind speed above 10 m/s (above) and 15 m/s (below).

6 The weather during the measurement period

In order to interpret the statistics of the lidar measurements it is necessary to check and compare the wind speed and direction distributions for the relative short period of measurements with the lidar, with a period which is long enough so that the conditions are representative for the actual wind climate.

6.1 Weather during the full measurement period

As stated in Table 3-2, the lidar was located at two different locations during the measurement period, near the mast in Hvassahraun and near a quarry some kilometres south of the mast (Figure 2-1). The first measurements were done on 30 April 2021 and ended on 10 May 2023. The lidar was not operational for extended parts of this, full measurement period, most notably in the late summer and early autumn of 2021 and 2022.

At the mast location, the simulated flow conditions at ~20 m above the surface of the ground are quite similar during the 1993 – 2023 as during the measurements (Figure 6-1). The main difference is that southerly and easterly flow was more frequent during the measurement period than during 1993 – 2023, while westerly and northerly winds were somewhat less frequent. The same behaviour is observed at ~200 m above the ground, but the differences in frequencies are however more exaggerated than at ~20 m. An investigation of the flow conditions at ~200 m above the quarry locations reveals the same (Figure 6-2); namely that southerly and easterly flow was considerably more common during the measurement period than in the wind climate, while westerly and northerly flow was less frequent.

Overall, Figure 6-1 and Figure 6-2 indicate that flow from the south and east may be somewhat over-represented during the measurement period. These are in fact the directions that are a priori most likely associated with topographically induced turbulence, which may affect flight conditions near an airport in Hvassahraun. However, successful wind speed retrievals from the lidar are strongly dependant on the flow conditions..

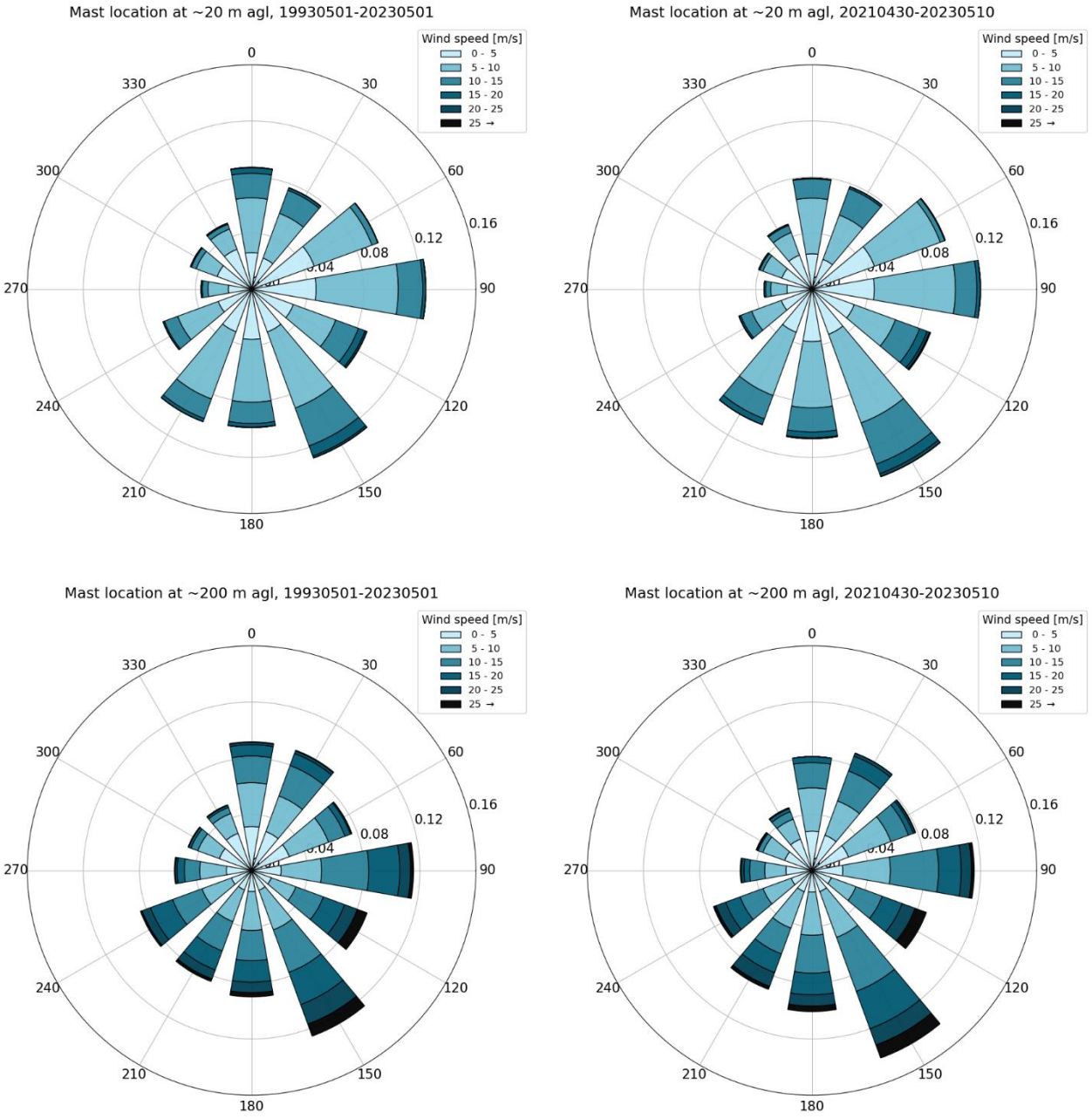

Figure 6-1 Wind roses based on simulated wind data with 2 km horizontal resolution, valid at the mast location in Hvassahraun at ~20 m agl (upper row) and at ~200 m agl (lower row). Roses in left column show the wind climate (30 year) while the right column shows flow conditions during the full measurement period.

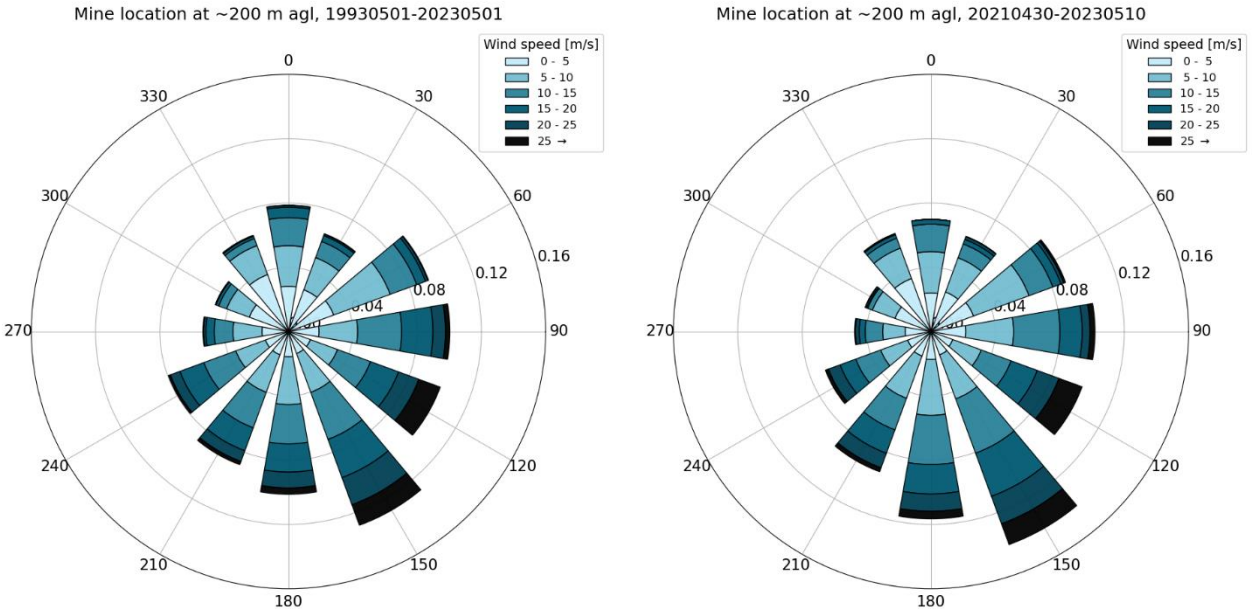

Figure 6-2 Wind roses based on simulated wind data with 2 km horizontal resolution, valid at ~200 m above ground at the quarry location. Left rose shows the wind climate (30 year) while the right column shows flow conditions during the full measurement period.

6.2 Weather during measurement sub-periods

The lidar has measured at two locations and in different modes, as indicated in Table 3-2 and Table 3-3. The full measurement period can thus be split into 4-5 sub-periods.

The KVTMeso dataset is as before used to provide wind data aloft during each sub-period, but only when concurrent with available and good lidar-measurements. The simulated data is available with an hourly resolution, and can, due to the models limited resolution, be considered to represent an temporal average on the order of 10-30 minutes. The lidar-data used is from the first sloping range gate at 345 m (for measurements until June 2022) and at 200 m agl for a vertical beam (from September 2022). The lidar-data has previously been aggregated to 10 minutes and the hourly simulated wind data nearest in time is used for all good and available lidar-data.

The first period of observations with a sloping beam at the mast location, was short but characterized by observations of relatively weak northerly flow and stronger southeasterly flow (Figure 6-3). During the second period there were strong winds from mostly east and southwest, but unstable lidar operations and technical issues degrade the quality of this data. The last period of sloping measurements had higher frequencies of northerly winds and somewhat less frequent southeasterly flow than compared to the full measurement period and wind climate. After the summer of 2022, the lidar only did vertical oriented observations, and the available measurements from the lidar are associated with a far higher frequency of easterly and norheasterly winds, and less frequent from other directions, than compared to the full measurement period (Figure 6-4). The difference in the wind roses in Figure 6-3 and Figure 6-4 compared to those in Figure 6-1 and Figure 6-2, is only partly explained by differences in the actual flow conditions during the sub-periods. The differences are presumably mostly associated with differences in lidar availability, based on wind direction and other weather conditions such as cloud and precipitation.

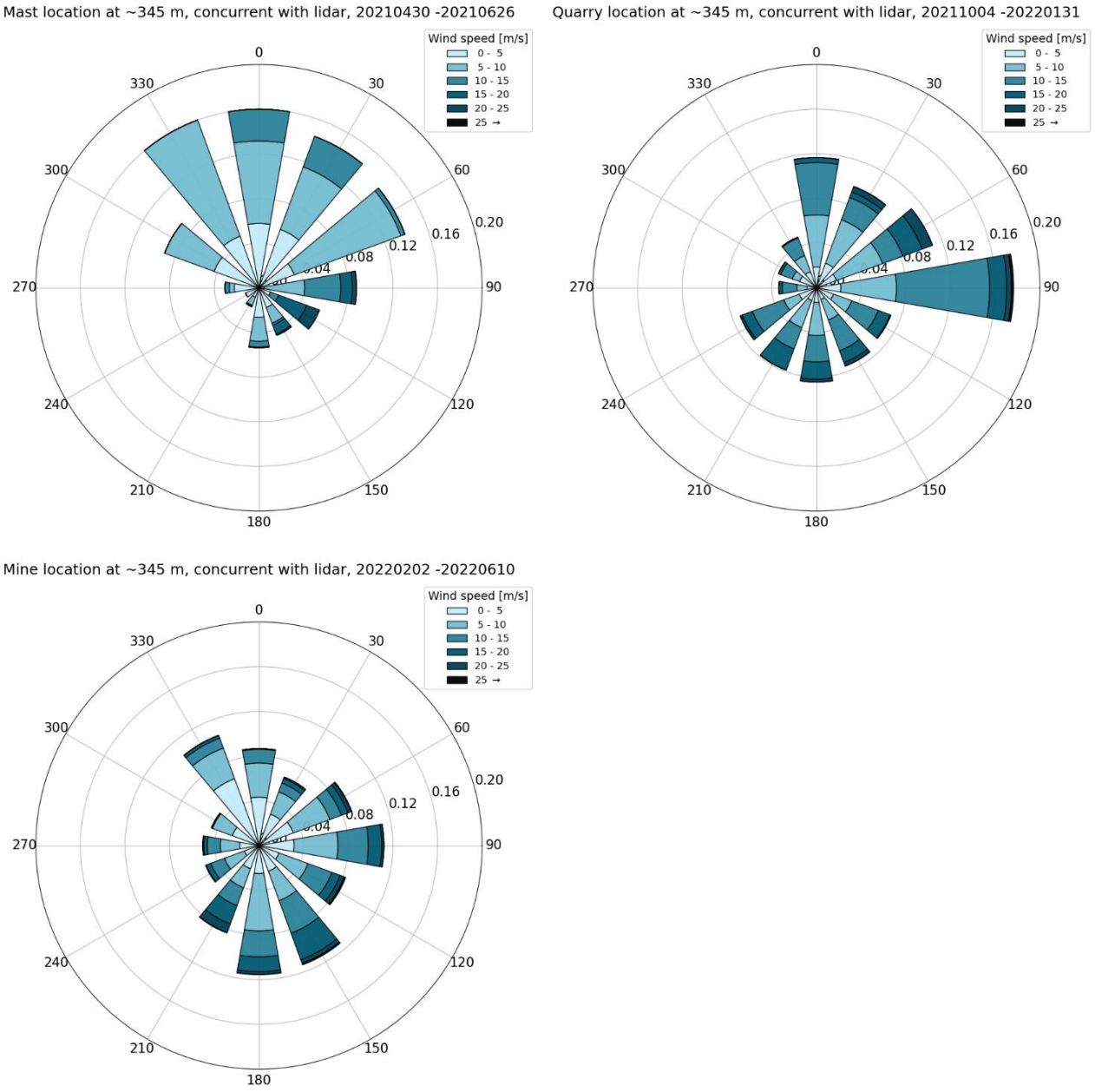

Figure 6-3 Wind roses based on simulated wind data with 2 km horizontal resolution, concurrent with valid lidar-data at 345 m along a sloping lidar beam.

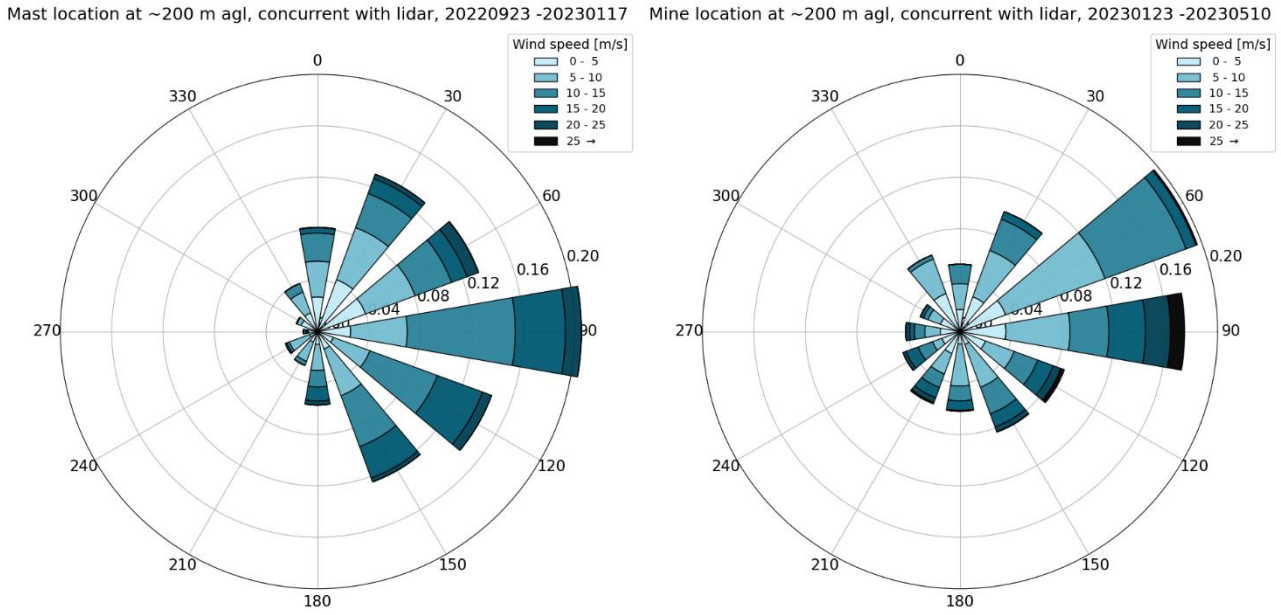

Figure 6-4 Wind roses based on simulated wind data with 2 km horizontal resolution, concurrent with valid lidar-data at 200 m agl lidar.

7 Concluding remarks

As a part of a detailed investigation to assess the conditions at a possible airport site in Hvassahraun, a scanning lidar was deployed in order to quantify the occurrence and magnitude of turbulence aloft.

The lidar was in operation for almost two years at two different sites, but not continuously. Reliable and good data was collected for a large part of the campaign, while technical issues degraded somewhat the data quality during extended periods. The dataset includes observations of the vertical component of the turbulence at levels from the surface and up to 1000 above ground level, but data availability decreases with height, in particular above approximately 500 m. Observations of wind speed variations along a sloping lidar beam were also done but are difficult to interpret in a general manner, and best suited as input to calibration with fine scale turbulence models as in [1]. Overall data availability and quality is considered good, and data are adequate for the analysis of turbulence aloft. However, we note that not all wind directions were as well sampled, and directions associated with the low turbulence are rather poorly represented in the dataset.

For the first part of the campaign, the lidar was located close to a 30 m mast in Hvassahraun and observations were cross-validated. The lidar derived wind observations reproduce the sonic observations from anemometers in the mast, both with regard to mean wind speed and directions, but also with regard to bulk quantities of turbulence such as turbulence intensity and turbulence energy. The main limitations of the lidar data with regard to point observations at high temporal resolution in sonic anemometer is related to technical differences due to the observation platform. Lidars cannot reproduce the higher temporal frequencies of the turbulence, i.e. small turbulent structures associated with the inertial subrange and dissipation are not observed. The lidar reproduces the lower frequency turbulence, typically up to or well into the low-frequency end of the inertial subrange. A result of this is that bulk-estimates of turbulence such at the turbulence intensity are typically on the order of 10% lower than when observed with a sonic anemometer. And the turbulence spectra from the lidar observations does not capture the high frequency part of the spectrum.

The lidar observations show a directional difference in the intensity of the turbulence and a general increase in turbulence with wind speed. Turbulence in the observations is generally weak from the west but the limited amount of available data for this sector means that the results are not easily generalized. Northerly wind is well represented in the data but not associated with particularly high turbulence. The strongest turbulence occurs in strong easterly and southerly flow, downstream of a 300-500 h mountain ridge. For these directions there is presumably a large orographic contribution in the turbulence aloft. The turbulence is generally stronger below 500 m agl than above, but this is not necessarily always the case for easterly and southerly flow. Strong turbulence at the mast location is presumably mostly locally generated due to surface roughness while aloft there is presumably a non-local contribution for flow from the east and south. The mast data may not be an optimal indicator for strong turbulence aloft for these directions.

The current work does not quantify the spatial and temporal long-term distributions of turbulence in the area of interest. As in [1], this could be done by calibration of the lidar derived observed turbulence with simulated turbulence from a high-resolution CFD model with adequate spatial resolution (~100 m) to resolve terrain features of relevance. Such model data is currently not available but can be readily produced. The model data should be produced to cover the entire period of available observations and forced with boundary data representing the actual wind conditions. The resulting model data can be used to describe the spatial distribution of the turbulence in the area, after comparing and calibration with the lidar observations which are only available for discrete points in time and space. Long time-series of such high-resolution CFD-simulations are expensive to produce so the long-term turbulence conditions would typically be estimated by calibration with coarser scale simulated wind data which is readily available for periods covering more than 40 years.

8 References

[1] H. Ágústsson og K. Harstveit, «Lofoten, værmessig tilgjengelighet for aktuelle flyplasslokaliteter, nr. KVT/HÁ/2019/R049_rev1,» Kjeller Vindteknikk, 2019.

[2] Samgöngu- og sveitarsjórnarráðuneytið, « Flugvallarkostir á suðvesturhorni landsins,» 2019.

[3] L. Magnússon, «Skýrsla um athuganir a flugskilyrðum yfir Kapelluhrauni 1969/1970,» 1970.

[4] G. N. Petersen, «Veðurmælingar í Hvassahrauni 2021 - 2022. Skýrsla VÍ 2023-005.,» Veðurstofa Íslands, 2023.

[5] G. Árnason og Þ. Pálsson, «In-Flight Measurements and Investigation of Air Turbulence over Hvassahraun,» Reykjavík University, 2024.

[6] H. Ágústsson, «E39, Sulafjorden, Møre & Romsdal, Analysis of LIDAR derived wind measurements, September 2018 - March 2021, RAP-KVT-LID-110-R1 / KVT/2021/R093/HÁrev1,» Kjeller Vindteknikk, Norconsult AS, 2021.

[7] R. B. Stull, An introduction to boundary layer meteorology, Kluwer Academic Press, 1988.

[8] J. D. Doyle og D. R. Durran, «Rotor and Subrotor Dynamics in the Lee of Three-Dimensional Terrain,» *J. Atm. Sci.,* vol. 64, pp. 4202 - 4221, 2007.

[9] M. Katurji, A. Sturman og P. Zawar-Reza, «An Investigation into Ridge-Top Turbulence Characteristics During Neutral and Weakly Stable Conditions: Velocity Spectra and Isotropy,» *Boundary Layer Meteorol.,* vol. 139, pp. 143 - 160, 2011.

[10] R. Sharman og T. Lane, Aviation turbulence: Processes, detection and prediction, 2016.

[11] E. Cheynet, J. B. Jakobsen, J. Snæbjörnsson, J. Mann, M. Courtney, G. Lea og B. Svardal, «Measurements of Surface-Layer Turbulence in a Wide Norwegian Fjord Using Synchronized Long-Range Doppler Wind Lidars,» *Remote Sens.,* vol. 9, p. 26, 2017.

[12] H. Ágústsson og Þ. Arason, «Samanburður á úrkomumælingum í Bláfjöllum og Reykjavík, greinargerð Veðurstofu Íslands nr. 01015,» 2001.

[13] H. Sundqvist, E. Berge og J. E. Kristjánsson, «Condensation and cloud parameterization studies with a Mesoscale Numerical Weather Prediction Model,» *Monthly Weather Review,* vol. 117, nr. 8, https://doi.org/10.1175/1520-0493(1989)117<1641:CACPSW>2.0.CO;2, p. 1641–1657 , 1989.

A. KVTMeso

KVTMeso is a product suite using the numerical weather forecast model WRF (Weather Research and Forecasting). WRF is a state-of-the-art meso-scale numerical weather prediction system, aiming at both operational forecasting and atmospheric research needs. Numerous WRF hindcasts have been produced and available at Kjeller Vindteknikk, Norconsult, covering different areas and time periods.

A detailed description of the modelling system can be found at the WRF home page[2]. The development of the WRF-model is supported by a strong scientific and administrative community in U.S.A. The number of users is large, and the code is accessible for the public.

One model simulation has been applied in this work. For this we have applied the numerical weather forecast model Weather Research and Forecasting model (WRF), as detailed in Table A-1, and in the sections below. Actual model runs were performed by Belgingur ehf as a part of the IceBox R&D project, in collaboration with Norconsult as well as Landsnet.

Table A-1: Details on model simulations.

Parameterisation	KVTMeso
Horizontal resolution	2 km x 2 km
Vertical resolution	51 levels
Simulation period	19910101-20230930
Boundary conditions	ERA5 + ERA5-Land
Micro physics	Thompson Aerosol aware (28)
PBL scheme	MYNN 2.5 (5)
Land surface scheme	NOAH (2)
Surface layer scheme	MYNN (5)
Radiation	RRTMG (4) with cloud fraction by [13]
WRF version	4.2.1

The most important input data are geographical data and meteorological data. The geographical data is from the National Oceanic and Atmospheric Administration (NOAA). The data includes topography, surface data, albedo, and vegetation. These parameters have high influence for the wind speed in the layers close to the ground. The model setup has been updated with a more detailed land use classification data set from the CORINE Land Cover mapping project[3].

The ERA5[4,5] reanalysis data is used as lateral boundary conditions, and the simulations are set up to use input data with a 3-hours interval. In addition to the lateral input updated every 3 hours spectral nudging is used at the higher atmospheric levels.

For KVTMeso3, land components are taken from ERA5-Land[6], which is run on close to 0.1-degree resolution. ERA5-Land is a so-called replay of the ERA5 land components, improving the spatial variability compared to ERA5.

[2] https://www.mmm.ucar.edu/weather-research-and-forecasting-model
[3] http://www.eea.europa.eu/publications/COR0-landcover
[4] Copernicus Climate Change Service (C3S) (2017): ERA5: Fifth generation of ECMWF atmospheric reanalyses of the global climate. Copernicus Climate Change Service Climate Data Store (CDS). https://cds.climate.copernicus.eu/cdsapp#!/home
[5] https://www.ecmwf.int/en/forecasts/datasets/reanalysis-datasets/era5
[6] https://confluence.ecmwf.int/display/CKB/ERA5-Land:+data+documentation

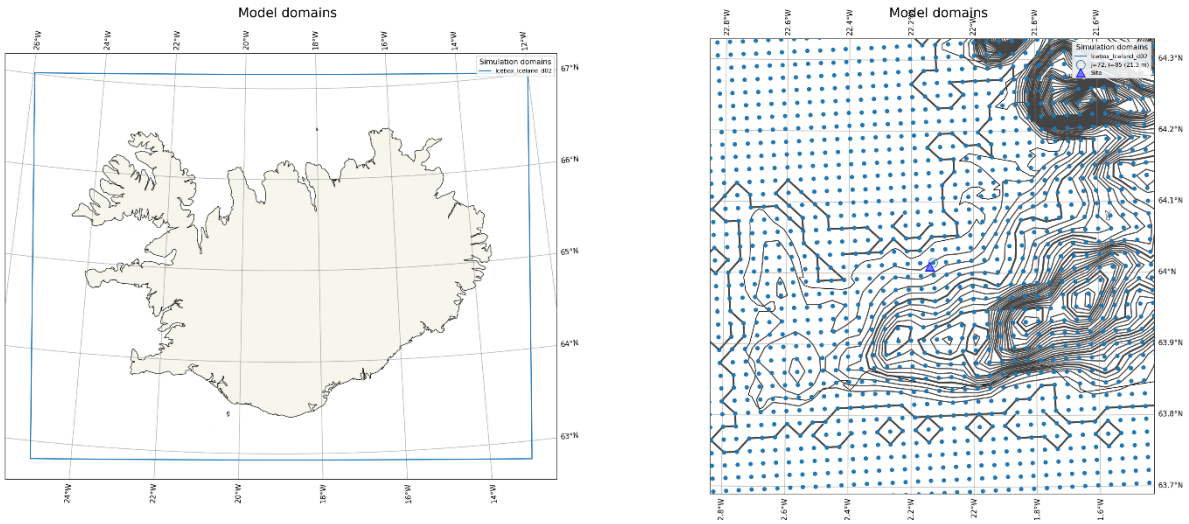

Figure A-1: Left: Overview of model domain 2 (blue) applied in this work. Right: model terrain (5 m contour lines) and grid points for the region of interest.

B. Timeseries of observed and simulated wind speed and direction during strong wind events

Simulated wind:

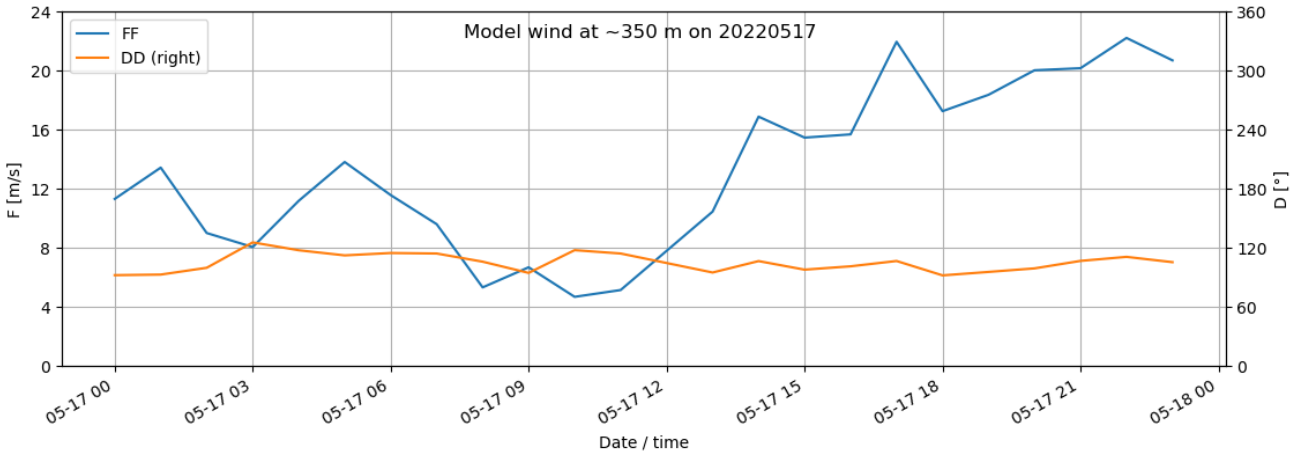

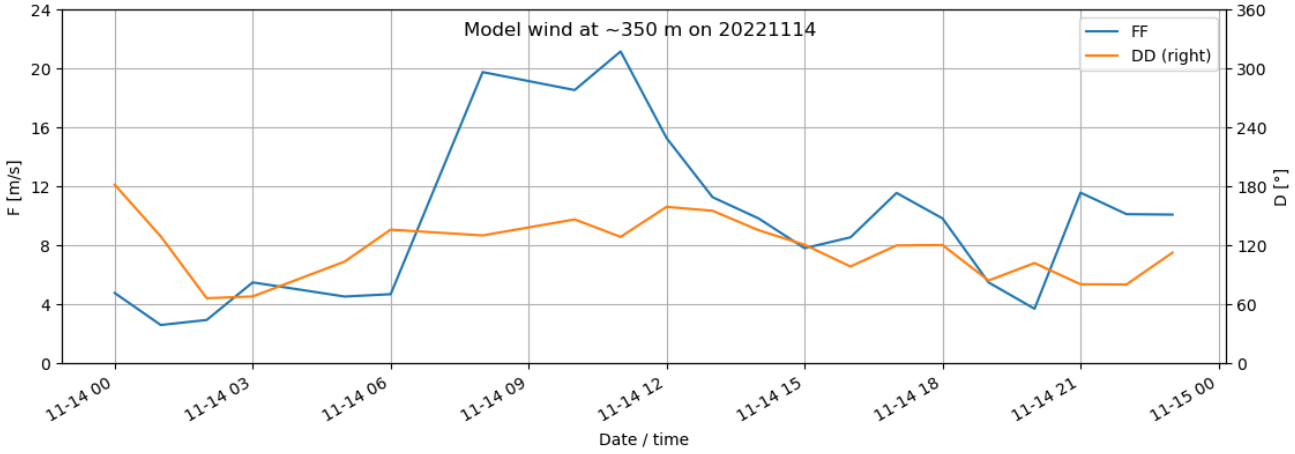
Model wind at ~350 m on 20221114
FF
DD (right)
F [m/s]
D [°]
Date / time
11-14 00
11-14 03
11-14 06
11-14 09
11-14 12
11-14 15
11-14 18
11-14 21
11-15 00

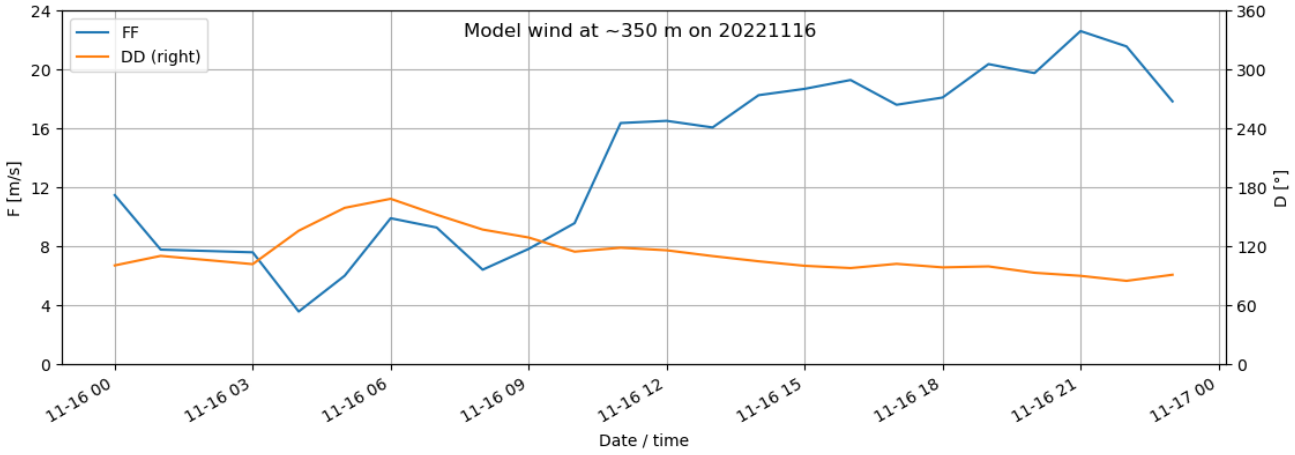
Model wind at ~350 m on 20221116
FF
DD (right)
F [m/s]
D [°]
Date / time
11-16 00
11-16 03
11-16 06
11-16 09
11-16 12
11-16 15
11-16 18
11-16 21
11-17 00

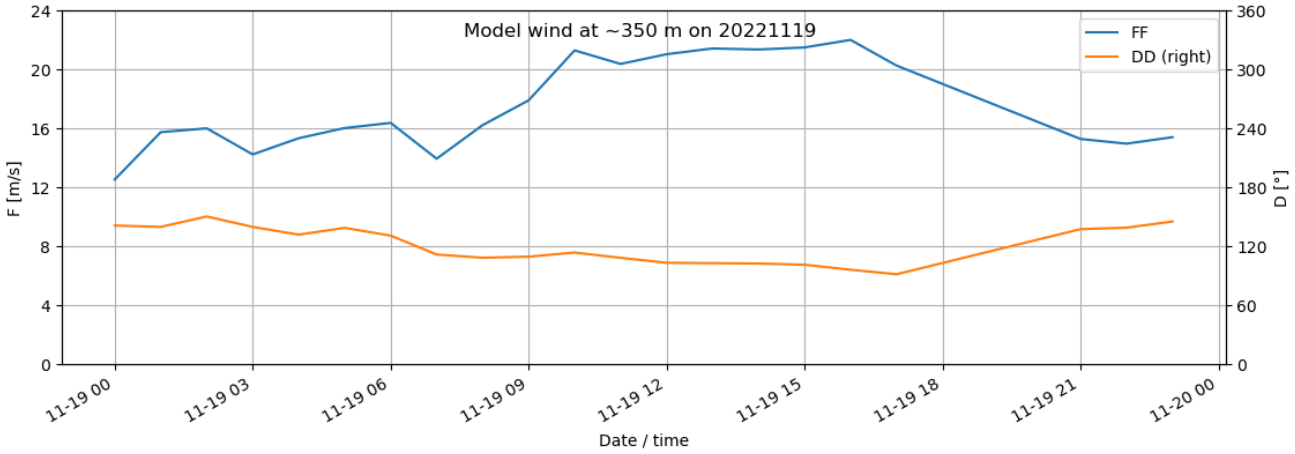
Model wind at ~350 m on 20221119
FF
DD (right)
F [m/s]
D [°]
Date / time
11-19 00
11-19 03
11-19 06
11-19 09
11-19 12
11-19 15
11-19 18
11-19 21
11-20 00

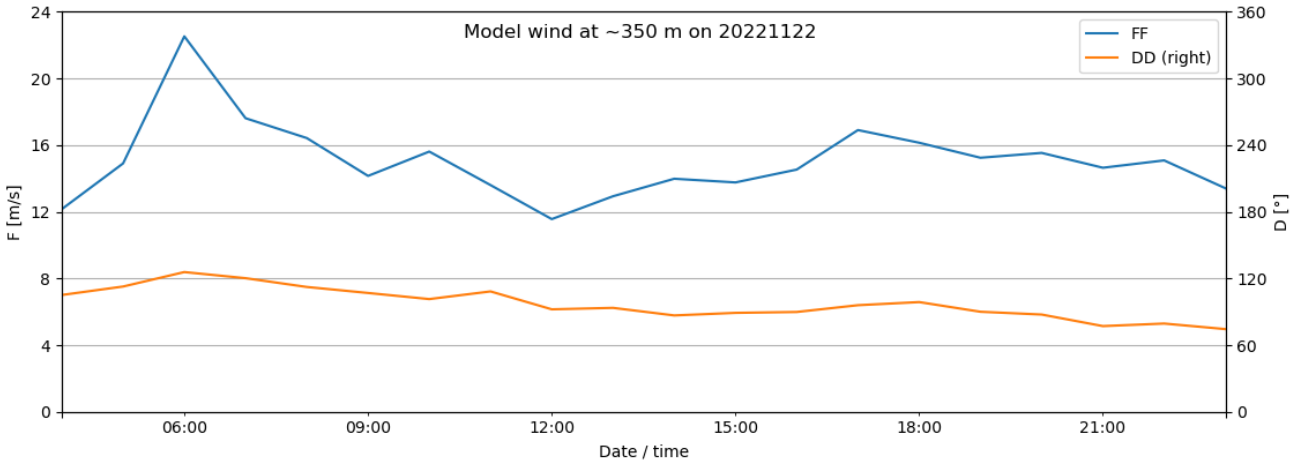
Model wind at ~350 m on 20221122
FF
DD (right)
F [m/s]
D [°]
Date / time
06:00
09:00
12:00
15:00
18:00
21:00

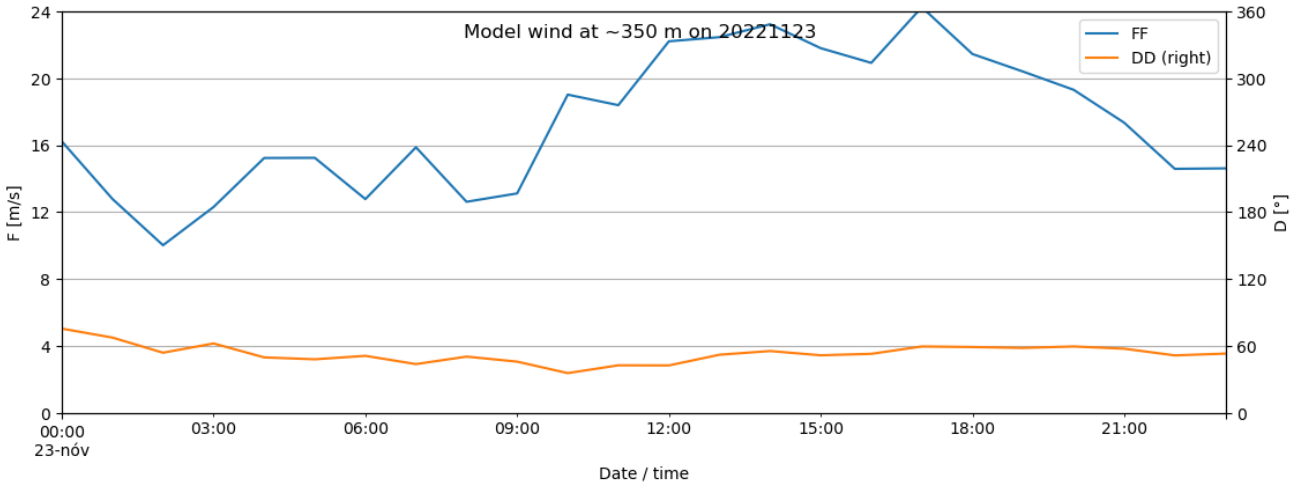
Model wind at ~350 m on 20221123
FF
DD (right)
F [m/s]
D [°]
Date / time
00:00
23-nóv
03:00
06:00
09:00
12:00
15:00
18:00
21:00

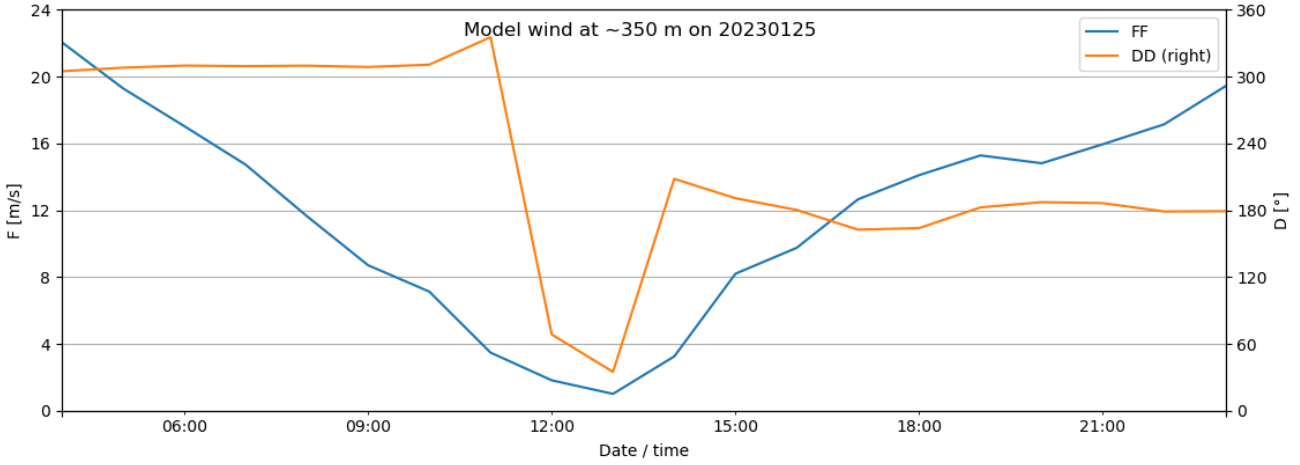
Model wind at ~350 m on 20230125
FF
DD (right)
F [m/s]
D [°]
Date / time
06:00
09:00
12:00
15:00
18:00
21:00

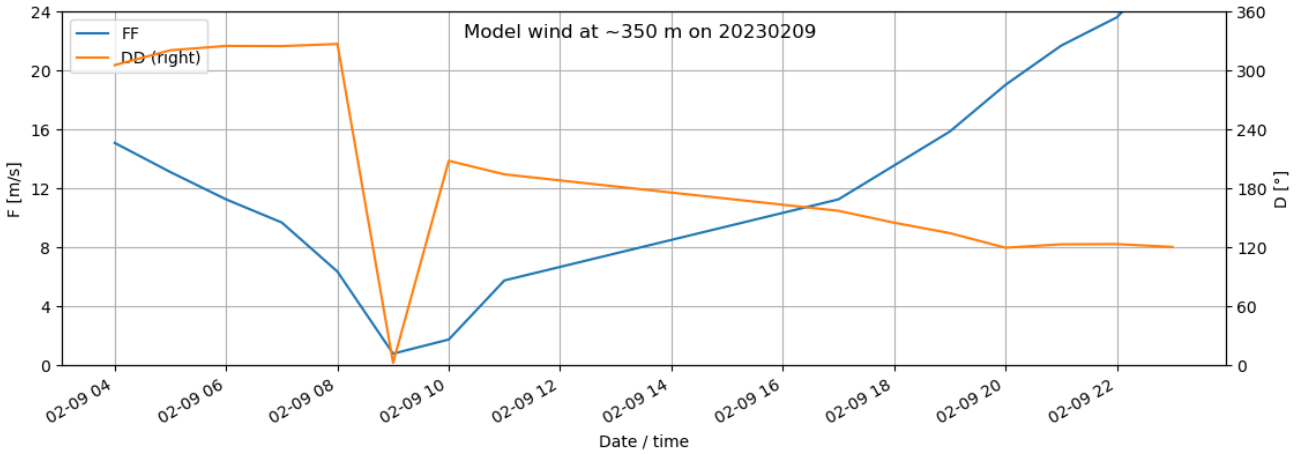
Model wind at ~350 m on 20230209
FF
DD (right)
F [m/s]
D [°]
Date / time
02-09 04
02-09 06
02-09 08
02-09 10
02-09 12
02-09 14
02-09 16
02-09 18
02-09 20
02-09 22

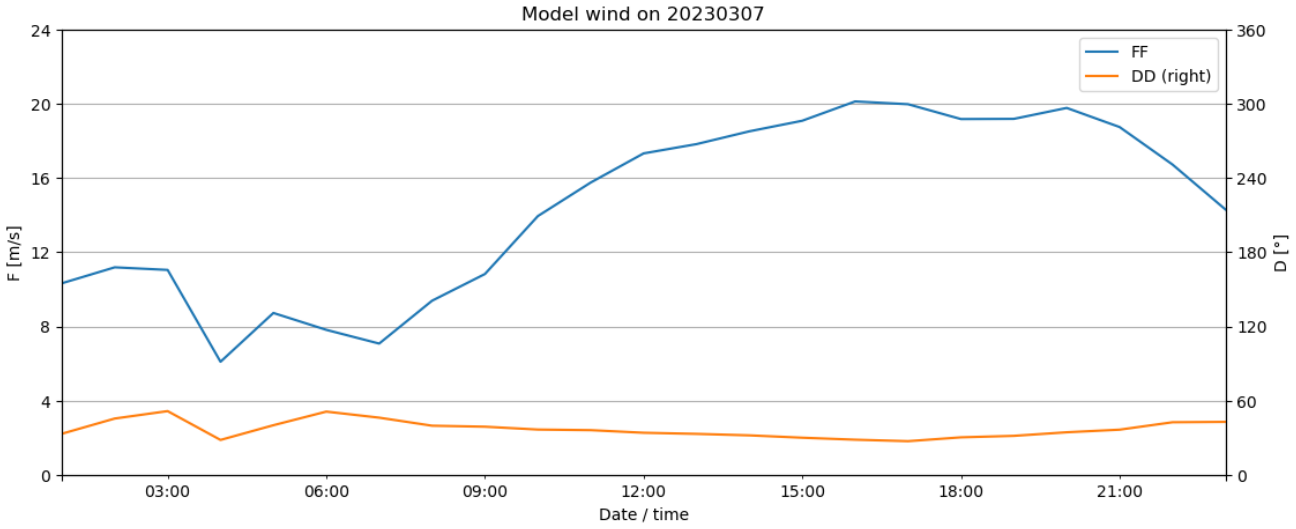
Model wind on 20230307
FF
DD (right)
F [m/s]
D [°]
Date / time
03:00
06:00
09:00
12:00
15:00
18:00
21:00

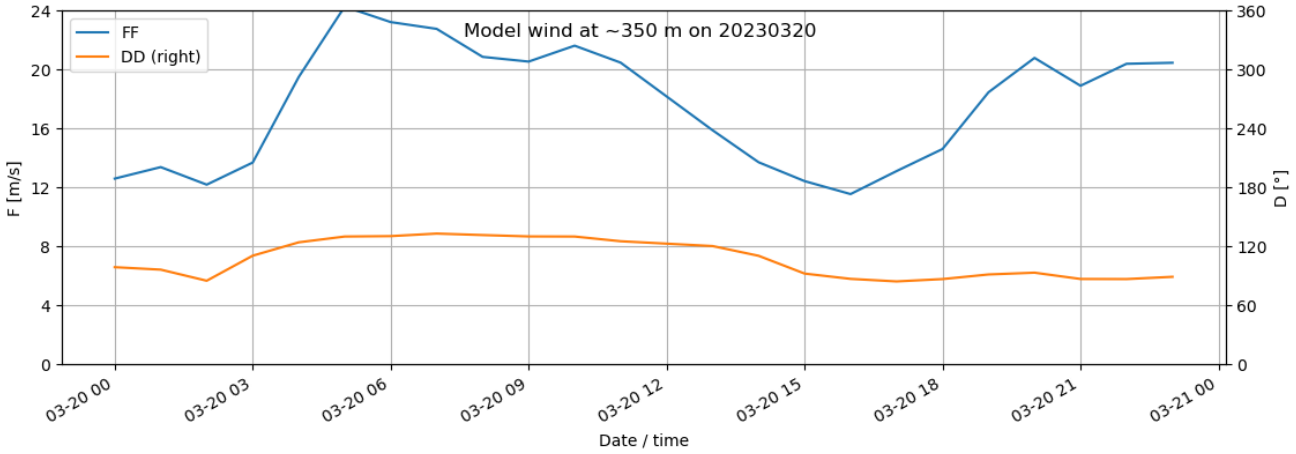
Model wind at ~350 m on 20230320
FF
DD (right)
F [m/s]
D [°]
Date / time
03-20 00
03-20 03
03-20 06
03-20 09
03-20 12
03-20 15
03-20 18
03-20 21
03-21 00

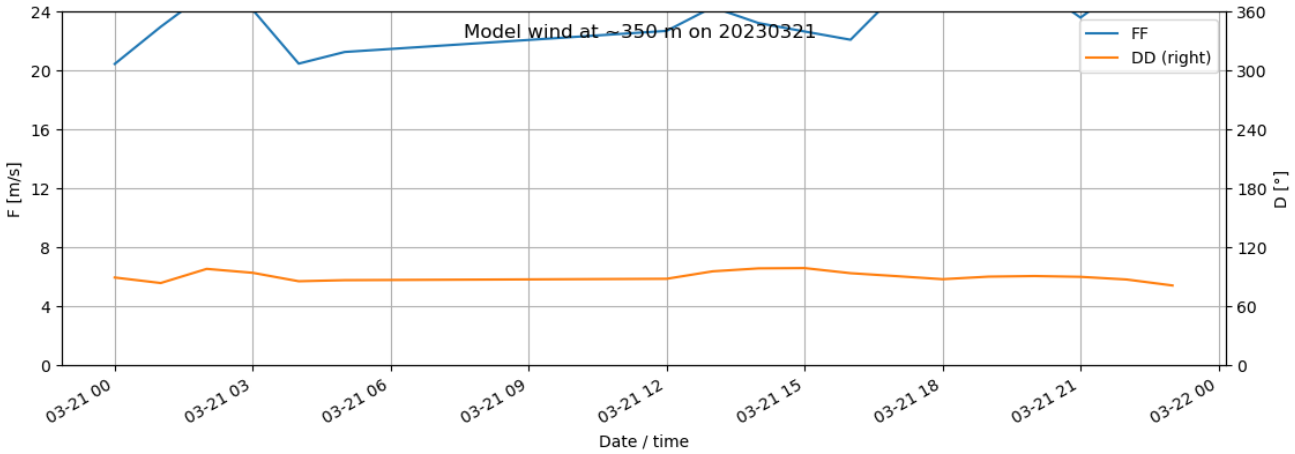
Model wind at ~350 m on 20230321
FF
DD (right)
F [m/s]
D [°]
Date / time
03-21 00
03-21 03
03-21 06
03-21 09
03-21 12
03-21 15
03-21 18
03-21 21
03-22 00

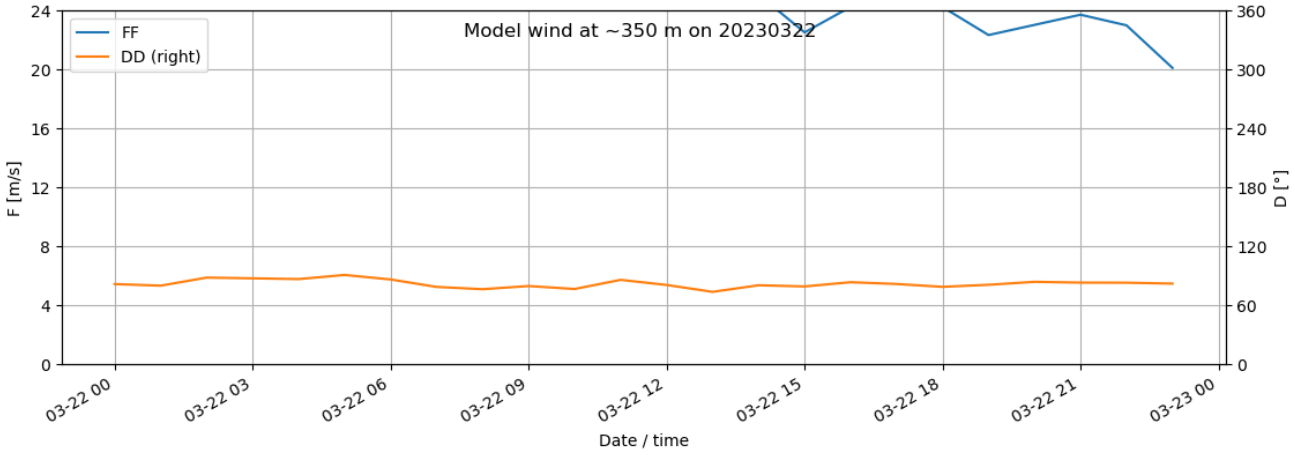
Model wind at ~350 m on 20230322
FF
DD (right)
F [m/s]
D [°]
Date / time
03-22 00
03-22 03
03-22 06
03-22 09
03-22 12
03-22 15
03-22 18
03-22 21
03-23 00

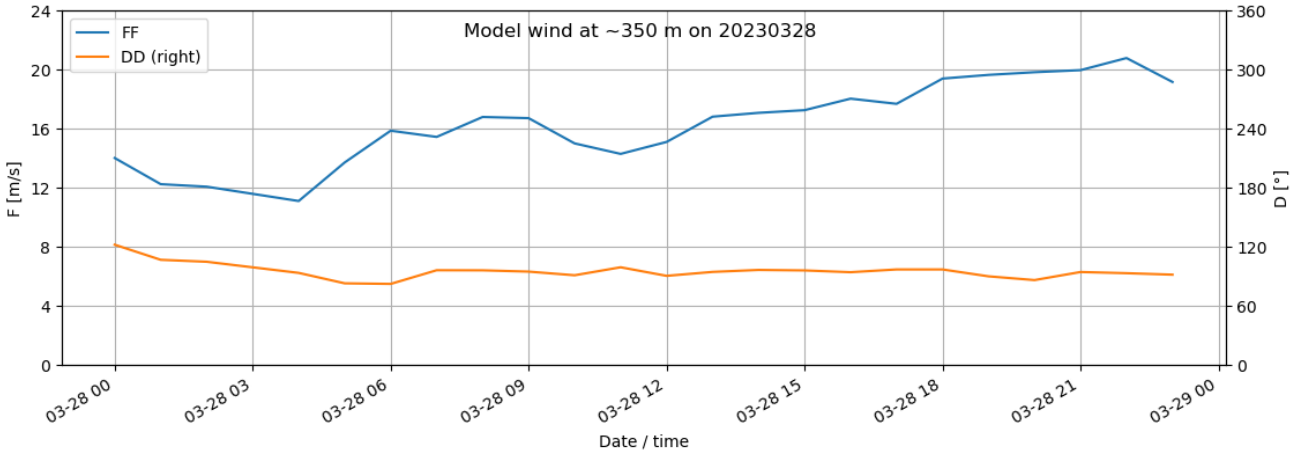
Model wind at ~350 m on 20230328
FF
DD (right)
F [m/s]
D [°]
Date / time
03-28 00
03-28 03
03-28 06
03-28 09
03-28 12
03-28 15
03-28 18
03-28 21
03-29 00

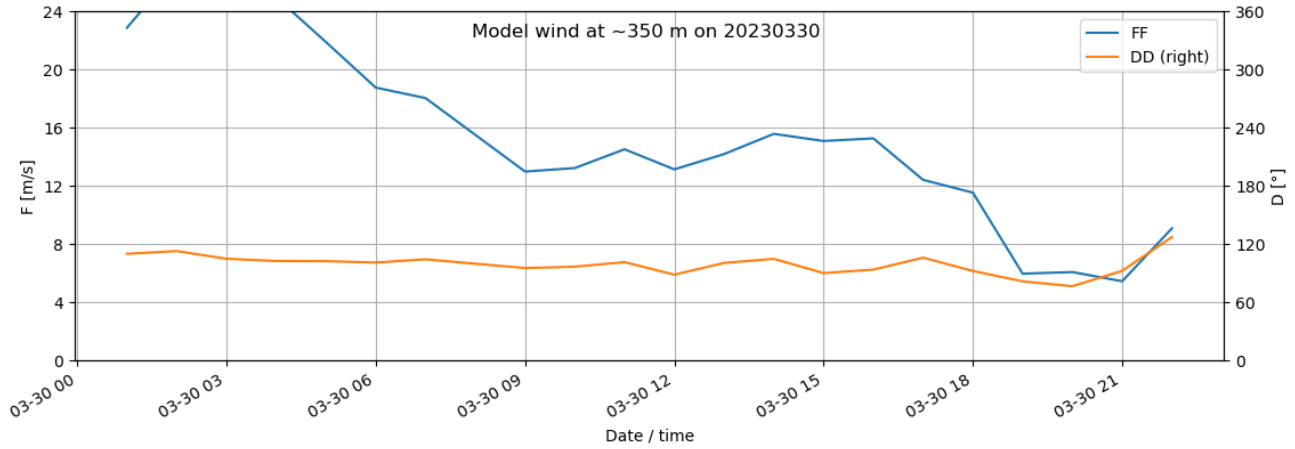

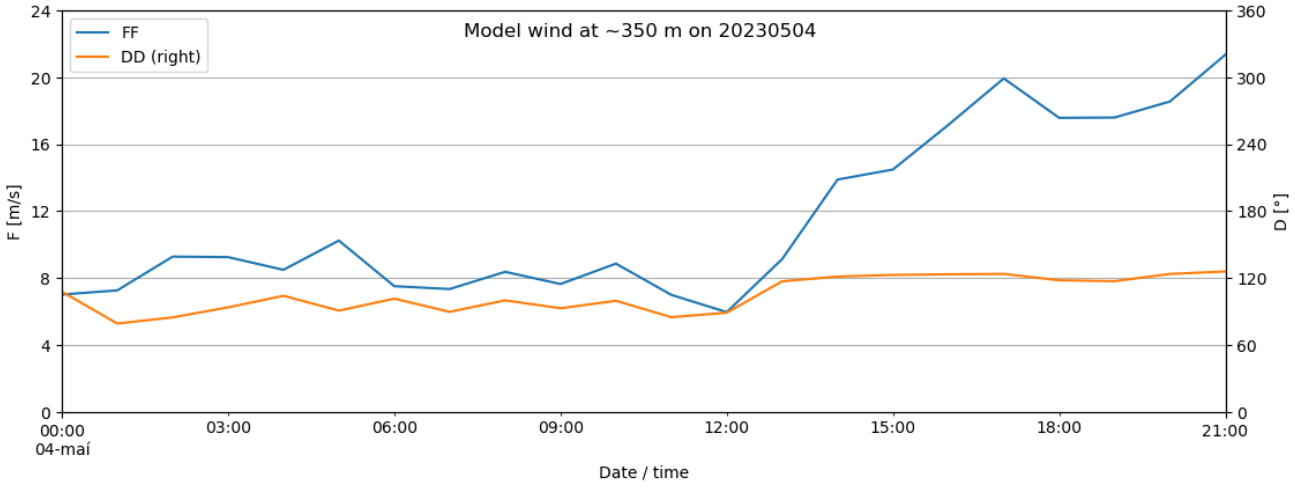

Observed wind:

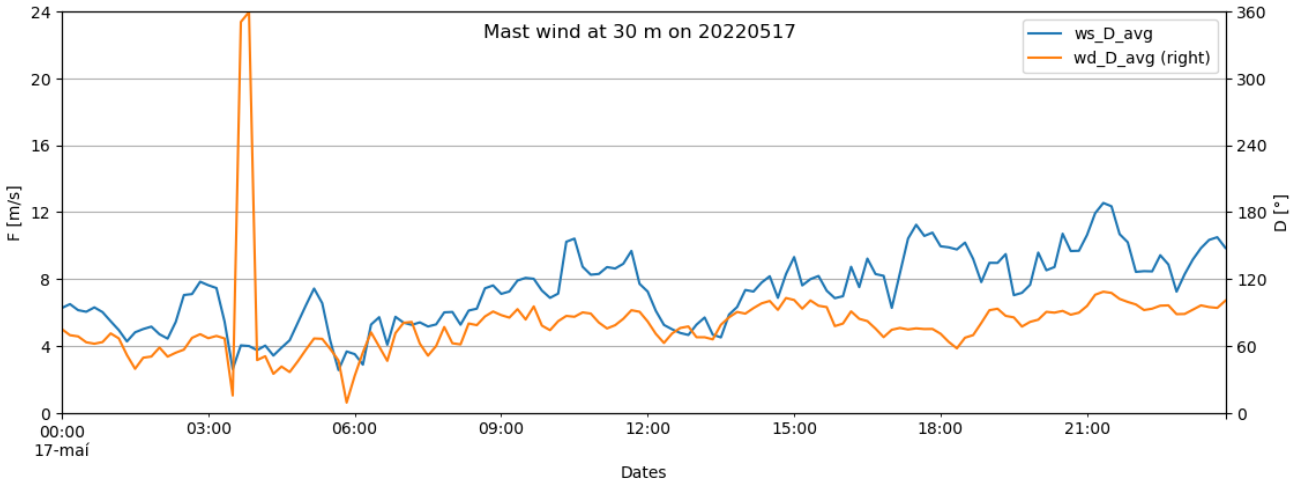

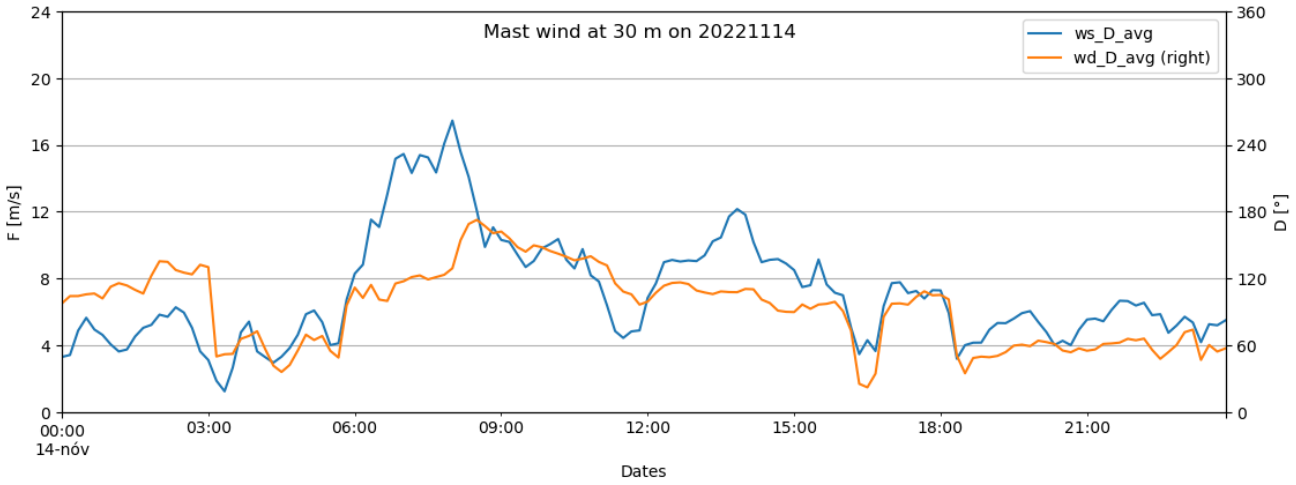
Mast wind at 30 m on 20221114
ws_D_avg
wd_D_avg (right)
F [m/s]
D [°]
00:00
14-nóv
03:00
06:00
09:00
12:00
15:00
18:00
21:00
Dates

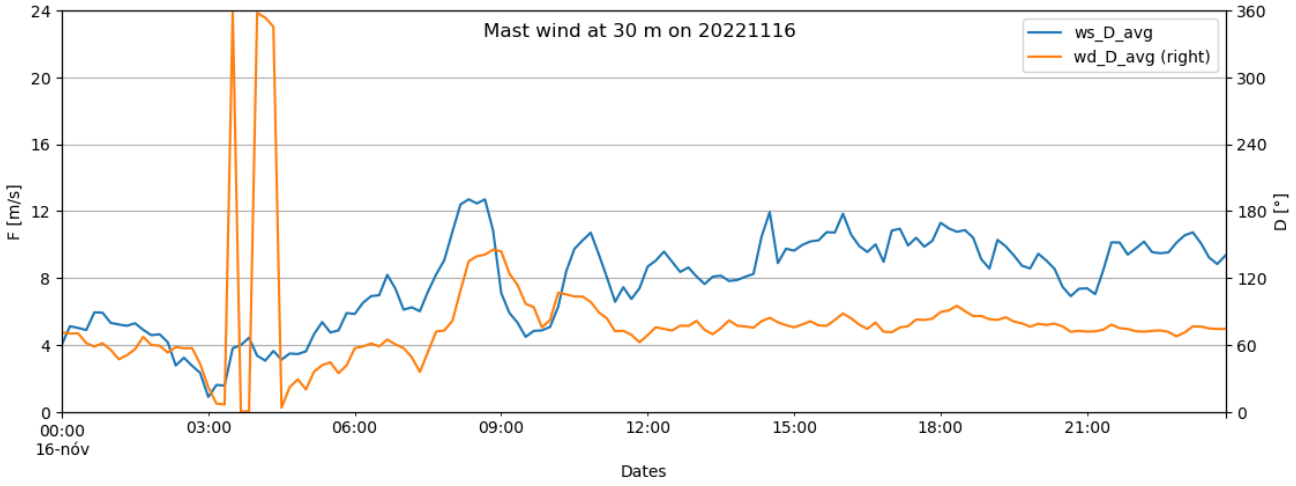
Mast wind at 30 m on 20221116
ws_D_avg
wd_D_avg (right)
F [m/s]
D [°]
00:00
16-nóv
03:00
06:00
09:00
12:00
15:00
18:00
21:00
Dates

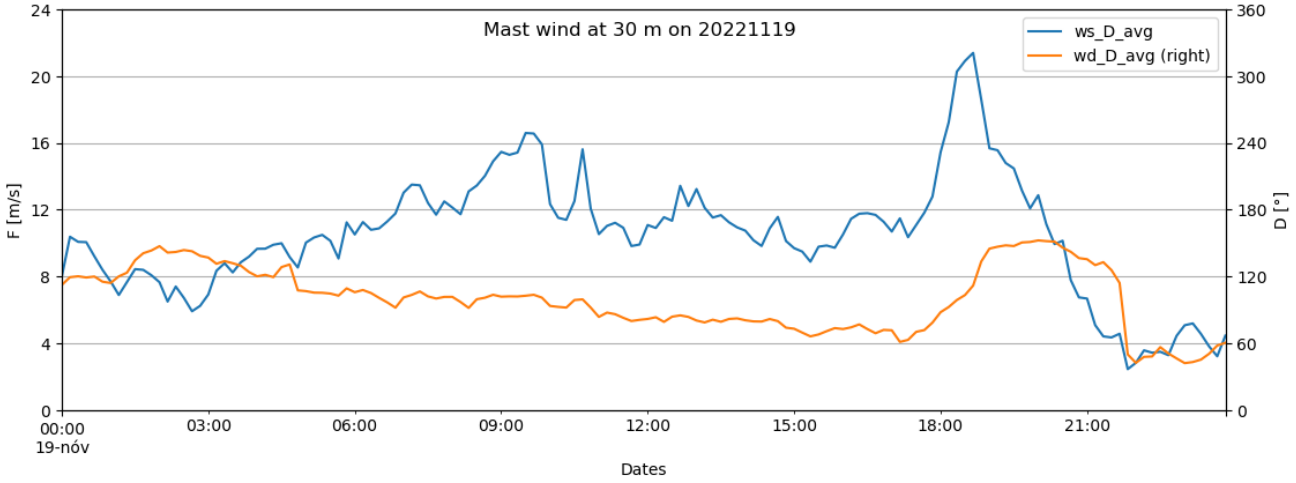
Mast wind at 30 m on 20221119
ws_D_avg
wd_D_avg (right)
F [m/s]
D [°]
00:00
19-nóv
03:00
06:00
09:00
12:00
15:00
18:00
21:00
Dates

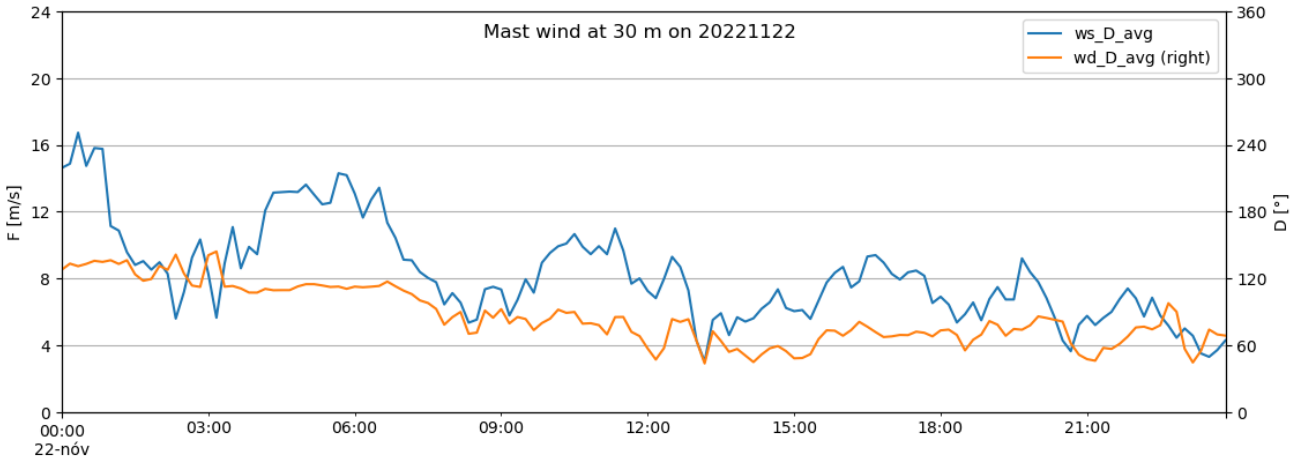
Mast wind at 30 m on 20221122
ws_D_avg
wd_D_avg (right)
F [m/s]
D [°]
00:00
22-nóv
03:00
06:00
09:00
12:00
15:00
18:00
21:00
Dates

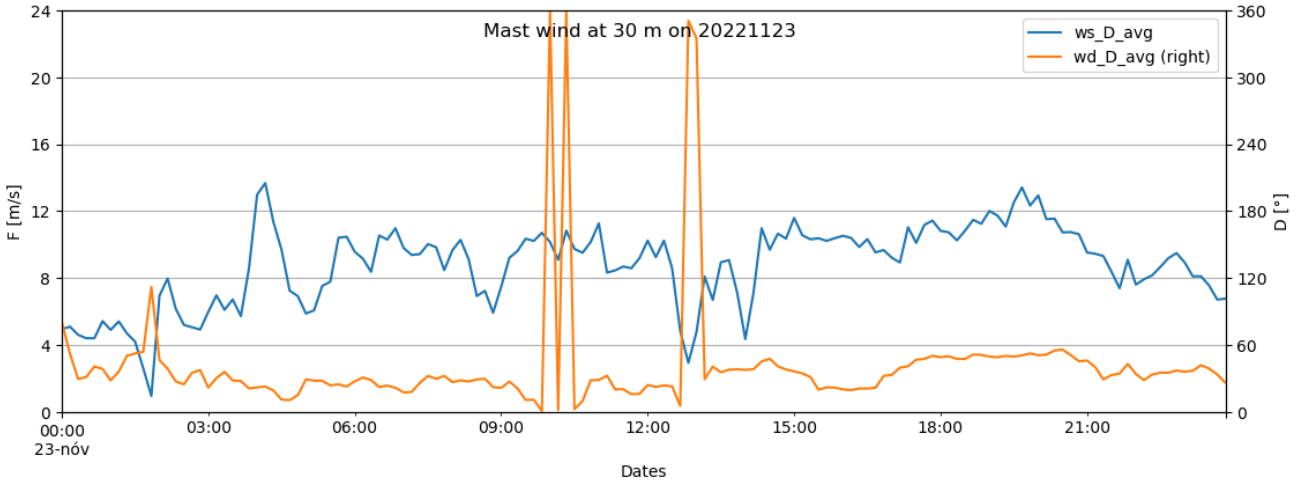
Mast wind at 30 m on 20221123
ws_D_avg
wd_D_avg (right)
F [m/s]
D [°]
00:00
23-nóv
03:00
06:00
09:00
12:00
15:00
18:00
21:00
Dates

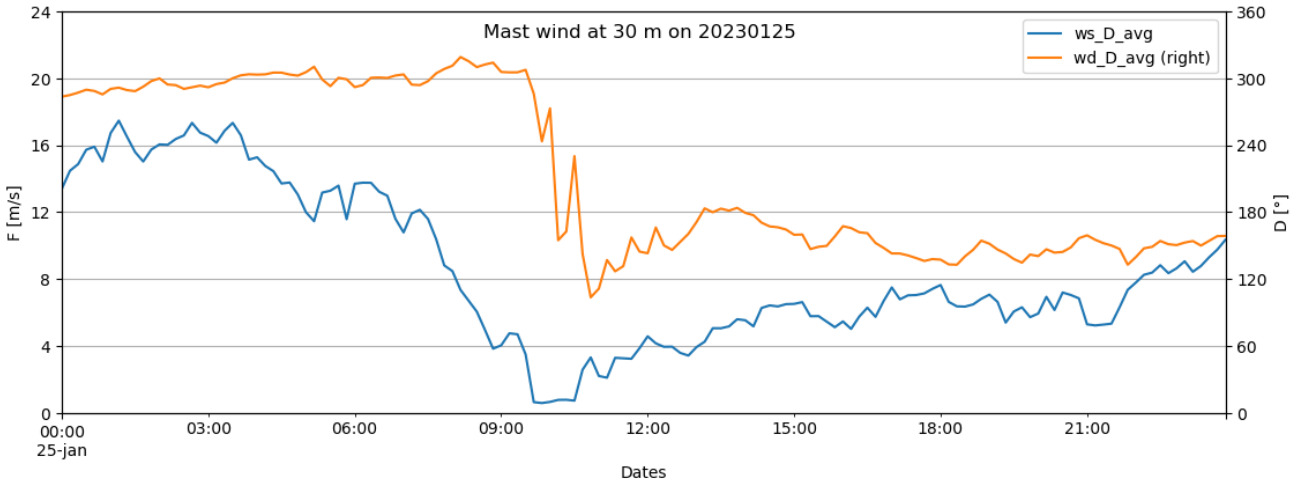
Mast wind at 30 m on 20230125
ws_D_avg
wd_D_avg (right)
F [m/s]
D [°]
00:00
25-jan
03:00
06:00
09:00
12:00
15:00
18:00
21:00
Dates

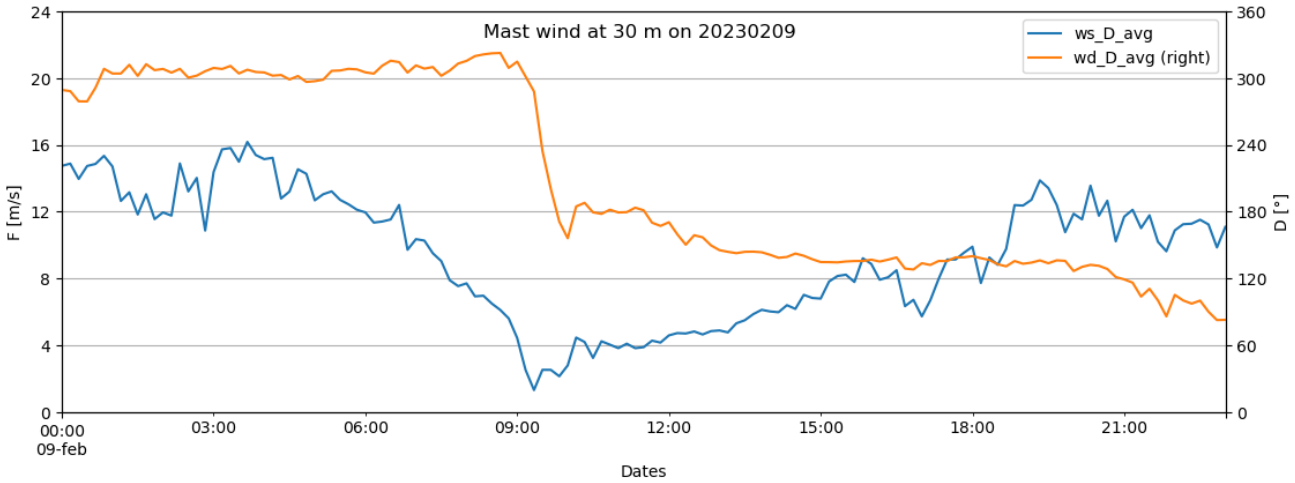
Mast wind at 30 m on 20230209
ws_D_avg
wd_D_avg (right)
F [m/s]
D [°]
00:00
09-feb
03:00
06:00
09:00
12:00
15:00
18:00
21:00
Dates

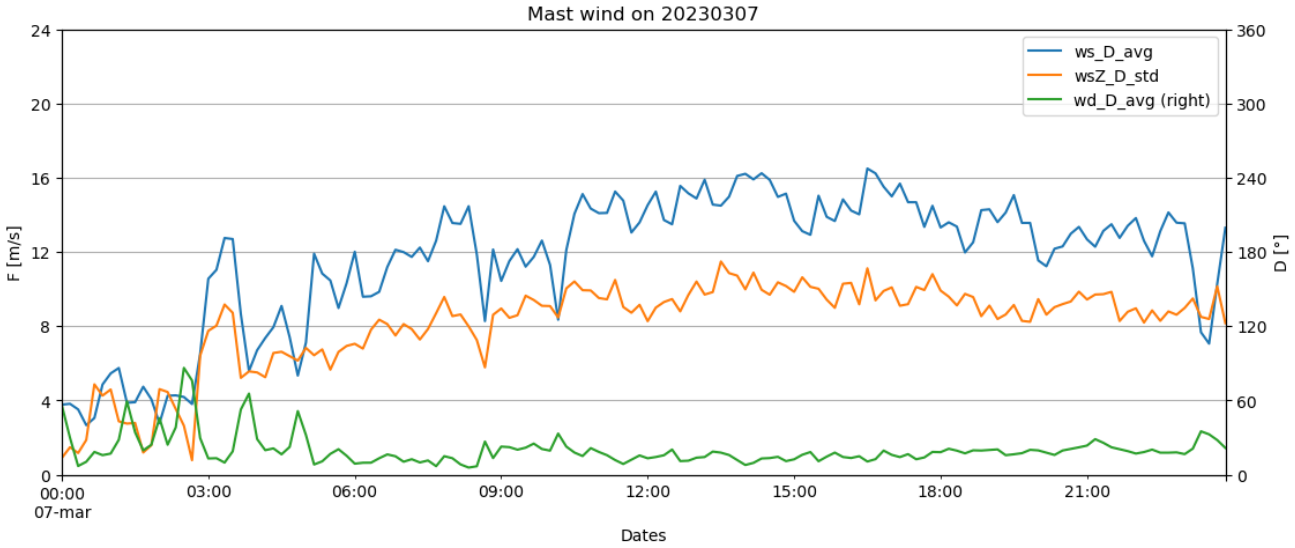
Mast wind on 20230307
ws_D_avg
wsZ_D_std
wd_D_avg (right)
F [m/s]
D [°]
00:00
07-mar
03:00
06:00
09:00
12:00
15:00
18:00
21:00
Dates

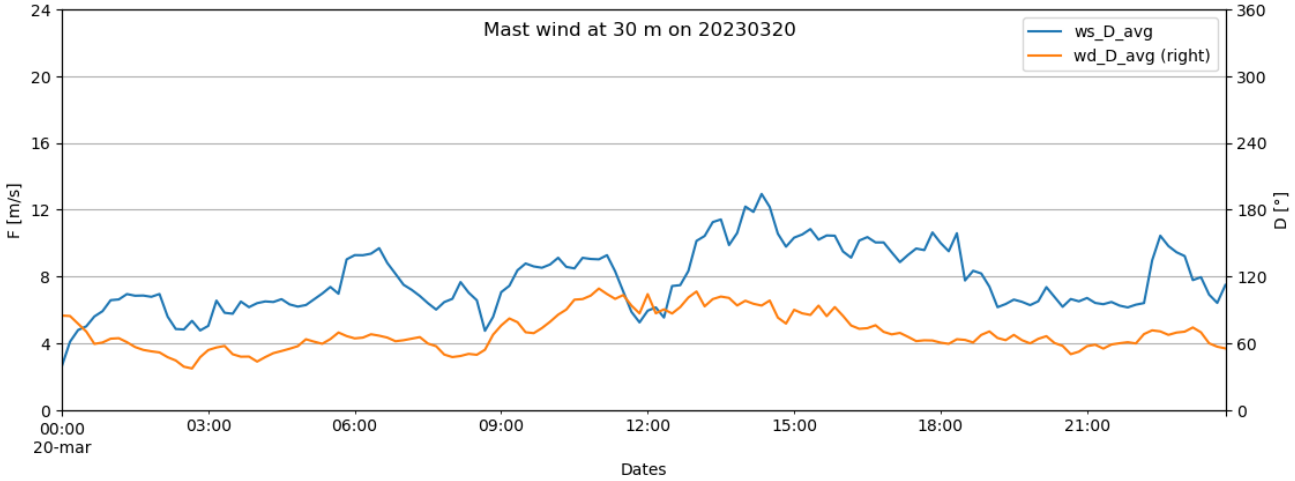
Mast wind at 30 m on 20230320
ws_D_avg
wd_D_avg (right)
F [m/s]
D [°]
00:00
20-mar
03:00
06:00
09:00
12:00
15:00
18:00
21:00
Dates

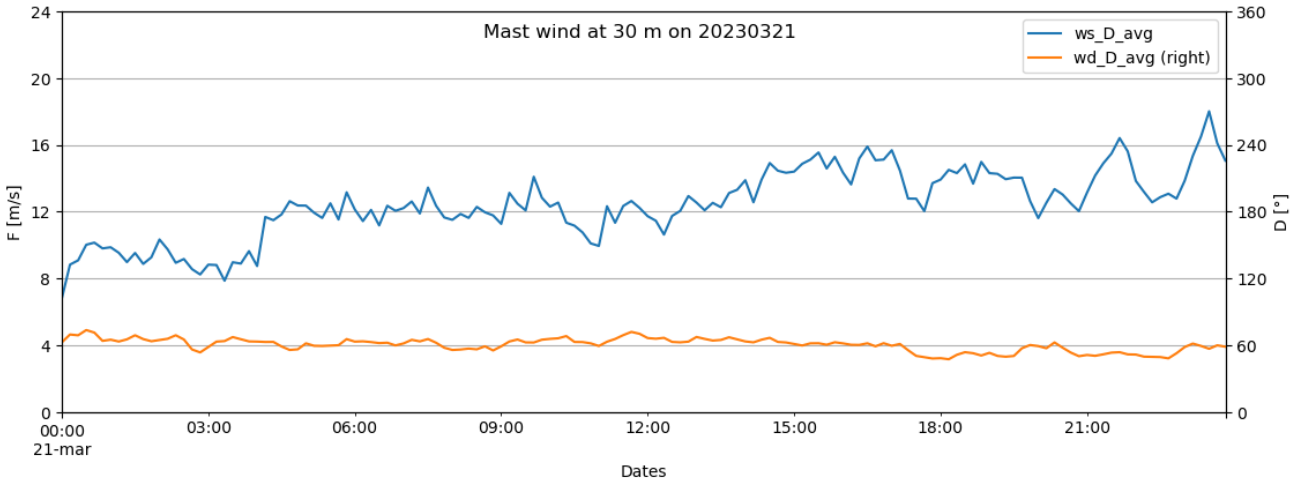
Mast wind at 30 m on 20230321
ws_D_avg
wd_D_avg (right)
F [m/s]
D [°]
00:00
21-mar
03:00
06:00
09:00
12:00
15:00
18:00
21:00
Dates

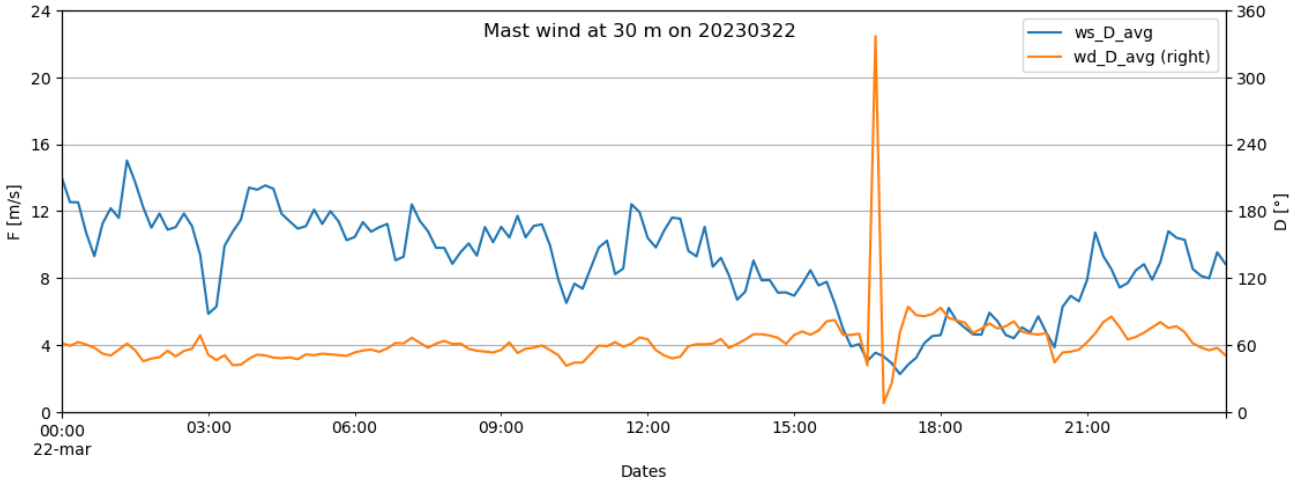
Mast wind at 30 m on 20230322
ws_D_avg
wd_D_avg (right)
F [m/s]
D [°]
00:00
22-mar
03:00
06:00
09:00
12:00
15:00
18:00
21:00
Dates

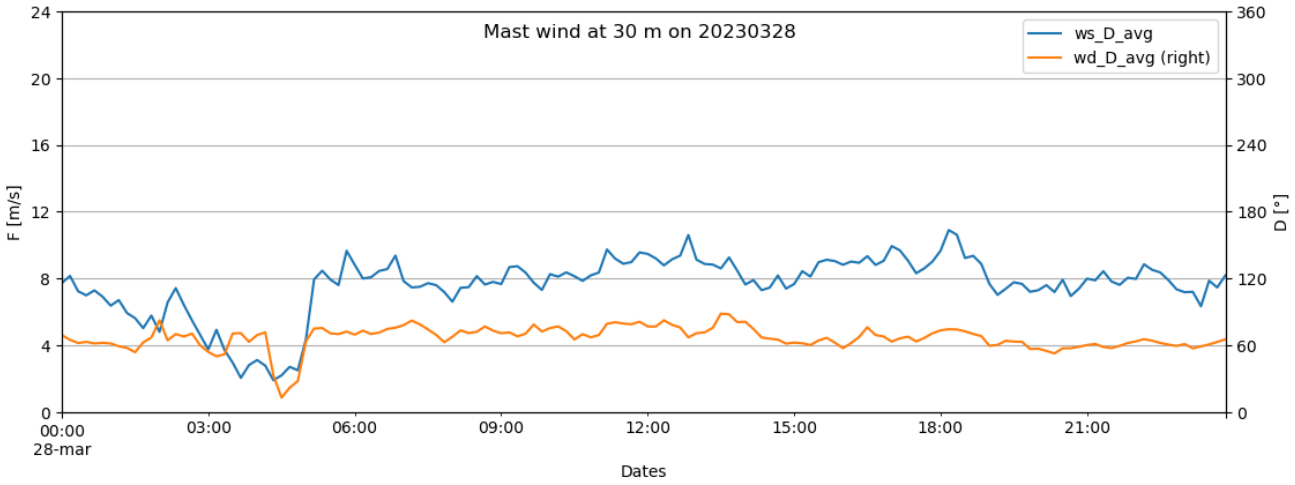
Mast wind at 30 m on 20230328
ws_D_avg
wd_D_avg (right)
F [m/s]
D [°]
0
4
8
12
16
20
24
0
60
120
180
240
300
360
00:00
28-mar
03:00
06:00
09:00
12:00
15:00
18:00
21:00
Dates

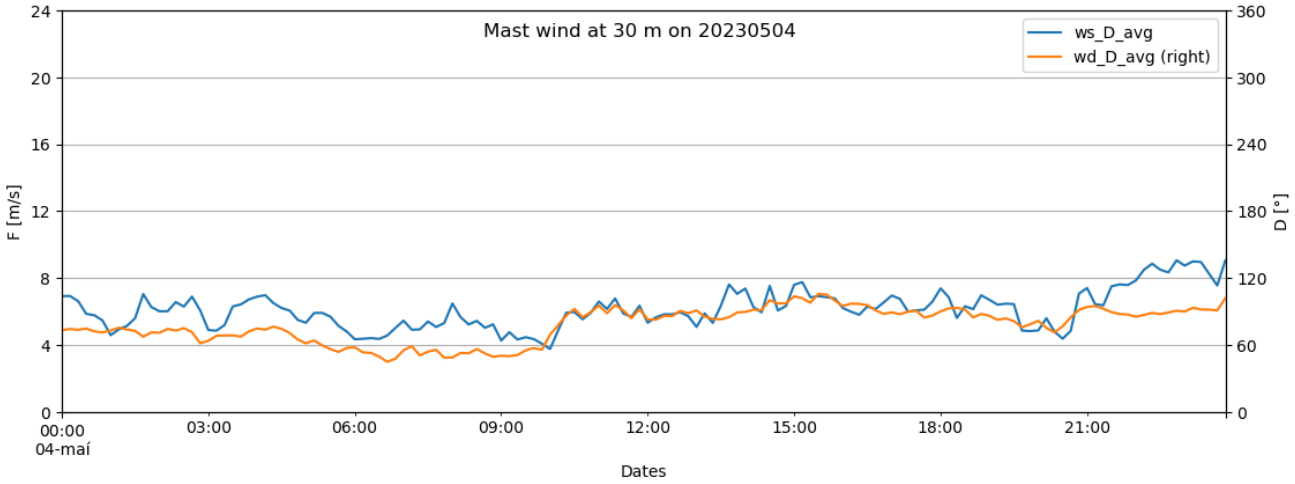
Mast wind at 30 m on 20230504
ws_D_avg
wd_D_avg (right)
F [m/s]
D [°]
0
4
8
12
16
20
24
0
60
120
180
240
300
360
00:00
04-maí
03:00
06:00
09:00
12:00
15:00
18:00
21:00
Dates

C. Lidar measurements for 8 standard wind sectors

Figures below show quantiles of standard deviation of radial wind speed from observed lidar data below 500 m and from vertical wind in mast top sensor. Only concurrent data is used and 8 standard directional sectors with a width of 45°, going clockwise with first sector centred at 0°.

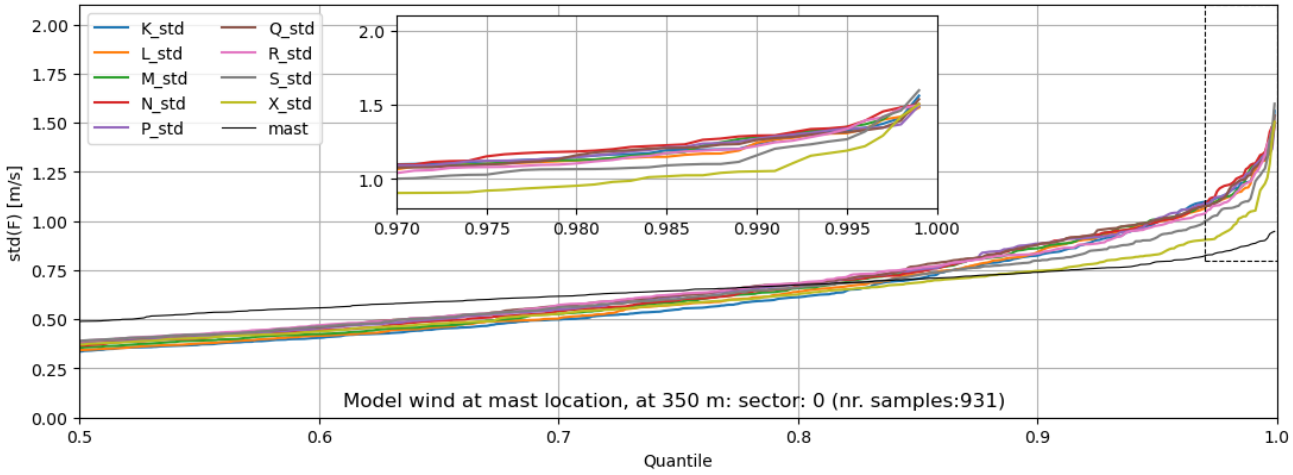

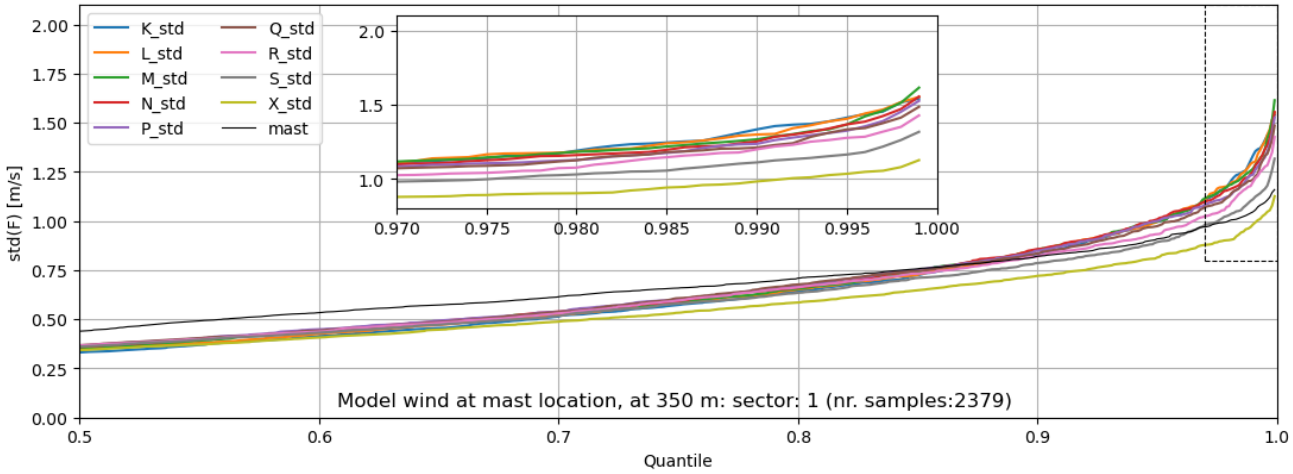

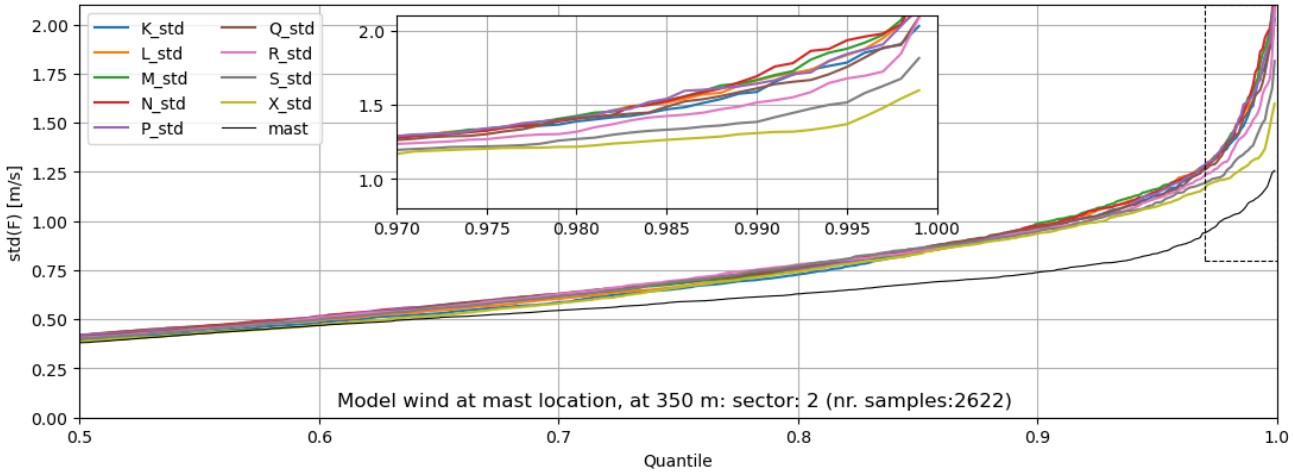
K_std
L_std
M_std
N_std
P_std
Q_std
R_std
S_std
X_std
mast
std(F) [m/s]
Quantile
Model wind at mast location, at 350 m: sector: 2 (nr. samples:2622)

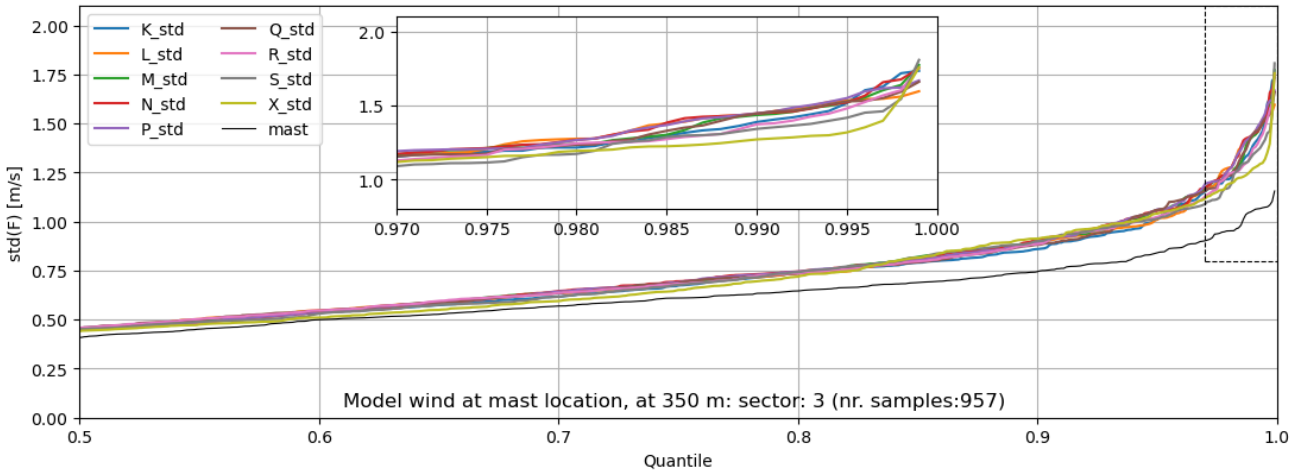
K_std
L_std
M_std
N_std
P_std
Q_std
R_std
S_std
X_std
mast
std(F) [m/s]
Quantile
Model wind at mast location, at 350 m: sector: 3 (nr. samples:957)

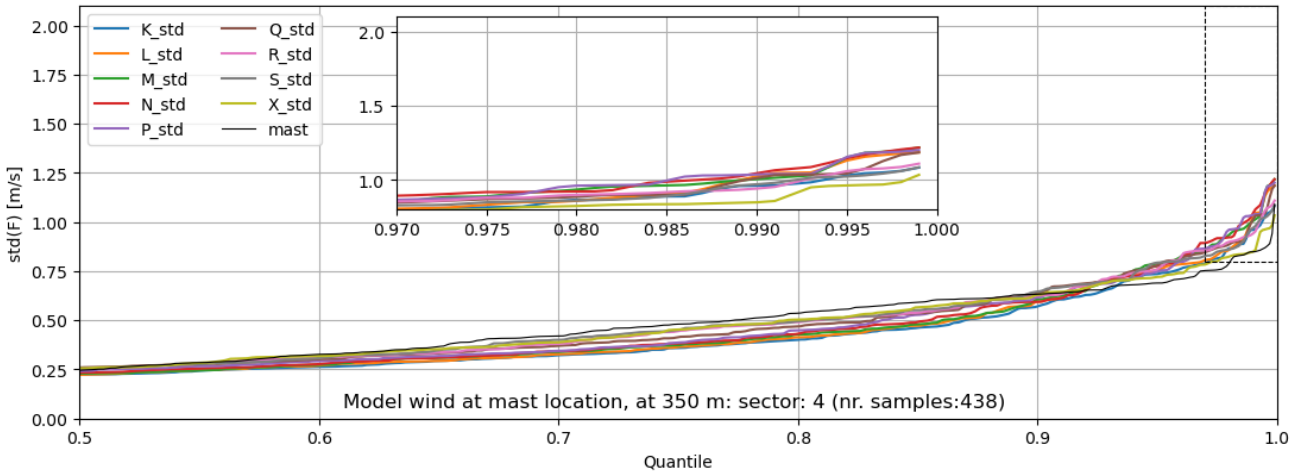
K_std
L_std
M_std
N_std
P_std
Q_std
R_std
S_std
X_std
mast
std(F) [m/s]
Quantile
Model wind at mast location, at 350 m: sector: 4 (nr. samples:438)

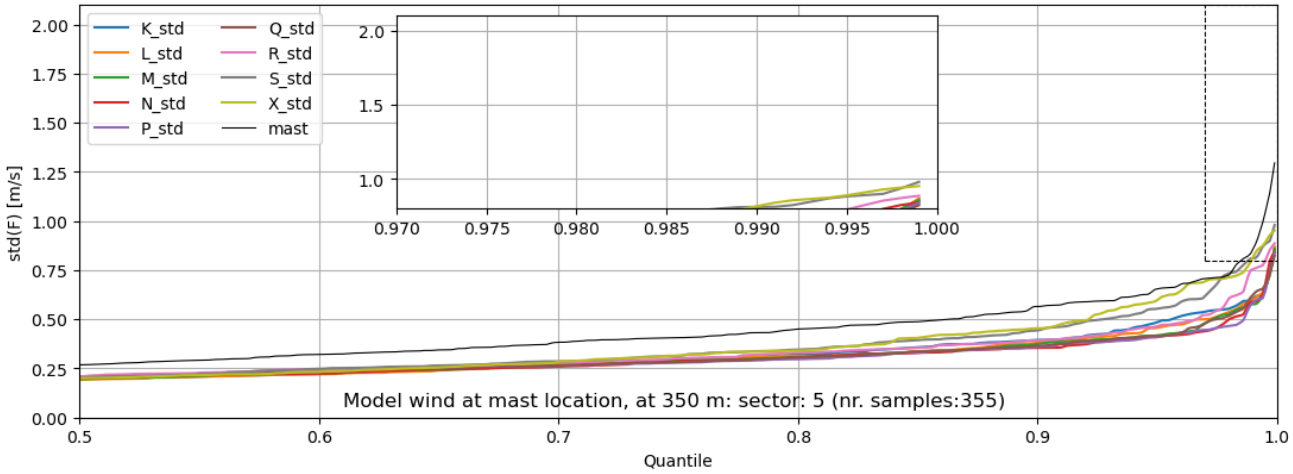
K_std
L_std
M_std
N_std
P_std
Q_std
R_std
S_std
X_std
mast
std(F) [m/s]
Quantile
Model wind at mast location, at 350 m: sector: 5 (nr. samples:355)

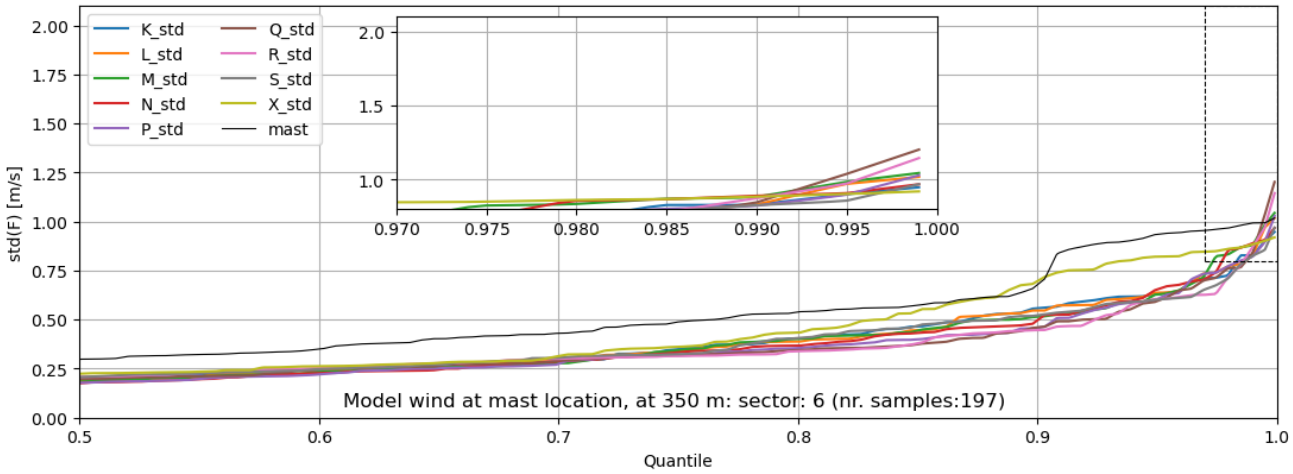
K_std
L_std
M_std
N_std
P_std
Q_std
R_std
S_std
X_std
mast
std(F) [m/s]
Quantile
Model wind at mast location, at 350 m: sector: 6 (nr. samples:197)

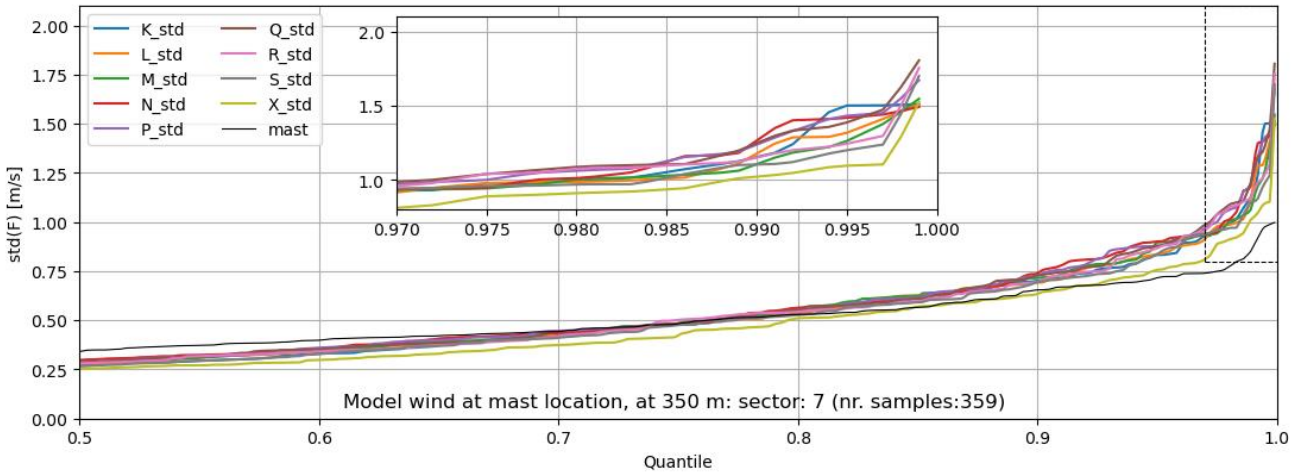
K_std
L_std
M_std
N_std
P_std
Q_std
R_std
S_std
X_std
mast
std(F) [m/s]
Quantile
Model wind at mast location, at 350 m: sector: 7 (nr. samples:359)